EUROPEAN ORGANIZATION FOR NUCLEAR RESEARCH (CERN)

CERN-EP-2023-201
2023/09/27

CMS-TOP-22-009



# Inclusive and differential cross section measurements of $\mathrm{t\bar{t}b\bar{b}}$ production in the lepton+jets channel at $\sqrt{s} = 13\,\mathrm{TeV}$

The CMS Collaboration*

## Abstract

Measurements of inclusive and normalized differential cross sections of the associated production of top quark-antiquark and bottom quark-antiquark pairs, $\mathrm{t\bar{t}b\bar{b}}$, are presented. The results are based on data from proton-proton collisions collected by the CMS detector at a centre-of-mass energy of 13 TeV, corresponding to an integrated luminosity of 138 $\mathrm{fb}^{-1}$. The cross sections are measured in the lepton+jets decay channel of the top quark pair, using events containing exactly one isolated electron or muon and at least five jets. Measurements are made in four fiducial phase space regions, targeting different aspects of the $\mathrm{t\bar{t}b\bar{b}}$ process. Distributions are unfolded to the particle level through maximum likelihood fits, and compared with predictions from several event generators. The inclusive cross section measurements of this process in the fiducial phase space regions are the most precise to date. In most cases, the measured inclusive cross sections exceed the predictions with the chosen generator settings. The only exception is when using a particular choice of dynamic renormalization scale, $\mu_{\mathrm{R}} = \frac{1}{2}\prod_{i=\mathrm{t},\bar{\mathrm{t}},\mathrm{b},\bar{\mathrm{b}}} m_{\mathrm{T},i}^{1/4}$, where $m_{\mathrm{T},i}^2 = m_i^2 + p_{\mathrm{T},i}^2$ are the transverse masses of top and bottom quarks. The differential cross sections show varying degrees of compatibility with the theoretical predictions, and none of the tested generators with the chosen settings simultaneously describe all the measured distributions.

*Submitted to the Journal of High Energy Physics*



*See Appendix F for the list of collaboration members

# 1 Introduction

The associated production of top and bottom quark-antiquark pairs, $\mathrm{t\bar{t}b\bar{b}}$, in proton-proton (pp) collisions at the CERN LHC is notoriously challenging to model because of the nonnegligible mass of the b quark, and the difference in the typical energy scales of interactions involving top and b quarks [1, 2]. Comparing predictions for $\mathrm{t\bar{t}b\bar{b}}$ production cross sections with inclusive and differential measurements is an important test of perturbative quantum chromodynamics (QCD) calculations. Furthermore, $\mathrm{t\bar{t}b\bar{b}}$ production is a leading background for searches and other measurements, such as the measurement of the associated production of top quark pairs with Higgs bosons ($\mathrm{t\bar{t}H}$), where the Higgs boson decays to a pair of b quarks ($\mathrm{H \to b\bar{b}}$) [3–8], and measurements of the simultaneous production of four top quarks ($\mathrm{t\bar{t}t\bar{t}}$) [9–19]. These two processes provide direct access to the top quark Yukawa coupling, a crucial parameter of the standard model (SM) [20, 21]. An improved understanding of $\mathrm{t\bar{t}b\bar{b}}$ production will help reduce the uncertainties in these important measurements.

Fixed-order calculations of inclusive and differential cross sections have been obtained at next-to-leading order (NLO) in QCD for $\mathrm{t\bar{t}b\bar{b}}$ production [22–26] and for the associated production of $\mathrm{t\bar{t}b\bar{b}}$ with one additional jet ($\mathrm{t\bar{t}b\bar{b}j}$) [1]. In addition, full NLO QCD corrections to off-shell $\mathrm{t\bar{t}b\bar{b}}$ production are available [27, 28]. While these fixed-order calculations provide important insights into the dynamics of the $\mathrm{t\bar{t}b\bar{b}}$ process, they cannot easily be compared with measurements because of the large extrapolations to the full parton-level phase space that this would involve. Instead, predictions obtained by matching matrix-element (ME) generators to parton showers (PSs) can be more directly compared to the data and can be used to model the $\mathrm{t\bar{t}b\bar{b}}$ background in other measurements. Such predictions have been obtained using different modelling approaches [29–34]. The current state of the art in simulating $\mathrm{t\bar{t}b\bar{b}}$ production uses ME calculations at NLO in QCD with massive b quarks and matching to a PS [2, 35, 36]. These calculations with massive b quarks use parton distribution functions (PDFs) of the proton in the four-flavour scheme (4FS), where b quarks are not part of the proton PDF. In particular, in final states with gluon splittings, $\mathrm{g \to b\bar{b}}$, the b quark mass is taken into account. These calculations provide a description of $\mathrm{t\bar{t}b\bar{b}}$ production based on the NLO MEs in the entire phase space where the $\mathrm{b\bar{b}}$ pair can be resolved as one or two b quark jets.

Measurements of inclusive and differential $\mathrm{t\bar{t}b\bar{b}}$ cross sections have previously been performed by the ATLAS and CMS Collaborations in pp collisions at centre-of-mass energies of 7, 8, and 13 TeV in final states with zero, one, or two charged leptons ($\ell = \mathrm{e}, \mu$), using samples corresponding to integrated luminosities of up to $41.5\,\mathrm{fb}^{-1}$ [37–45]. To date, $\mathrm{t\bar{t}b\bar{b}}$ simulations have shown a tendency to underpredict the inclusive $\mathrm{t\bar{t}b\bar{b}}$ cross sections. Normalized differential distributions are generally in agreement with the predictions from event generators, within experimental and theoretical uncertainties, although the size of these uncertainties has not yet made it possible to definitively rule out or prefer specific modelling approaches. The dominant uncertainties in previous studies were those related to b tagging calibration, jet energy scale (JES), and the limited precision of the NLO calculations, i.e. the choice of renormalization ($\mu_\mathrm{R}$) and factorization scales ($\mu_\mathrm{F}$).

This paper reports the measurement of inclusive and normalized differential cross sections of $\mathrm{t\bar{t}b\bar{b}}$ production in four fiducial phase space regions in the lepton+jets channel. The measurement uses pp collision data recorded with the CMS detector at the LHC from 2016 to 2018 at $\sqrt{s} = 13\,\mathrm{TeV}$, corresponding to an integrated luminosity of $138\,\mathrm{fb}^{-1}$. Top quarks almost always decay into a W boson and a b quark. We consider events in which one W boson decays into a pair of quarks, and the other W boson decays into a charged lepton (electron or muon) and a neutrino. Decays of the W boson into a tau lepton decaying into an electron or muon are also implicitly considered. After hadronization of the quarks, and including the b quarks not originating from the top quarks, the considered $t\bar{t}b\bar{b}$ events contain one electron or muon and at least five jets, of which three result from the hadronization of b quarks (b jets).

We measure inclusive cross sections and normalized differential cross sections, where the latter correspond to the ratios of the absolute differential cross sections to the inclusive ones. Measurements are performed in different phase space regions, targeting distinct aspects of $t\bar{t}b\bar{b}$ production. One phase space region targets fully resolved $t\bar{t}b\bar{b}$ events (labelled as $t\bar{t}b\bar{b}$). Another, more inclusive, phase space region requires only three b jets, so as to select $t\bar{t}b\bar{b}$ events in which the pairs of additional b quarks are reconstructed as a single jet, or in which one b jet is outside of the detector acceptance (labelled as $t\bar{t}b$). Finally, we measure cross sections aimed at the study of additional QCD radiation in $t\bar{t}b$ or $t\bar{t}b\bar{b}$ events (labelled as $t\bar{t}bj$ and $t\bar{t}b\bar{b}j$, respectively), as these have been shown to be sensitive to the modelling of $t\bar{t}b\bar{b}$ production [1].

The observed distributions are unfolded to the particle level using binned maximum likelihood fits, whereby the data from muon and electron channels from all data-taking years are fitted simultaneously, and uncertainties are estimated using a nuisance parameter profiling procedure. Differential cross sections are measured for several observables, using two complementary approaches for the event interpretation given below.

In the first approach, no attempt is made at directly identifying the additional b jets in $t\bar{t}b\bar{b}$ events in either data or simulation. The generator-level observables are defined using stable particles exclusively, with no reference to the simulated event history or the origin of b jets from top quark decays or QCD radiation. This ensures that the observable definitions at the generator and detector levels are highly consistent. Furthermore, the distributions unfolded in this way can be compared with predictions from event generators which do not provide any information about the origin of b quarks in the final state. In the phase space region with four b jets ($t\bar{t}b\bar{b}$), observables are defined via the pair of b jets with the smallest angular separation to target b jets produced through the splitting of gluons into $b\bar{b}$.

In the second approach, the b jets not originating from top quark decays are identified at the generator level using the simulated event history, and a multivariate algorithm is developed to identify the resulting reconstructed b jets among all observed jets. This approach is more accurate at identifying additional b jets and thus these observables can be more sensitive to the modelling of additional heavy-quark production in $t\bar{t}$ events, at the cost of restricting future reinterpretations of the results and introducing additional modelling assumptions about the parton history.

The unfolded results are compared to different predictions based on various NLO ME calculations, interfaced with different PS simulations. Tabulated results are provided in the HEPData record for this analysis [46].

This paper is organized as follows. Section 2 describes the CMS detector. The event generation and detector simulation are detailed in Section 3. The reconstruction of electrons, muons, and jets and the identification of b jets, as well as the corresponding definition of particle-level objects, are discussed in Section 4. Section 5 describes the event selection and the definition of the measured observables at the generator and detector levels. In Section 6, the extraction of the signal, the identification of additional b jets using a multivariate algorithm, and the unfolding of the observables are presented. The treatment of systematic uncertainties is detailed in Section 7, and the results, compared to several theoretical predictions, are presented in Section 8. Finally, a summary of the results is provided in Section 9.

## 2 The CMS detector

The central feature of the Compact Muon Solenoid (CMS) apparatus is a superconducting solenoid of 6 m internal diameter, providing a magnetic field of 3.8 T. Within the solenoid volume are a silicon pixel and strip tracker, a lead tungstate crystal electromagnetic calorimeter (ECAL), and a brass and scintillator hadron calorimeter (HCAL), each composed of a barrel and two endcap sections. Forward calorimeters extend the pseudorapidity ($\eta$) coverage provided by the barrel and endcap detectors. Muons are measured in gas-ionization detectors embedded in the steel flux-return yoke outside the solenoid. A more detailed description of the CMS detector, together with a definition of the coordinate system used and the relevant kinematic variables, can be found in Refs. [47, 48].

Events of interest are selected using a two-tiered trigger system. The first level (L1), composed of custom hardware processors, uses information from the calorimeters and muon detectors to select events at a rate of around 100 kHz within a fixed latency of about 4 $\mu$s [49]. The second level, known as the high-level trigger, consists of a farm of processors running a version of the full event reconstruction software optimized for fast processing, and reduces the event rate to around 1 kHz before data storage [50].

## 3 Simulated samples

Samples of simulated events, produced with Monte Carlo (MC) event generators, are used in this analysis to estimate the contributions from background processes, model the correspondence between the observables at the generator and detector levels for unfolding, and compare the unfolded results with theoretical predictions.

For all simulated samples, additional pp interactions in the same or neighbouring bunch crossings (pileup) are generated with PYTHIA (v8.240) [51] and overlapped with the simulated hard interactions to match the pileup multiplicity measured in data. The detector response is modelled using a detailed simulation of the CMS detector, based on GEANT4 [52].

The response of the detector and event reconstruction of the $\mathrm{t\bar{t}b\bar{b}}$ signal is modelled using a sample of $\mathrm{t\bar{t}b\bar{b}}$ events generated using POWHEG-BOX-RES [53] and OPENLOOPS [54], referred to as the nominal $\mathrm{t\bar{t}b\bar{b}}$ sample (or POWHEG+OL+P8 $\mathrm{t\bar{t}b\bar{b}}$ 4FS), where the $\mathrm{t\bar{t}b\bar{b}}$ MEs are calculated at NLO in QCD with massive b quarks [2], and matched with PYTHIA for parton showering and hadronization. The 4FS NNPDF3.1 next-to-NLO (NNLO) PDF set is used for the description of the proton structure. The b quark mass is set to 4.75 GeV and the POWHEG damping parameter that regulates the damping of real emissions in the NLO calculation when matching to the PS is set to a value of $h_{\mathrm{damp}} = 1.379 m_{\mathrm{t}}$. Dynamic $\mu_{\mathrm{F}}$ and $\mu_{\mathrm{R}}$ scales were chosen as $\mu_{\mathrm{F}} = H_{\mathrm{T}}/4$ and $\mu_{\mathrm{R}} = \frac{1}{2}\prod_{i=\mathrm{t},\bar{\mathrm{t}},\mathrm{b},\bar{\mathrm{b}}} m_{\mathrm{T},i}^{1/4}$, respectively, where $H_{\mathrm{T}} = \sum_{i=\mathrm{t},\bar{\mathrm{t}},\mathrm{b},\bar{\mathrm{b}},\mathrm{g}} m_{\mathrm{T},i}$ and the transverse mass $m_{\mathrm{T},i} = \sqrt{m_i^2 + p_{\mathrm{T},i}^2}$, following Ref. [1]. The choice of renormalization scale is a geometric average of top and bottom quark transverse masses and is a natural choice for taking into account the widely separated energy scales of both particles. The factorization scale is based on the maximum momentum of final state radiation that is still resummed into the PDF and hence is parameterized as the scalar sum of transverse top and bottom quark masses.

The sensitivity of the detector response to the modelling of the $\mathrm{t\bar{t}b\bar{b}}$ process is evaluated using an alternative sample of $\mathrm{t\bar{t}b\bar{b}}$ events, obtained from the inclusive $\mathrm{t\bar{t}}$ simulation with POWHEG (v2) matched to PYTHIA (also referred to as POWHEG+P8 $\mathrm{t\bar{t}}$ 5FS). The b quarks are assumed to be massless, and accordingly, five flavour scheme (5FS) proton PDFs (also NNPDF3.1 NNLO) are used in the calculation. In that sample, events with one additional b quark are modelled by the ME at leading order (LO) in QCD, while any further b quarks are generated by the PS. In particular, in $g \to b\bar{b}$ splittings only the emission of the gluon off initial-state partons or the top quarks is described at the ME-level. Hence, for a description of $t\bar{t}b\bar{b}$, the modelling of the splitting itself is necessarily handled by the PS. Since it has been shown that $g \to b\bar{b}$ splittings are the dominant mechanism for the production of additional b jets with top quark pairs, both in $t\bar{t}b$ and $t\bar{t}b\bar{b}$ events [2], this results in large uncertainties from the choice of the $\mu_R$ scale used for the strong coupling constant in the final-state PS. Conversely, in $t\bar{t}b\bar{b}$ samples generated in the 4FS, the dominant uncertainty comes from the choice of $\mu_R$ scale in the MEs, while uncertainties from the PS scale are smaller. The $\mu_F$ and $\mu_R$ scales in the POWHEG+P8 $t\bar{t}$ 5FS sample were set to $\mu_F = \mu_R = m_{T,t}$.

In addition to the above, we consider several alternative predictions of $t\bar{t}b\bar{b}$ cross sections, to be compared with the measurements. The generator settings used for the POWHEG+OL+P8 $t\bar{t}b\bar{b}$ 4FS and inclusive $t\bar{t}$ simulation, as well as a number of alternative generator setups described below, which are used for comparison of results.

The POWHEG inclusive $t\bar{t}$ generator is also interfaced with HERWIG (v7.13) for parton showering and hadronization [55, 56], using the CH3 underlying event tune [57] (referred to as POWHEG+H7 $t\bar{t}$ 5FS). Two other sets of simulated $t\bar{t}b\bar{b}$ events in the 4FS at NLO in QCD were obtained using MADGRAPH5_aMC@NLO (referred to as MG5_aMC+P8 $t\bar{t}b\bar{b}$ 4FS), and SHERPA (v2.2.4) [35, 58] with OPENLOOPS (referred to as SHERPA+OL $t\bar{t}b\bar{b}$ 4FS). The MG5_aMC+P8 $t\bar{t}b\bar{b}$ 4FS simulation is matched with PYTHIA and uses MADSPIN to decay the top quarks; the $\mu_F$ and $\mu_R$ scales are set to the sums of the transverse masses $m_T$ of all partons in the final state ($\sum m_T$). In the SHERPA+OL $t\bar{t}b\bar{b}$ 4FS sample, the ME and PS are matched in the MC@NLO scheme, the PDF set used is NNPDF3.0 NNLO in the 4FS, and the scales are set to $\mu_F = H_T/2$ and $\mu_R = \prod_{i=t,\bar{t},b,\bar{b}} m_{T,i}^{1/4}$. Finally, MADGRAPH5_aMC@NLO is used to generate a sample of $t\bar{t}$+jets events with up to two additional jets described at NLO QCD in the ME calculations, merged in the FxFx scheme [33] and using massless b quarks (referred to as MG5_aMC+P8 $t\bar{t}$+jets FxFx 5FS). The $\mu_F$ and $\mu_R$ scales are set to $\mu_F = \mu_R = \sum m_T$, while the jet cutoff in the ME calculations is set to 20 GeV and the merging scale to 40 GeV. The generator settings of all $t\bar{t}b\bar{b}$ simulation approaches are summarized in Table 1.

Table 1: Generator settings for different modeling approaches of $t\bar{t}b\bar{b}$ production. The top quark mass value is set to $m_t = 172.5$ GeV for all generator setups, and for the generator setups using massive b quarks, the b quark mass value is set to $m_b = 4.75$ GeV. In the scale settings, $H_T$ corresponds to the scalar $m_T$ sum, $H_T = \sum_{i=t,\bar{t},b,\bar{b},g} m_{T,i}$, and $m_{T,i} = \sqrt{m_i^2 + p_{T,i}^2}$ is the transverse mass. For generators setups using POWHEG the $h_{damp}$ value is specified. Other generator setups do not use this parameter and are marked with (—).

| Generator setup | Process/ME order | Generator/Shower | Tune | PDF set | $h_{damp}$ | Scales |
|---|---|---|---|---|---|---|
| POWHEG+P8 $t\bar{t}$ 5FS | $t\bar{t}$/ NLO | POWHEG v2/ PYTHIA 8.240 | CP5 | 5FS NNPDF3.1 NNLO | $1.379 m_t$ | $\mu_F = \mu_R = m_{T,t}$ |
| POWHEG+H7 $t\bar{t}$ 5FS | $t\bar{t}$/ NLO | POWHEG v2/ HERWIG 7.13 | CH3 | 5FS NNPDF3.1 NNLO | $1.379 m_t$ | $\mu_F = \mu_R = m_{T,t}$ |
| POWHEG+OL+P8 $t\bar{t}b\bar{b}$ 4FS | $t\bar{t}b\bar{b}$/ NLO | POWHEG-BOX-RES/ PYTHIA 8.240 | CP5 | 4FS NNPDF3.1 NNLO as 0118 | $1.379 m_t$ | $\mu_R = \frac{1}{2}\prod_{i=t,\bar{t},b,\bar{b}} m_{T,i}^{1/4}$, $\mu_F = H_T/4$ |
| SHERPA+OL $t\bar{t}b\bar{b}$ 4FS | $t\bar{t}b\bar{b}$/ NLO | SHERPA 2.2.4 | SHERPA | 4FS NNPDF3.0 NNLO as 0118 | — | $\mu_R = \prod_{i=t,\bar{t},b,\bar{b}} m_{T,i}^{1/4}$, $\mu_F = H_T/2$ |
| MG5_aMC+P8 $t\bar{t}b\bar{b}$ 4FS | $t\bar{t}b\bar{b}$/ NLO | MADGRAPH5_aMC@NLO v2.4.2/ PYTHIA 8.230 | CP5 | 4FS NNPDF3.1 NNLO as 0118 | — | $\mu_F = \mu_R = \sum m_T$ |
| MG5_aMC+P8 $t\bar{t}$+jets FxFx 5FS | $t\bar{t}$+jets FxFx/ NLO [$\leq$2 jets] | MADGRAPH5_aMC@NLO v2.6.1/ PYTHIA 8.240 | CP5 | 5FS NNPDF3.1 NNLO | — | $\mu_F = \mu_R = \sum m_T$, qCut = 40 GeV, qCutME = 20 GeV |

The predictions from the exclusive $t\bar{t}b\bar{b}$ samples are normalized using the total $t\bar{t}b\bar{b}$ cross sections obtained at NLO in QCD from the corresponding generators, whereas the inclusive $t\bar{t}$ and $t\bar{t}$+jets samples are normalized using the total cross section for $t\bar{t}$ production, $\sigma(t\bar{t}) = 833.9\,\text{pb}$, computed at NNLO in QCD using TOP++ (v2.0) [59], including soft-gluon resummations to next-to-next-to-leading logarithmic accuracy [60], and assuming a top quark mass of $m_t = 172.5\,\text{GeV}$.

The POWHEG+P8 $t\bar{t}$ 5FS sample is used for the estimation of the inclusive $t\bar{t}$ background. However, using the nominal $t\bar{t}b\bar{b}$ sample for the signal in conjunction with the inclusive $t\bar{t}$ sample for the backgrounds would result in a double counting of the $t\bar{t}b\bar{b}$ contribution. This overlap is avoided by removing from the inclusive sample events containing at least one b jet not originating from a top quark (as defined below in Section 4.2), with $p_T > 20\,\text{GeV}$ and $|\eta| < 2.4$. Conversely, in the nominal $t\bar{t}b\bar{b}$ sample only the events with at least one additional b jet are kept. Henceforth the $t\bar{t}B$ process is defined as the production of events passing these criteria. All simulated events in our measured fiducial phase spaces (see Section 5.2) are found to pass the $t\bar{t}B$ selection criteria. The remaining events in the inclusive $t\bar{t}$ samples are categorized into a $t\bar{t}C$ contribution, with events containing at least one charm (c) jet (also with $p_T > 20\,\text{GeV}$ and $|\eta| < 2.4$) for which the simulation histories of the matched c hadrons do not include any top quark, and a $t\bar{t}$+light contribution with all remaining events.

Simulated samples of minor backgrounds include single top quark production in the $t$ and $s$ channels, as well as tW production (collectively Single t); $t\bar{t}W$, $t\bar{t}H$, and $t\bar{t}Z$ production (collectively $t\bar{t}X$); and the production of $Z/\gamma^*$ or W in association with jets (collectively V+jets). An overview of the simulation settings used for these backgrounds is given in Table 2.

For all of these minor background samples, the proton structure is described by the NNPDF3.1 set of NNLO PDFs [69], and parton showering and hadronization are simulated with PYTHIA, using the CP5 tune [70] for the underlying event description. The value of the Higgs boson mass is assumed to be 125 GeV, while the top quark mass value is set to $m_t = 172.5\,\text{GeV}$. In the POWHEG samples, the $h_{\text{damp}}$ parameter is set to a value of $h_{\text{damp}} = 1.379 m_t$ as a part of the CP5 tune.

The cross sections for $t\bar{t}$, Z+jets, W+jets, and single top quark production are obtained at NNLO in QCD [59, 60, 71]. Samples for $t\bar{t}W$, $t\bar{t}Z$, and $t\bar{t}H$ production are normalized to predictions at NLO in QCD [32, 66].

Table 2: Generator settings for various minor background samples simulated with POWHEG [34, 61–66] or MADGRAPH5_aMC@NLO [32]. The "Group" column refers to the grouping of processes in the maximum likelihood fits.

| Process | Group | ME order | Generator | Notes |
|---|---|---|---|---|
| tW | Single t | NLO | POWHEG v2 | |
| $t$ channel | Single t | NLO | POWHEG v2 | MADSPIN for heavy particle decays [67] |
| $s$ channel | Single t | NLO | MADGRAPH5_aMC@NLO v2.6.1 | |
| $t\bar{t}H$ | $t\bar{t}H$ | NLO | POWHEG v2 | |
| $t\bar{t}Z$ | $t\bar{t}V$ | NLO | MADGRAPH5_aMC@NLO v2.6.1 | MADSPIN for heavy particle decays [67] |
| $t\bar{t}W$ | $t\bar{t}V$ | NLO | MADGRAPH5_aMC@NLO v2.6.1 | FxFx merging up to 1 additional jet [33]<br>MADSPIN for heavy particle decays [67] |
| W+jets | V+jets | LO | MADGRAPH5_aMC@NLO v2.6.5 | MLM merging up to 4 additional jets [68] |
| Z+jets | V+jets | LO | MADGRAPH5_aMC@NLO v2.6.5 | MLM merging up to 4 additional jets [68] |

# 4 Event reconstruction

## 4.1 Detector-level object reconstruction and identification

A particle-flow (PF) algorithm [72] is applied to reconstruct and identify each individual particle in an event, with an optimized combination of information from the various elements of the CMS detector. The primary vertex (PV) is taken to be the vertex corresponding to the hardest scattering in the event, evaluated using tracking information alone, as described in Section 9.4.1 of Ref. [73].

The energy of electrons is determined using a multivariate algorithm from a combination of the electron momentum at the PV as determined by the tracker, the energy of the corresponding ECAL cluster, and the energy sum of all bremsstrahlung photons, obtained from the ECAL, spatially compatible with originating from the electron track [74]. Electrons are identified by placing requirements on the cluster shape in the ECAL, the track quality, and the compatibility between the track and the ECAL cluster. Electrons from photon conversions are rejected. The electrons used in this analysis are required to have $|\eta| < 2.5$ and $p_{\mathrm{T}} > 29\,\mathrm{GeV}$ for data collected in 2016. In data collected in 2017–2018, the $p_{\mathrm{T}}$ threshold is raised to 34 GeV, except for electrons with $|\eta| < 2.1$, for which the threshold is 30 GeV. These requirements are chosen to be as low as possible so as to maximize the signal selection efficiency while staying above the trigger thresholds in the respective data-taking periods. Electrons with a cluster pseudorapidity $|\eta_{\mathrm{SC}}|$ between 1.444 and 1.566 are not considered, in order to avoid the gap between the barrel and endcap ECAL sections. The average identification efficiency for the primary electrons is about 70%, including the isolation requirements described below. Another looser set of requirements with 95% selection efficiency is also considered, with $p_{\mathrm{T}} > 15\,\mathrm{GeV}$ and $|\eta| < 2.5$, and relaxed identification criteria. These define the "veto" electrons, which are used to reject events with more than one lepton.

The $p_{\mathrm{T}}$ of muons is obtained from the curvature of the corresponding track, combining information from the inner tracker and the outer muon detector system [75]. The muons are identified based on the quality of the combined track fit and on the number of hits in the different tracking detectors, with an efficiency of about 95%. Muons are required to have $|\eta| < 2.4$ and $p_{\mathrm{T}} > 26$ (29) GeV in 2016 (2017–2018), while "veto" muons are defined with $p_{\mathrm{T}} > 15\,\mathrm{GeV}$, $|\eta| < 2.4$, and looser identification criteria.

Electron or muon tracks are required to have a longitudinal and transverse distance to the PV smaller than 0.5–5 mm, depending on the lepton flavour and $|\eta|$. In order to suppress backgrounds from hadrons misidentified as leptons, or from leptons produced from hadrons decaying inside of jets, the leptons are required to be isolated from hadronic activity. The lepton isolation is defined as the ratio between the scalar $p_{\mathrm{T}}$ sum of all PF candidates in a cone around the lepton excluding the lepton itself, and the lepton $p_{\mathrm{T}}$. The cone size is $\Delta R < 0.4$ (0.3) for electrons (muons). The isolation is corrected by removing contributions from pileup [76]. The maximum primary (veto) electron isolation varies between 0.03–0.08 (0.20–0.27), decreasing with $p_{\mathrm{T}}$ and increasing with $|\eta_{\mathrm{SC}}|$. For primary (veto) muons, the isolation is required to be $<$0.15 ($<$0.25). Residual differences between lepton reconstruction, identification, and isolation efficiencies in data and simulation are corrected. The efficiencies are measured as a function of lepton $p_{\mathrm{T}}$ and $\eta$ in data samples enriched in $\mathrm{Z} \to \ell^+\ell^-$ events using a "tag-and-probe" method. For electrons (muons), the corrections are between 1–5% ($<$2%) with uncertainties of less than 2 (1)% [74, 75].

The energy of charged hadrons is determined from a combination of their momentum measured in the tracker and the matching ECAL and HCAL energy deposits, corrected for the response function of the calorimeters to hadronic showers. The energy of neutral hadrons is obtained from the corresponding corrected ECAL and HCAL energies. Hadronic jets are reconstructed by clustering PF candidates using the anti-$k_{\mathrm{T}}$ algorithm [77], as implemented in the FASTJET package [78], with a distance parameter of $R = 0.4$. Jet momentum is determined as the vectorial sum of all particle momenta in the jet, and is found from simulation to be, on average, within 5–10% of the true momentum over the whole $p_{\mathrm{T}}$ spectrum and detector acceptance. The jet energy resolution (JER) amounts typically to 10 (15–20)% at 100 (30) GeV [79]. Pileup interactions can contribute additional tracks and calorimetric energy depositions, increasing the apparent jet momentum. To mitigate this effect, tracks identified to be originating from pileup vertices are discarded and an offset correction is applied to correct for remaining contributions [76]. Jet energy corrections are derived from simulation studies so that the average measured energy of jets becomes identical to that of jets at generator level. In-situ measurements of the momentum balance in dijet, $\gamma$+jet, Z+jet, and multijet events are used to determine any residual differences between the JES in data and in simulation, and appropriate corrections are applied to data [79]. Additional selection criteria are applied to each jet to remove jets potentially falsely reconstructed, with dominant contributions from instrumental effects or reconstruction failures. A multivariate algorithm is used to identify and remove jets likely originating from pileup interactions [76]. Jets used in the analysis are required to have $p_{\mathrm{T}} > 30$ GeV and $|\eta| < 2.4$ and to be separated from the selected electron or muon by $\Delta R > 0.4$.

The DEEPJET algorithm is used to identify b jets [80–82]. This algorithm uses a deep neural network (DNN) discriminant to combine information from charged and neutral PF candidates clustered in the jet with features of secondary vertices within the jet. Jets are labelled as b tagged if they pass a "medium" working point of the discriminant, corresponding to an efficiency for correctly identifying b jets in $\mathrm{t\bar{t}}$ events of 75–80% and to a misidentification probability of about 15–17% for c jets and about 1.5–2% for other jets. We will also refer to jets failing the medium working point as light-tagged jets. Another, more restrictive, ("tight") b tagging working point is also used, yielding a misidentification rate of 2.5–3.5 for c jets and 0.15–0.25% for other jets. This improved mistagging rate comes at the cost of reducing the b jet identification efficiency to around 60%.

The b jet (mis)identification probabilities in the simulation are corrected to match the efficiencies measured in data at both the medium and tight working points [80]. The tagging efficiency in data for b jets is obtained from a combination of five different measurements, three of which make use of a sample of multijet events enriched in b jets, by requiring jets to contain a muon, while the remaining two use samples enriched in $\mathrm{t\bar{t}}$ events and containing respectively one or two isolated electrons or muons. These three samples are statistically independent of each other and with the events used in this analysis and yield compatible measurements of the b tagging efficiency. The b tagging efficiency correction factors are measured as functions of jet $p_{\mathrm{T}}$ and vary between 0.9–1.0 depending on the tagger working point, the data period, and the jet $p_{\mathrm{T}}$, and have uncertainties of up to 10%. For c jets, the misidentification efficiency in the simulation is corrected using the same correction factors as for b jets, but with double their uncertainty. This has been shown to cover the true c jet misidentification probability [80]. For other jets, the misidentification probability is measured as a function of jet $p_{\mathrm{T}}$ in an inclusive sample of multijet events. The corresponding simulation-to-data correction factors vary between 0.6–1.9, depending on the tagger working point, the data period, and the jet $p_{\mathrm{T}}$. Their uncertainties vary from 10–30%.

### 4.2 Particle-level object definitions

The fiducial phase space regions and observables for the inclusive and differential cross sections reported in this paper are defined based on the properties of stable final-state particles, with proper lifetimes $\tau_0 > 10\,\text{mm}$. Particles with $|\eta| > 5$ are not considered. The definition of objects at the particle level, which follow closely those at the detector level introduced earlier, is described in the following.

Prompt particle-level electrons are selected with $p_{\mathrm{T}} > 29\,\text{GeV}$ and $|\eta| < 2.5$ and are "dressed" with photons from final-state radiation (FSR) by adding to their four-momentum the momentum of any photon within $\Delta R < 0.1$. Prompt particle-level muons are required to have $p_{\mathrm{T}} > 26\,\text{GeV}$ and $|\eta| < 2.4$. A similar FSR dressing procedure as for the electrons is applied to the muons. Furthermore, "veto" electrons and muons are defined by relaxing the thresholds to $p_{\mathrm{T}} > 15\,\text{GeV}$, and are then used to reject events with more than one lepton.

Jets are obtained by clustering all particles, excluding any neutrinos, using the anti-$k_{\mathrm{T}}$ algorithm with $R = 0.4$. They are required to have $p_{\mathrm{T}} > 25\,\text{GeV}$ and $|\eta| < 2.4$ and are not considered if they are within $\Delta R < 0.4$ of a prompt electron or muon. At the particle level, the flavour of jets is defined unambiguously by rescaling the momenta of all generated b hadrons to a negligible value and including them in the jet clustering procedure [83]. Jets thus matched to at least one b hadron are considered as b jets, while all remaining jets are labelled as light jets.

For the purpose of defining observables for the second approach introduced in Section 1, and the definition of the $\mathrm{t\bar{t}B}$ process, we also define as "additional" b jets those particle-level b jets for which the simulation histories of the matched b hadrons do not include any top quark. This definition is therefore not uniquely based on stable particles, since it refers to the simulated parton-level event content, which is specific to each generator and not provided by every generator.

## 5 Event selection and definition of fiducial phase space regions and observables

### 5.1 Event selection

Data are collected using a set of triggers requiring the presence of one isolated electron or muon. The lepton $p_{\mathrm{T}}$ thresholds applied by these single-lepton triggers vary between 27–32 (24–27) GeV for electrons (muons), depending on the data-taking period. In addition, triggers selecting events with one isolated electron and a scalar jet $p_{\mathrm{T}}$ sum ($H_{\mathrm{T}}$) above 150 GeV are used, allowing the electron $p_{\mathrm{T}}$ threshold to be set to 28 GeV for $|\eta| < 2.1$. The trigger selections used in collision data are also applied in the simulation, and residual differences between data and simulation are corrected. For electron triggers, efficiencies are measured in a control region enriched with $\mathrm{t\bar{t}}$ events, collected using triggers requiring the presence of missing transverse momentum. These present a negligible correlation with the triggers used in this analysis. Muon trigger efficiencies are measured using the tag-and-probe technique in a control region enriched in $\mathrm{Z} \to \ell^+\ell^-$ events.

Data from the different data-taking periods (2016, 2017, 2018) are analyzed separately and are only combined at the likelihood level, as will be explained in Section 6.3. Additionally, data collected in 2016 are split into two groups, the "2016preVFP" and "2016postVFP" eras, due to substantial changes in the detector conditions between them. At the beginning of the 2016 period, saturation effects in the readout chips of the strip tracker led to lower signal-to-noise ratios and fewer hits on tracks. This issue was mitigated by changing the feedback pre-amplifier bias voltage (VFP) during the 2016 data-taking run [84].

## 5.2 Fiducial phase space regions

The measured cross sections are derived from the fiducial phase space regions and observables described below. The definitions at the particle and detector levels follow each other as closely as possible in order to minimize extrapolations outside of the detector acceptance. Both at the particle and detector levels, events are first required to have exactly one primary electron or muon, and no additional "veto" electrons or "veto" muons, as defined in Section 4. At the particle level, events with electrons and muons are combined, and no requirement is placed on the decay channels of the top quarks, so that the fiducial phase space regions can also contain $t\bar{t}b\bar{b}$ events in which both top quarks decay leptonically, but one lepton is outside the detector acceptance and is not selected as a "veto" lepton. Furthermore, electrons and muons produced indirectly through the decay of a tau lepton are included. At the detector level, events with electrons or muons are classified into two distinct channels in this measurement.

Four different and partially overlapping phase space regions are then considered, each targeting different aspects of $t\bar{t}b\bar{b}$ production, as introduced in Section 1. The most inclusive selection considered, labelled as 5j3b (or $\geq$5 jets: $\geq$3b ) and targeting $t\bar{t}b$, requires the presence of at least five jets, of which at least three must be b(-tagged) jets at particle (detector) level. In a second selection, labelled as 6j4b (or $\geq$6 jets: $\geq$4b ) and targeting $t\bar{t}b\bar{b}$, at least six jets are required, of which at least four are b(-tagged) jets. Two additional selections are defined which help target the properties of additional light jets produced in the event, targeting $t\bar{t}bj$ and $t\bar{t}b\bar{b}j$. These are the 6j3b3l phase space (also labelled $\geq$6 jets: $\geq$3b, $\geq$3 light), requiring at least six jets, including at least three b(-tagged) jets and at least three light(-tagged) jets; and the 7j4b3l phase space (also labelled $\geq$7 jets: $\geq$4b, $\geq$3 light), requiring at least seven jets, including at least four b(-tagged) jets and at least three light(-tagged) jets.

## 5.3 Observables

As described in Section 1, we consider two classes of observables for unfolding. In the first class, all observables are defined using stable particles exclusively, without reference to any simulated event history. This implies that no strict distinction is made between b jets originating from the decay of top quarks, or from additional radiation. In this way, there is a close correspondence between particle- and detector-level observables (see Sections 4.1 and 4.2), and the definition of the observables is independent of any specific event generator. In order to probe different features of $t\bar{t}b\bar{b}$ production, and in particular the properties of b jets produced from QCD radiation, we distinguish different categories of objects using simple kinematic criteria.

In the 5j3b phase space, we focus the measurements on the b jet with the third-largest $p_T$, which at the generator level is a true additional b jet (not coming from top quark decays) in the nominal signal simulation in approximately 49% of 5j3b events. This identification allows for the study of the properties of the additional b jets even in the case where they cannot be individually resolved. In that phase space, we measure, each independently, the number of jets in the event ($N_{\text{jets}}$), the number of b jets in the event ($N_b$), the $p_T$ and $|\eta|$ of the 3rd b jet ($p_T(b_3)$, $|\eta(b_3)|$), the scalar $p_T$ sum of all jets ($H_T$), and the scalar $p_T$ sum of all b jets ($H_T^b$).

In the 6j4b phase space where there are at least four b jets in the event, in order to measure properties that are expected to be sensitive to the modelling of gluon splittings to $b\bar{b}$, we define the "extra" b jets as the pair of b jets with the smallest angular separation, defined by

$$\Delta R_{\mathrm{bb}} = \sqrt{(\Delta\phi_{\mathrm{bb}})^2 + (\Delta\eta_{\mathrm{bb}})^2}, \quad (1)$$

where $\Delta\phi_{\mathrm{bb}}$ and $\Delta\eta_{\mathrm{bb}}$ are the angular separations of the pair of b jets in azimuthal angle $\phi$ (in radians) and $\eta$, respectively. We denote that pair by $\mathrm{bb}^{\mathrm{extra}}$ in the following. With this strategy, in the fiducial generator-level phase space, the two $\mathrm{bb}^{\mathrm{extra}}$ jets correspond to true additional b jets in $\sim$49% of events in the 6j4b phase space. Other choices, such as picking the pairs of jets with the 3rd and 4th largest $p_{\mathrm{T}}$, result in smaller probabilities of correctly identifying the additional jets ($\sim$28%).

In the 6j4b phase space, we measure, each independently, the number of jets in the event, the $p_{\mathrm{T}}$ and $|\eta|$ of the 3rd and 4th b jets ($p_{\mathrm{T}}(\mathrm{b}_3)$, $p_{\mathrm{T}}(\mathrm{b}_4)$, $|\eta(\mathrm{b}_3)|$, $|\eta(\mathrm{b}_4)|$), the scalar jet $p_{\mathrm{T}}$ sum ($H_{\mathrm{T}}$), and the scalar b-jet $p_{\mathrm{T}}$ sum ($H_{\mathrm{T}}^{\mathrm{b}}$). Considering all possible pairs of distinct b jets, we independently measure the average $\Delta R_{\mathrm{bb}}$ over all pairings ($\Delta R_{\mathrm{bb}}^{\mathrm{avg}}$), and the largest invariant mass ($m_{\mathrm{bb}}^{\mathrm{max}}$). For the $\mathrm{bb}^{\mathrm{extra}}$ pair, we measure, each independently, the distance in $\eta$ between the two b jets of the pair ($\Delta R(\mathrm{bb}^{\mathrm{extra}})$), the invariant mass of the pair ($m(\mathrm{bb}^{\mathrm{extra}})$), the $p_{\mathrm{T}}$ and $|\eta|$ of the pair ($p_{\mathrm{T}}(\mathrm{bb}^{\mathrm{extra}})$, $|\eta(\mathrm{bb}^{\mathrm{extra}})|$), and the $p_{\mathrm{T}}$ and $|\eta|$ of the leading ($\mathrm{b}_1^{\mathrm{extra}}$) and sub-leading ($\mathrm{b}_2^{\mathrm{extra}}$) b jets in the pair ($p_{\mathrm{T}}(\mathrm{b}_1^{\mathrm{extra}})$, $p_{\mathrm{T}}(\mathrm{b}_2^{\mathrm{extra}})$, $|\eta(\mathrm{b}_1^{\mathrm{extra}})|$, $|\eta(\mathrm{b}_2^{\mathrm{extra}})|$).

In the 6j3b3l and 7j4b3l phase space regions, we target the properties of the additional light jets (see Sections 4.1 and 4.2). In each of these phase space regions, we measure the scalar $p_{\mathrm{T}}$ sum of the light jets in the event ($H_{\mathrm{T}}^{\mathrm{light}}$). We then remove from consideration the pair of light jets with the invariant mass closest to the W boson mass obtained from a fit to the two detector- or particle-level jets matched to the W boson decay in simulation. We then measure, independently, the $p_{\mathrm{T}}$ of the leading remaining light jet ($p_{\mathrm{T}}(\mathrm{lj}_1^{\mathrm{extra}})$), and the $\Delta\phi$ between that light jet and the lowest $p_{\mathrm{T}}$ b jet ($|\Delta\phi(\mathrm{lj}_1^{\mathrm{extra}}, \mathrm{b}_{\mathrm{soft}})|$). The latter variable probes the amount of recoil against additional QCD radiation in $\mathrm{t\bar{t}b\bar{b}}$ events that is absorbed by the softest b jet [1]. In the 6j3b3l and 7j4b3l phase space regions, the leading remaining light jet corresponds to a light jet not from top quark decays in $\sim$94% of cases. The softest b jet is an additional b jet in $\sim$50 (65)% of cases in the 6j3b3l (7j4b3l) phase space.

In the second class of observables, we focus on the 6j4b phase space and explicitly target the b jets that do not originate from decaying top quarks. At the particle level, these are the additional b jets as defined in Section 4.2, labelled as $\mathrm{bb}^{\mathrm{add.}}$. In case more than two additional b jets are present, the two additional b jets leading in $p_{\mathrm{T}}$ are selected. At the detector level, the pair of b-tagged jets most consistent with the true additional b jets is identified using a DNN discriminant, described in Section 6.2. For the $\mathrm{bb}^{\mathrm{add.}}$ pair defined in this way, we measure the opening angle between the two b jets of the pair ($\Delta R(\mathrm{bb}^{\mathrm{add.}})$), the invariant mass of the pair ($m(\mathrm{bb}^{\mathrm{add.}})$), the $p_{\mathrm{T}}$ and $|\eta|$ of the pair ($p_{\mathrm{T}}(\mathrm{bb}^{\mathrm{add.}})$, $|\eta(\mathrm{bb}^{\mathrm{add.}})|$), and the $p_{\mathrm{T}}$ and $|\eta|$ of the leading and subleading b jets in the pair ($p_{\mathrm{T}}(\mathrm{b}_1^{\mathrm{add.}})$, $p_{\mathrm{T}}(\mathrm{b}_2^{\mathrm{add.}})$, $|\eta(\mathrm{b}_1^{\mathrm{add.}})|$, $|\eta(\mathrm{b}_2^{\mathrm{add.}})|$).

A summary of all observables is given in Table 3. In the measurement of each observable we also measure the inclusive cross section in the respective phase space ($\sigma_{\mathrm{fid}}$).

# 6 Signal extraction and unfolding

In the selected regions with at least three b-tagged jets, the data are highly enriched in $\mathrm{t\bar{t}}$+jets events, which consist of about 30% $\mathrm{t\bar{t}B}$, 20% $\mathrm{t\bar{t}C}$, and 50% $\mathrm{t\bar{t}}$+light events, with minor background contributions, in descending order of importance, from single top quark production, $\mathrm{t\bar{t}H}$, V+jets, $\mathrm{t\bar{t}Z}$, and $\mathrm{t\bar{t}W}$ processes. Events from $\mathrm{t\bar{t}H}$, $\mathrm{t\bar{t}Z}$, or $\mathrm{t\bar{t}W}$ processes are referred to

Table 3: Description of all measured observables for each of the four fiducial phase space regions. Observables marked as ($\checkmark^*$) rely on the definition of additional b jets, and do not fully correspond to the 6j4b fiducial phase space defined at the particle level, but also require the presence of b jets without top (anti)quarks in their simulated history.

| | Observable | 5j3b | 6j4b | 6j3b3l | 7j4b3l |
|---|---|---|---|---|---|
| $\sigma_{\text{fid}}$ | Inclusive cross section | ✓ | ✓ | ✓ | ✓ |
| Global observables | | | | | |
| $N_{\text{jets}}$ | Jet multiplicity | ✓ | ✓ | | |
| $N_{\text{b}}$ | b jet multiplicity | ✓ | | | |
| $H_{\text{T}}^{\text{j}}$ | Scalar $p_{\text{T}}$ sum of all jets | ✓ | ✓ | | |
| $H_{\text{T}}^{\text{b}}$ | Scalar $p_{\text{T}}$ sum of all b jets | ✓ | ✓ | | |
| $H_{\text{T}}^{\text{light}}$ | Scalar $p_{\text{T}}$ sum of all light jets | | | ✓ | ✓ |
| Observables related to b jets | | | | | |
| $p_{\text{T}}(\text{b}_3)$ | $p_{\text{T}}$ of third hardest b jet | ✓ | ✓ | | |
| $\lvert\eta(\text{b}_3)\rvert$ | $\lvert\eta\rvert$ of third hardest b jet | ✓ | ✓ | | |
| $p_{\text{T}}(\text{b}_4)$ | $p_{\text{T}}$ of fourth hardest b jet | | ✓ | | |
| $\lvert\eta(\text{b}_4)\rvert$ | $\lvert\eta\rvert$ of fourth hardest b jet | | ✓ | | |
| Observables considering all pairs of b jets (bb) | | | | | |
| $\Delta R_{\text{bb}}^{\text{avg}}$ | Average $\Delta R$ of all bb pairs | | ✓ | | |
| $m_{\text{bb}}^{\text{max}}$ | Highest invariant mass among all bb pairs | | ✓ | | |
| Observables related to the pair of b jets closest in $\Delta R$ ($\text{bb}^{\text{extra}}$) | | | | | |
| $p_{\text{T}}(\text{b}_1^{\text{extra}})$ | $p_{\text{T}}$ of leading extra b jet | | ✓ | | |
| $\lvert\eta(\text{b}_1^{\text{extra}})\rvert$ | $\lvert\eta\rvert$ of leading extra b jet | | ✓ | | |
| $p_{\text{T}}(\text{b}_2^{\text{extra}})$ | $p_{\text{T}}$ of subleading extra b jet | | ✓ | | |
| $\lvert\eta(\text{b}_2^{\text{extra}})\rvert$ | $\lvert\eta\rvert$ of subleading extra b jet | | ✓ | | |
| $\Delta R(\text{bb}^{\text{extra}})$ | $\Delta R$ of $\text{bb}^{\text{extra}}$ pair | | ✓ | | |
| $\lvert\eta(\text{bb}^{\text{extra}})\rvert$ | $\lvert\eta\rvert$ of $\text{bb}^{\text{extra}}$ pair | | ✓ | | |
| $m(\text{bb}^{\text{extra}})$ | invariant mass of $\text{bb}^{\text{extra}}$ pair | | ✓ | | |
| $p_{\text{T}}(\text{bb}^{\text{extra}})$ | $p_{\text{T}}$ of $\text{bb}^{\text{extra}}$ pair | | ✓ | | |
| Observables related to the pair of b jets not from $\text{t}\bar{\text{t}}$ decay ($\text{bb}^{\text{add.}}$) | | | | | |
| $p_{\text{T}}(\text{b}_1^{\text{add.}})$ | $p_{\text{T}}$ of leading additional b jet | | ✓* | | |
| $\lvert\eta(\text{b}_1^{\text{add.}})\rvert$ | $\lvert\eta\rvert$ of leading additional b jet | | ✓* | | |
| $p_{\text{T}}(\text{b}_2^{\text{add.}})$ | $p_{\text{T}}$ of subleading additional b jet | | ✓* | | |
| $\lvert\eta(\text{b}_2^{\text{add.}})\rvert$ | $\lvert\eta\rvert$ of subleading additional b jet | | ✓* | | |
| $\Delta R(\text{bb}^{\text{add.}})$ | $\Delta R$ of $\text{bb}^{\text{add.}}$ pair | | ✓* | | |
| $\lvert\eta(\text{bb}^{\text{add.}})\rvert$ | $\lvert\eta\rvert$ of $\text{bb}^{\text{add.}}$ pair | | ✓* | | |
| $m(\text{bb}^{\text{add.}})$ | invariant mass of $\text{bb}^{\text{add.}}$ pair | | ✓* | | |
| $p_{\text{T}}(\text{bb}^{\text{add.}})$ | $p_{\text{T}}$ of $\text{bb}^{\text{add.}}$ pair | | ✓* | | |
| Observables related to extra light jets | | | | | |
| $p_{\text{T}}(\text{lj}_1^{\text{extra}})$ | $p_{\text{T}}$ of leading extra light jet | | | ✓ | ✓ |
| $\lvert\Delta\phi(\text{lj}_1^{\text{extra}}, \text{b}_{\text{soft}})\rvert$ | $\Delta\phi$ of leading extra light jet and softest b jet | | | ✓ | ✓ |

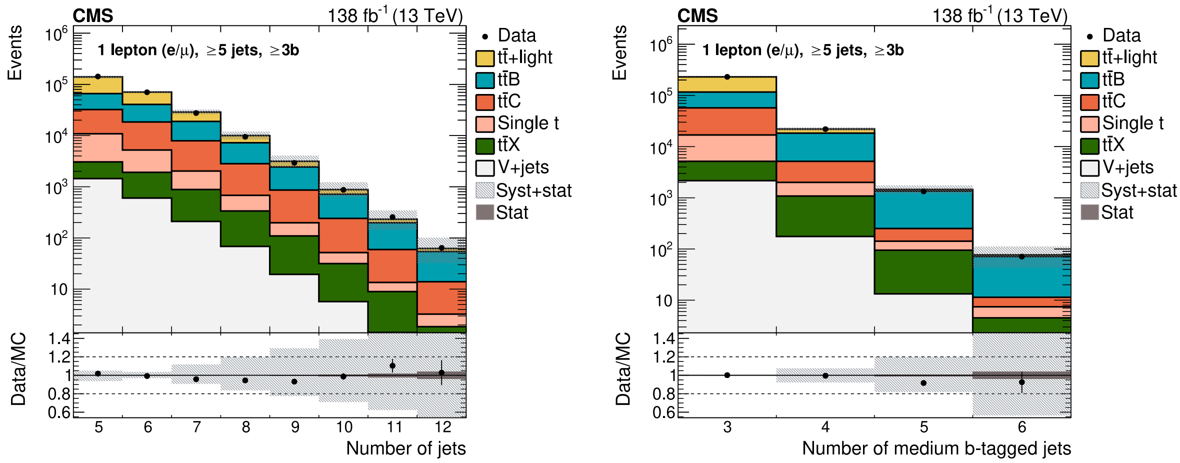


Figure 1: Jet (left) and b-tagged jet (right) multiplicity with the $\geq$5 jets: $\geq$3b selection prior to any fit, shown for both lepton channels and all data periods combined. For the purpose of visualisation, the contributions from simulation have been scaled by a common factor to match the yield in data. The $t\bar{t}X$ contribution includes the $t\bar{t}H$, $t\bar{t}W$, and $t\bar{t}Z$ processes. The shaded bands include all a priori uncertainties described in Section 7, including the $t\bar{t}B$ cross section uncertainty estimated from the nominal $t\bar{t}b\bar{b}$ simulation. Only effects on the shape of the distributions are considered. The last bins also contain the overflow.

as a combined $t\bar{t}X$ contribution if a distinction is not necessary. In the other selected regions with at least four b-tagged jets, the $t\bar{t}B$ contribution is about two thirds of all events. Background contamination from inclusive multijet production, where a jet or a nonisolated lepton is misidentified as a primary lepton, has been verified with simulated multijet events to be negligible at the level of the precision of this measurement ($\leq$1% in the 5j3b phase space), and this background is therefore not considered further. The prefit composition of the events as a function of number of jets and number of b-tagged jets at the medium working point is shown in Figure 1, with the 5j3b selection applied. The events displayed in these distributions are the superset of events used for the measurements presented in Sec. 8.

For each observable, the cross section is measured using a dedicated binned maximum likelihood fit, which simultaneously yields the inclusive cross section in the corresponding fiducial phase space and the unfolded normalized differential cross section of the observable (Section 6.3). In order to improve the separation between the signal and background components, thereby better constraining the background contributions using the data, we use an “ancillary” variable that divides the detector-level selections into signal- and background-enriched categories, which are then fitted simultaneously.

## 6.1 Ancillary variable

We use the number of jets passing the tight b tagging working point as an ancillary variable. The distributions of the number of tight b-tagged jets with the 5j3b and 6j4b selections applied are shown in Fig. 2. The regions with three or more tight b-tagged jets are highly enriched in $t\bar{t}B$ signal events, as defined in Section 3, since they typically feature three or four true b jets after fiducial selection, whereas the regions with 0–2 tight b-tagged jets are dominated by $t\bar{t}C$ or $t\bar{t}$+light backgrounds where c or light jets have been misidentified as medium b-tagged jets and, therefore, serve as control regions for these backgrounds. In the fits of observables in the 5j3b and 6j3b3l phase space regions we use three ancillary regions containing zero or one, two, or three or more tight b-tagged jets. In the other phase space regions we only use two

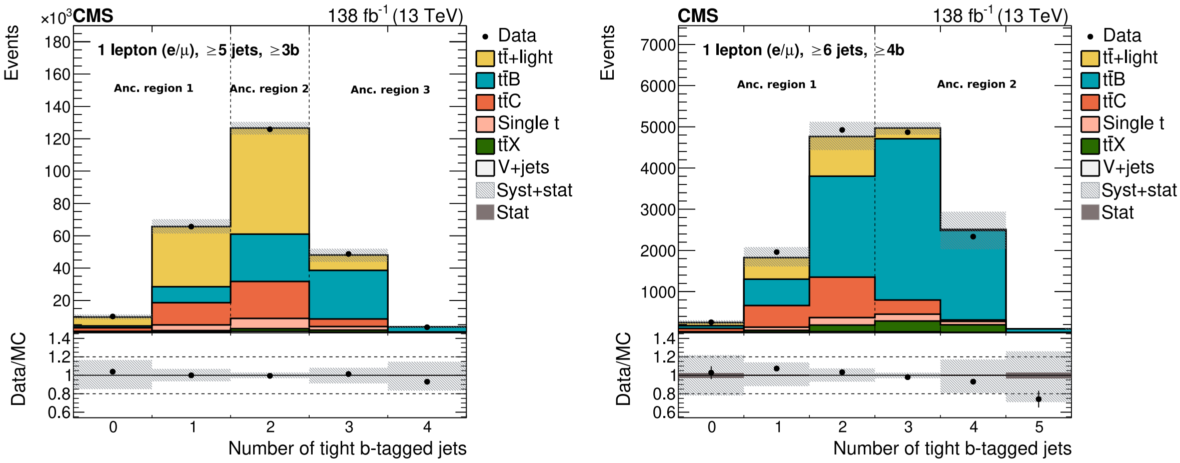


Figure 2: Number of jets b tagged at the tight working point with the ≥5 jets: ≥3b (left) and ≥6 jets: ≥4b selections (right) prior to any fit, shown for all lepton channels and years combined. For the purpose of visualisation, the contributions from simulation have been scaled by a common factor to match the yield in data. The shaded bands include all uncertainties described in Section 7, including the $\mathrm{t\bar{t}B}$ cross section uncertainty estimated from the nominal $\mathrm{t\bar{t}b\bar{b}}$ simulation. Only effects on the shape of the distributions are considered. The last bins also contain the overflow. The vertical dashed lines indicate the ancillary regions.

ancillary regions: one containing events with fewer than three tight b-tagged jets, and another one containing events with at least three tight b-tagged jets. The use of ancillary variables is not only useful for obtaining signal-enriched regions but also allows for the constraint of b tagging related uncertainties in the fit.

## 6.2 Multivariate algorithm for jet assignment

For the eight observables in the 6j4b phase space with explicit identification of the additional b jets, a multivariate algorithm based on a DNN is used to identify the pair of b-tagged jets most consistent with the true additional b jets as defined by the generator-level information. The four b-tagged jets in an event with the highest $p_{\mathrm{T}}$, in the following referred to as candidate jets, are grouped into six permutations of candidate jet pairs, depending on their ranking in $p_{\mathrm{T}}$. Permutations within a pair are not treated separately. A detector-level jet is considered correctly identified as an additional jet if it lies within an angular distance of $\Delta R < 0.4$ to an additional particle-level b jet.

An illustration of the DNN architecture is shown in Fig. 3. The DNN makes use of two sets of input variables, targeting jet-specific input information and global event information separately.

For the input variables targeting jet-specific information, i.e. features of the four candidate jets, an automated feature engineering is performed for each jet using five convolutional neural network (CNN) layers [85] with filter matrices of size 1×1 [81]. The size of the filter matrices is chosen such that they aggregate the different features, separately for each jet, into higher-level features of the consecutive layers. These layers are followed by a long short-term memory (LSTM) cell [86], where the independent jet features are combined into a sequence, allowing the network to learn from the correlations of the jet features. The five features used for each candidate jet are the $p_{\mathrm{T}}$, $\eta$, a flag indicating whether it passes the tight b tagging working point, the angular separation ($\Delta R$) with the charged lepton, and the invariant mass with the charged lepton. The 30 input variables targeting global event information include the properties of the

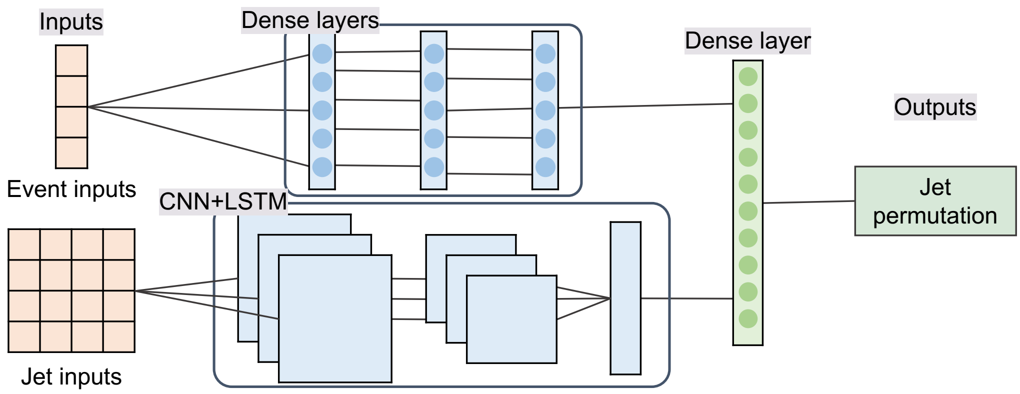


Figure 3: Structural representation of the neural network used for the assignment of the additional b-jet pair. The neural network uses two sets of input variables: global event information is connected to three dense network layers, and jet-specific information is connected via convolutional network layers (CNN) and a long short-term memory (LSTM) cell. The input sequences are concatenated into one dense layer. The output layer consists of six nodes, each representing one of the six possible candidate jet combinations.

six dijet combinations of the four candidate b jets. These input variables are connected via three dense network layers. The inputs consist of the scalar $p_{\mathrm{T}}$ sum of the four candidate b jets, the $p_{\mathrm{T}}$, $\eta$, and $\phi$ of the charged lepton, the $\Delta\phi$, $\Delta\eta$, and invariant mass of the dijet combinations, the $\Delta R$ of the dijet combinations and the charged lepton, and the jet and b-tagged jet multiplicities. Both input sequences are concatenated into one dense layer, which is connected to an output layer consisting of six nodes, each representing one of the six possible candidate jet combinations. The pair of b-tagged jets with the highest DNN output value per event is chosen as the additional b-jet pair to be used further in the analysis.

The training of the DNN is performed with simulated events passing the fiducial 6j4b phase space definition using the KERAS [87] package with a TENSORFLOW [88] backend and the ADAM optimizer [89]. In the training, the categorical cross-entropy loss function is minimized. To reduce biases from imbalances in the numbers of events for the different dijet categories, events are weighted in the training such that each category has the same number of weighted events. Potential overfitting is mitigated using a dropout percentage of 10% [90] and an early-stopping procedure to stop the training if no decrease in the loss minimization has been achieved for 20 epochs (iterations over the training data set) on a set of spectator events not used for the training (validation data set). In order not to bias the evaluation of the DNN, events from the POWHEG+P8 $\mathrm{t\bar{t}}$ 5FS simulation passing the fiducial 6j4b definition are used in the training, while the evaluation for the measurement is performed with the nominal $\mathrm{t\bar{t}b\bar{b}}$ sample. It has been validated that the performance of the DNN is independent of the choice of which of those samples of simulated $\mathrm{t\bar{t}b\bar{b}}$ events is used for the training or the evaluation. This implies that the measurements of the DNN-based observables are not biased by the choice of signal model used for training the DNN.

The performance of the DNN is evaluated in the simulation based on the fraction of events in which it selects the correct pair of additional b jets (accuracy). The accuracy of the DNN is determined to be about 49%, which represents a significant increase in identification accuracy compared to choosing the two b jets closest in $\Delta R$ (as in Section 5), which only yields an accuracy of about 41%.

## 6.3 Unfolding methodology

The observed distributions are unfolded to the particle level by removing estimated background contributions and correcting for resolution, acceptance and efficiency effects of the detector and event reconstruction so that the measured distributions can be directly compared to theoretical predictions provided by MC event generators.

Unfolding is performed through a maximum likelihood fit by constructing, for each observable, a statistical model that links the distributions at the particle and detector levels. The values of the particle-level cross sections which maximize the agreement between the predicted detector-level distributions and the observed data are determined from the fit. In these models, freely floating parameters of interest determine the total cross section of the signal process in the corresponding phase space, as well as the normalized differential cross section of the signal process in discrete bins of the considered observable. The models are constructed using the simulated signal and background samples described in Section 3 and include nuisance parameters that model the effect of systematic uncertainties in the signal and background predictions. The fit is performed by minimizing the negative-log-likelihood (NLL) of the data with respect to the parameters of the model. The calculation of the NLL and its minimization are performed using SMOOFIT [91], itself relying on the JAX package [92] for automatic differentiation of the NLL function, providing fast and numerically stable evaluations of the NLL gradients and of the second derivative (Hessian) matrix. Both the central values and confidence intervals for the absolute and normalized differential cross sections are extracted from the fit.

The electron and muon channels as well as the four data-taking eras (2016preVFP, 2016postVFP, 2017, and 2018) and the ancillary variable regions are combined at the likelihood level. The likelihood used to measure the unfolded distributions can be written as

$$L(\vec{\mu},\vec{\alpha}) = \left[\prod_{e,i} \mathrm{Poi}\left(D_{e,i} \middle| S_{e,i}(\vec{\mu},\vec{\alpha}) + \sum_{p\in\mathrm{bkg.}} N^{p}_{e,i}(\vec{\alpha})\right)\right] \mathcal{N}(\vec{\alpha}), \tag{2}$$

where the parameters $\vec{\mu}$ are freely-floating parameters of interest, $\vec{\alpha}$ are profiled nuisance parameters used to model systematic uncertainties, $D_{e,i}$ are the observed yields in data-taking era $e$ and detector-level bin $i$ (including the lepton channels and ancillary regions), $N^{p}_{e,i}$ are the predicted yields of background process $p$ in era $e$ and bin $i$, $S_{e,i}$ are the predicted signal yields in era $e$ and bin $i$, $\mathrm{Poi}(d|\nu)$ is the Poisson probability mass function for counts $d$ with mean $\nu$, and $\mathcal{N}(\vec{\alpha})$ is the Gaussian constraint term (with mean of zero and width of one) of the nuisance parameters.

We denote by $M^{e}_{ij}$ the expected number of signal events in the fiducial phase space in the detector-level bin $i$ and generator-level bin $j$ for the data-taking era $e$. For every generator-level bin there are, therefore, up to

$$(4 \text{ eras}) \times (2 \text{ channels}) \times (2 \text{ or } 3 \text{ anc. regions}) = 16 \text{ or } 24 \text{ detector-level bins}, \tag{3}$$

depending on the phase space. In addition, the detector-level binning is chosen to be finer than the generator-level binning, with every bin at the detector level being about half the width of the generator-level bins (except for discrete observables such as the number of jets or b jets, and the observables in the 7j4b3l region where the data yields are the lowest). This improves the separation between signal and background. Including other control regions in the fit or using a finer binning at the detector level has not been found to provide any significant further improvements in the sensitivity of the measurements. The expected event yields in era $e$ can be written as $M^{e}_{ij} = \mathcal{L}_e \sigma^0_j K^{e}_{ij}$, where $\mathcal{L}_e$ is the integrated luminosity in era $e$, $\sigma^0_j$ is the prefit cross section in bin $j$ estimated using the nominal $\mathrm{t\bar{t}b\bar{b}}$ sample, and $K^e_{ij}$ are response matrices, i.e. the probability for a simulated event in era $e$ and generator-level bin $j$ to be reconstructed and selected in detector-level bin $i$. The total expected signal yields $S$ in Eq. (2) are computed as functions of the parameters of interest as

$$S_{e,i}(\vec{\mu},\vec{\alpha}) = \mu_{\mathrm{fid}} \sum_{j=1}^{n} \mu_j M^e_{ij}(\vec{\alpha}), \tag{4}$$

where $\mu_{\mathrm{fid}} = \sigma_{\mathrm{fid}}/\sigma^0_{\mathrm{fid}}$ is the signal-strength modifier for the inclusive cross section and $\mu_j$ are the parameters varying the fraction of signal events in each generator-level bin $j$. To preserve unity, the yields in the last generator-level bin $n$ are not scaled independently, but as a function of the other bins as

$$\mu_n(\mu_1 \ldots \mu_{n-1}) = \frac{1}{F_n}\left(1 - \sum_{i=1}^{n-1} \mu_i F_i\right). \tag{5}$$

where $F_j = \sigma^0_j/\sigma^0_{\mathrm{fid}} = \sigma^0_j / \sum_{i=1}^{n} \sigma^0_i$ is the *a priori* fractional cross section in bin $j$. In this way, the measured inclusive cross section is directly obtained as $\hat{\sigma}_{\mathrm{fid}} = \hat{\mu}_{\mathrm{fid}}\sigma^0_{\mathrm{fid}}$. Furthermore, the measured normalized differential cross section in bin $j$ is extracted as $1/\hat{\sigma}_{\mathrm{fid}}\, \mathrm{d}\hat{\sigma}_j/\mathrm{d}X = \hat{\mu}_j F_j/w_j$, where $w_j$ is the width of generator-level bin $j$. Thus, the yields in the last bin $n$ are constrained through Eq. (5) to conserve the total signal normalization for a given value of $\mu_{\mathrm{fid}}$. The covariance matrix of all fit parameters is obtained from the inverse Hessian of the NLL at the minimum and is used to compute confidence intervals on the measured cross sections. We have verified that the resulting intervals are equivalent to those obtained by finding the level crossings of the profiled NLL, and we have validated the frequentist coverage properties of the confidence intervals using pseudo-experiments.

Figure 4 shows the response matrix for an example observable, both with and without ancillary variables. For the purpose of visualization, the response matrices shown are averaged across eras and lepton channels and are normalized so that the values sum to 100% across each column (generator-level bin). Most response matrices are highly diagonal, which can be explained by the close correspondence between the particle- and detector-level definitions of the observables. Compared to these purely particle-level based observables, there is considerably more migration for the observables based on the additional b jets, which are defined via the simulated history at the particle level but only identified with limited accuracy by the DNN at the detector level.

Despite a careful definition of the fiducial phase space at the generator and detector level, a fraction of the events selected at the detector level consists of simulated $\mathrm{t\bar{t}B}$ events that do not pass the corresponding generator-level fiducial phase space definitions. There is an inherent ambiguity on how to treat this contribution, labelled as "out of acceptance" (OOA). While technically part of the $\mathrm{t\bar{t}b\bar{b}}$ process being measured, these events are outside of the fiducial phase space and should not be included in the measured cross sections. Therefore, we treat this OOA contribution as a background and assign to it theoretical systematic uncertainties estimated using the nominal $\mathrm{t\bar{t}b\bar{b}}$ simulation. This OOA contribution constitutes about 40% of selected $\mathrm{t\bar{t}B}$ events in the 6j4b and 7j4b3l regions and reduces to about 20 and 12% in the more inclusive 6j3b3l and 5j3b regions, respectively.

Two distinct mechanisms explain the presence of OOA events in the detector-level selection. First, mismeasurements of the energy or direction of leptons or jets can cause events that are outside the generator-level phase space to pass the detector-level selection. This class of events features a similar topology to the fiducial signal events. Second, the misidentification of light or

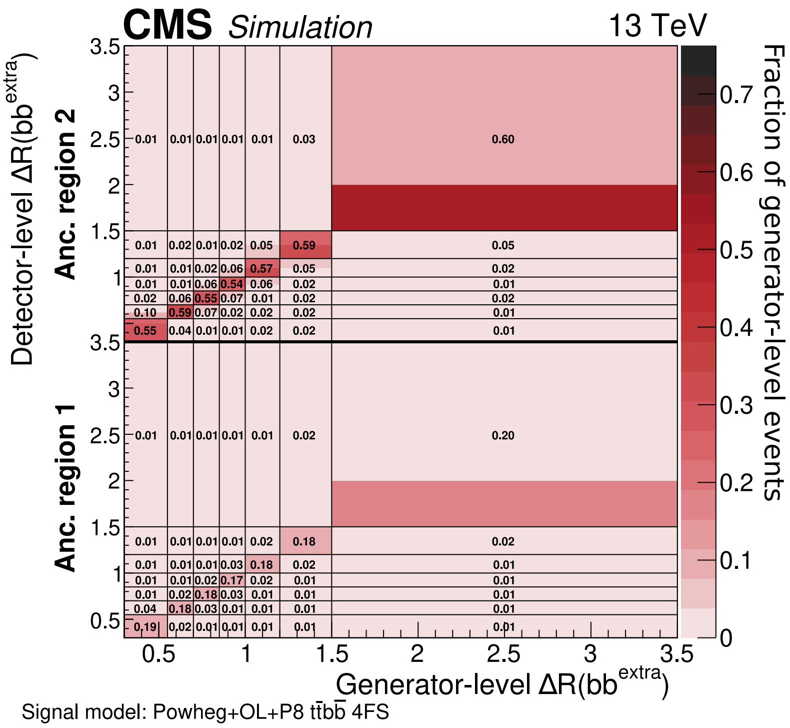


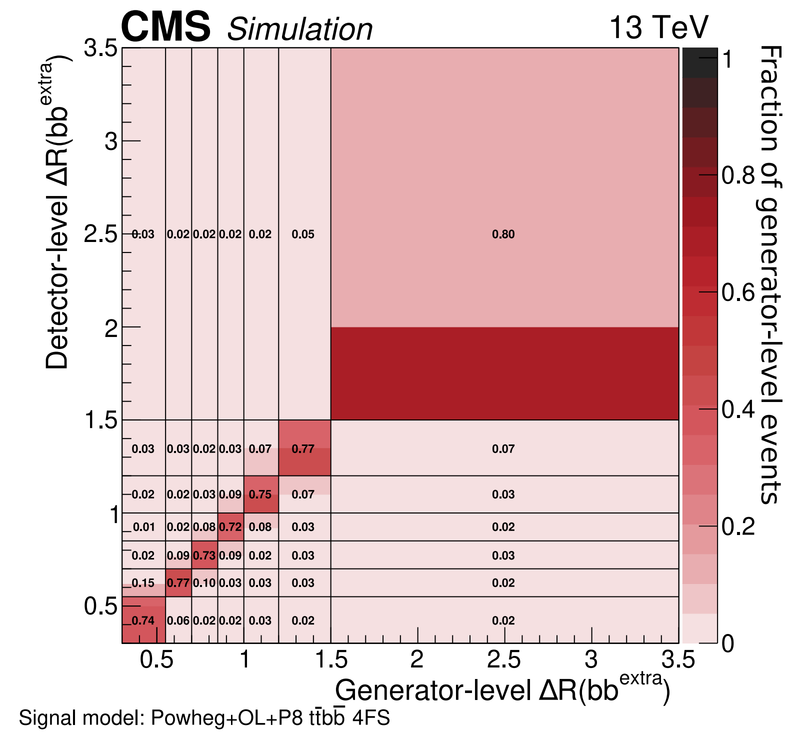


Figure 4: Response matrix for $\Delta R(\mathrm{bb}^{\mathrm{extra}})$ in the $\geq$6 jets: $\geq$4b phase space. The $x$ ($y$) axes show the generator- (detector-)level observables. The upper figure includes the ancillary variable, unrolled on the same axis as the detector-level observable, so that the binning of the detector-level observable, stacked vertically, is repeated twice. For the lower figure, the ancillary variables are projected out to more easily visualize the correspondence between true and reconstructed values. The coloured bins show the finer binning used at reconstructed level (bins split in two), while the numbers show the values one would obtain when using the same binning at the generator and detector level.

c jets as b jets can lead to events with only two or three b jets within the fiducial acceptance to be selected in the regions requiring the presence of three or four b-tagged jets, respectively. This latter mechanism is dominant in the two regions with four b jets, 6j4b and 7j4b3l, and explains why the OOA contribution is larger in these regions, while the fractions of OOA events are reduced in the signal-enriched ancillary regions. However, $t\bar{t}B$ events with only three b jets selected within the generator-level fiducial volume feature a distinct topology from those with four b-tagged jets, since they might either contain a soft (low-$p_T$) or forward (high-$|\eta|$) b jet, or a b jet resulting from the hadronization of a collinear $b\bar{b}$ quark pair. Due to this difference, the two OOA configurations are treated as separate background sources in the 6j4b and 7j4b3l regions and are labelled as $t\bar{t}b$ OOA and $t\bar{t}b\bar{b}$ OOA, respectively, based on the presence of one or two "additional" b jets (in the sense of Section 4.2).

For some of the unfolded distributions, there is no well-defined upper bound on the measured observable. In order to include all observed events in the measurement, while keeping the upper edge of the unfolded distributions at a reasonable value, we normalize the differential cross sections in these bins by the width of the bin as it appears in the histogram, while at the same time including any overflow events, both in the data and in the simulation, into these last bins.

In order to assess the presence of biases due to the choice of the nominal signal model (POWHEG+OL+P8 $t\bar{t}b\bar{b}$ 4FS), bias tests were performed with the POWHEG+P8 $t\bar{t}$ 5FS simulation. These tests consisted of unfolding pseudo-data generated using signal predictions from the POWHEG+P8 $t\bar{t}$ 5FS simulation, while using response matrices constructed from the POWHEG+OL+P8 $t\bar{t}b\bar{b}$ 4FS samples, thereby verifying whether the differences in signal modelling and response matrices resulted in any biases in the measurements. These studies showed that the unfolded results were compatible with the expectations of the POWHEG+P8 $t\bar{t}$ 5FS signal prediction within systematic uncertainties, supporting the validity of using the response matrices of the POWHEG+OL+P8 $t\bar{t}b\bar{b}$ 4FS model for unbiased unfolding.

# 7 Systematic uncertainties

Systematic uncertainties are evaluated by appropriate variations of the signal and background simulations. The uncertainty sources may affect background yields and distributions, as well as the selection efficiency and the kinematic distributions of the signals. These uncertainties are taken into account via nuisance parameters in the likelihood fits.

In certain cases where the statistical uncertainty of a systematic variation is comparable to or larger than the size of the systematic variation or there is significant bin-to-bin variation, the systematic templates need to be smoothed. This is done via a lowess-based smoothing algorithm, which constrains the shape differences between the upward and downward fluctuations if they have a shape effect (smoothing) or, if not, converts them to rate-only effects. If, on the other hand, the systematic uncertainty in question is determined not to have a shape or rate effect, then it is removed altogether.

A summary of all systematic uncertainties is given in Table 4 and in the following sections, grouped by experimental uncertainties in Section 7.1 and modelling uncertainties in Section 7.2.

## 7.1 Experimental uncertainties

**Integrated luminosity:** The integrated luminosities of the data-taking periods are individually measured with uncertainties of 1.2, 2.3, and 2.5% for 2016, 2017, and 2018 data-taking periods, respectively [93–95]. The uncertainty in the integrated luminosity of the combined

Table 4: Summary of the systematic uncertainty sources in the inclusive and differential $t\bar{t}b\bar{b}$ cross section measurements. The first column lists the source of the uncertainty. The second (third) column indicates the treatment of correlations of the uncertainties between different data-taking periods (processes), where ✓ means fully correlated, ∼ means partially correlated (i.e. contains sub-sources that are either fully correlated or uncorrelated), × means uncorrelated, and —means not applicable.

| | Source | Corr. (period) | Corr. (process) |
|---|---|---|---|
| Experimental | Integrated luminosity | ∼ | ✓ |
| | Pileup reweighting | ✓ | ✓ |
| | Electron reconstruction and identification | ✓ | ✓ |
| | Muon reconstruction and identification | ✓ | ✓ |
| | Trigger efficiencies | × | ✓ |
| | L1 prefiring | ✓ | ✓ |
| | JES | ∼ | ✓ |
| | JER | × | ✓ |
| | b tagging | ∼ | ✓ |
| Theoretical | $\mu_R$ scale | ✓ | ∼ |
| | $\mu_F$ scale | ✓ | ∼ |
| | Top quark $p_T$ modelling | ✓ | ✓ |
| | PDF | ✓ | ✓ |
| | PS scales: ISR | ✓ | × |
| | PS scales: FSR | ✓ | × |
| | ME-PS matching ($h_{damp}$) | ✓ | ∼ |
| | Underlying-event tune | ✓ | ✓ |
| | Colour reconnection | ✓ | ✓ |
| | b quark fragmentation | ✓ | ✓ |
| | Inclusive $t\bar{t}C$ cross section | ✓ | — |

data set is 1.6% when taking into account the correlations between the periods.

**Pileup reweighting:** The prediction of the number of pileup interactions in simulation is performed by assuming a total inelastic pp cross section of 69.2 mb. Changes in the assumed pileup multiplicity are estimated by varying the total inelastic cross section by ±4.6% [76]. This uncertainty is treated as fully correlated between the data-taking periods.

**Lepton reconstruction and identification:** Separate uncertainties are assigned to the corrections applied to the reconstruction and identification efficiencies for electrons in the simulation. Similarly, the muon tracking, identification, and isolation efficiencies are estimated and the associated uncertainties are propagated to signal and background distributions used in the fits. These uncertainties are taken to be fully correlated across the data-taking periods.

**Trigger efficiencies:** The trigger efficiency scale factors are varied within their uncertainties, separately for electron and muon triggers and for each data-taking period.

**L1 prefiring:** During the 2016–2017 data-taking periods, a gradual shift in the timing of the inputs of the ECAL L1 trigger in the forward endcap region ($|\eta| > 2.4$) led to a specific inefficiency, known as "prefiring". A similar effect is present for the muon system due to its limited time resolution, most pronounced in 2016, but also impacting data collected in 2017–2018. Corrections of this effect are applied to simulated events, and 20% of the corrections are assigned as the associated uncertainties.

**Jet energy scale and resolution:** Uncertainties in the determination of the JES are taken into account by shifting the jet momenta in the simulation up and down, separately for several sources of uncertainty such as the overall energy scale, differences in flavour response, and residual differences between energy scale measurements. Some of these sources are treated separately per data-taking period, while some are correlated for all periods. Uncertainties in the JER are evaluated by increasing or decreasing the variation of jet energies between the reconstructed and particle levels, or by smearing the measured jet energy in case no matching particle-level jet could be found [79]. This uncertainty is uncorrelated between data-taking periods.

**b tagging:** Differences in the b tagging efficiency between data and simulation are corrected by applying correction factors to simulated events, derived as a function of jet $p_{\mathrm{T}}$ and $|\eta|$. Systematic uncertainties are considered separately for light jets and b/c jets. For b and c jets, nine different sources of uncertainties from the measurements of the correction factors are considered [80]. Included amongst these uncertainties are effects from variations in b fragmentation and gluon to $\mathrm{b\bar{b}}$ splitting. Scale factors and their uncertainties on the b tagging efficiency and mistag rates are split based on the flavour of the intiating quark, but do not discriminate based on the origin of the b quark as coming, for example, from a gluon splitting or top quark decay. Statistical uncertainties in the scale factor measurements are treated independently for the medium and tight b tagging working points, and for the four data-taking periods. All other sources of uncertainties are correlated between the data-taking periods and the b tagging working points.

## 7.2 Modelling uncertainties

This analysis is affected by uncertainties in the modelling of the background processes and the migration matrices linking the measured particle-level observables with the detector-level observables. Variations applied to the signal process are defined such that the predicted yields at generator level remain constant for all values of the corresponding nuisance parameters, independently for each bin of the generator-level distributions. This procedure ensures that the modelling uncertainties only have an effect on the signal selection efficiency, due to shape variations within each generator-level bin. All modelling uncertainties are correlated between the data-taking eras. Some uncertainties are not correlated between processes. In the phase space regions where the OOA contribution is separated into $\mathrm{t\bar{t}b}$ OOA and $\mathrm{t\bar{t}b\bar{b}}$ OOA contributions, the two components can have different correlations with the signal. However, by repeating the fits with different correlation assumptions for the signal and the OOA processes, it has been verified that the results were not sensitive to this choice.

**Renormalization and factorization scales:** Uncertainties covering the choice of $\mu_{\mathrm{R}}$ and $\mu_{\mathrm{F}}$ scales in the ME generators are considered by shifting the scales independently up and down by a factor of two. These uncertainties are treated separately for each process but correlated for $\mathrm{t\bar{t}}$+light and $\mathrm{t\bar{t}C}$, as these contributions are estimated using the same POWHEG+P8 $\mathrm{t\bar{t}}$ 5FS simulation. Where separate $\mathrm{t\bar{t}b\bar{b}}$ OOA and $\mathrm{t\bar{t}b}$ OOA contributions are considered, the uncertainty in the former contribution is correlated with the signal while the latter taken as uncorrelated. For the $\mathrm{t\bar{t}B}$ OOA processes, shape and normalization effects of the $\mu_{\mathrm{R}}$ scale are decorrelated, and both are uncorrelated with the signal.

**Top quark $p_T$ modelling:** Because of discrepancies between the observed and simulated $p_T$ spectrum of top quarks in $t\bar{t}$ events, simulated events are reweighted to match the top quark $p_T$ distribution predicted at NNLO [96]. This procedure improves the agreement of the simulated predictions with the data. We consider as uncertainty in this reweighting the full effect of the reweighting itself. The uncertainty is applied to all $t\bar{t}$ subprocesses (including the signal and all OOA processes), but not to single top quark or $t\bar{t}X$ production.

**PDF:** The uncertainties in the PDFs are evaluated by using replicas of the NNPDF set [69]. For the 4FS set used for the $t\bar{t}b\bar{b}$ signal simulation, uncertainties are estimated using the root-mean-square of all residuals in the predictions obtained using the PDF replicas, as these are defined by sampling from the covariance matrix of the PDF fit. For the 5FS set used in all the other simulated samples, the replicas correspond to the leading eigenvectors of the PDF fit covariance matrix, and the uncertainties are obtained as the quadratic sum of the residuals in the predictions across the replicas. This uncertainty is treated as correlated for all processes. An additional uncertainty from the value of the strong coupling constant, $\alpha_S$, used in the PDF, is also included.

**PS scales:** The uncertainty from the choice of scale at which the strong coupling constant is evaluated in the PS is estimated by varying the scale up and down by a factor of two, independently for initial-state radiation (ISR) and final state radiation (FSR). These uncertainties are considered as uncorrelated for all processes. Accordingly, the $t\bar{t}B$ OOA processes is considered uncorrelated with the signal. Where separate $t\bar{t}b\bar{b}$ OOA and $t\bar{t}b$ OOA contributions are considered, the $t\bar{t}b\bar{b}$ OOA contribution is correlated with the signal, and $t\bar{t}b$ OOA is treated separately.

**ME-PS matching ($h_{damp}$):** In the POWHEG generator, the scale that separates the phase space of the first QCD emission into soft and hard parts is controlled by the $h_{damp}$ parameter. The nominal value of the $h_{damp}$ parameter in the CP5 tune [70] is $h_{damp} = 1.379 m_t$ and the uncertainties are estimated with varied values of $h_{damp} = 2.305 m_t$ and $0.874 m_t$ for the $t\bar{t}$ and $t\bar{t}b\bar{b}$ samples. This uncertainty is treated as correlated for $t\bar{t}$+light and $t\bar{t}C$ processes but decorrelated from the $t\bar{t}B$ contributions. This uncertainty is only applied to $t\bar{t}$ subprocesses, which does not include single top or $t\bar{t}X$ production.

**Underlying event tune:** The simulation of the underlying event is based on the CP5 tune of the PYTHIA event generator, and uncertainties are estimated via varied tune settings [70], applied to the $t\bar{t}$ samples. This uncertainty is only applied to $t\bar{t}B$, $t\bar{t}$+light, and $t\bar{t}C$ processes and is treated as correlated.

**Colour reconnection:** The default colour reconnection model in the PYTHIA PS simulation is replaced by three alternative models [97, 98]. These uncertainties are treated as correlated for $t\bar{t}B$, $t\bar{t}$+light, and $t\bar{t}C$ processes. This uncertainty is only applied to $t\bar{t}$ subprocesses, which does not include single top or $t\bar{t}X$ production.

**b quark fragmentation:** We include a theoretical uncertainty for the fragmentation of the b quarks into hadrons. The fragmentation of the initiating parton into observable hadrons is subject to modelling uncertainties. We estimate this effect by varying simultaneously the generator- and detector-level momenta of b jets up and down by 1% in the simulated samples. This is consistent with the effect from reasonable variations of the fragmentation functions on the b jet $p_T$ distribution in Ref. [99]. Residual effects on the efficiency to identify b jets, due to a possible mismodelling of the fragmentation of b quarks, are already accounted for by the calibration of the b tagging efficiency in the simulation.

**Inclusive $t\bar{t}C$ cross section:** For the $t\bar{t}C$ process an additional 20% normalization uncertainty is applied, corresponding to the precision of the inclusive $t\bar{t}C$ cross section measurement by CMS [45]. This measurement found that the $t\bar{t}C$ cross section agreed with the POWHEG+P8 $t\bar{t}$ 5FS prediction.

No additional cross section uncertainties are considered for the backgrounds since the uncertainties listed above already result in variations in the predicted event yields that cover the uncertainties in the theoretical cross sections used to normalize the background contributions.

The finite size of the simulated MC samples is taken into account as a systematic uncertainty, following a method similar to the one proposed by Barlow and Beeston [100, 101]. For every bin of the detector-level distributions, a single Gaussian-constrained nuisance parameter varies the predicted yields, summed over all processes including the signal, within their statistical uncertainty.

The impact of a group of $k$ nuisance parameters $\alpha_{n_1} \ldots \alpha_{n_k}$ on the parameter of interest $p$ is computed as

$$I_p = \sqrt{\sum_{i,j=1}^{k} C_{pn_i} \widetilde{C}^{-1}_{n_i n_j} C_{n_j p}}, \tag{6}$$

where $C$ is the covariance matrix between all parameters, and $\widetilde{C}$ is the covariance matrix restricted to the parameters $n_1 \ldots n_k$. In this way, the effects of a set of nuisance parameters are combined while taking into account their correlation in the fit. The total systematic uncertainties are calculated by considering all nuisance parameters in the sum in Eq. (6), and the statistical uncertainties as the difference in quadrature between the total uncertainties and the total systematic uncertainties.

Table 5 shows the contributions of various sources of uncertainties to the total uncertainties in the inclusive cross sections, obtained from the combined impacts $I_{\mu_{\text{fid}}}$ on the parameters scaling the inclusive cross sections in the fits of the representative observables discussed in Section 8.1. For these fits, the contributions of the 20 single nuisance parameters with the largest contributions to the uncertainty in the inclusive cross section can be found in Appendix A. Figure 5 shows the effect of the sources of uncertainty on the normalized differential cross section measurements for the $H_T$ of b jets in the 5j3b phase space. For the four representative observables, corresponding figures are shown in Appendix B. The uncertainties in the inclusive cross sections are dominated by systematic sources, while the precision in the differential measurements is mainly limited by the statistical uncertainty in the data since the rate-based effects of many systematic uncertainties cancel out in the ratio between the absolute differential cross sections and the inclusive cross sections. The leading systematic uncertainties originate from the calibration of the b tagging and of the JES, the choice of $\mu_R$ scale in the signal $t\bar{t}b\bar{b}$ and background $t\bar{t}$ processes, and, for the differential measurements only, the finite number of simulated events. Previous measurements of the inclusive $t\bar{t}b\bar{b}$ cross section by the ATLAS [39] and CMS [42–44] Collaborations had the same leading sources of systematic uncertainty.

The nuisance parameter associated with the normalization of the $t\bar{t}C$ process is not found to be constrained significantly beyond its prefit expectation and also shows no significant deviation from its expected value, which is consistent with the results of Ref. [45]. The correlation of that nuisance parameter with the inclusive $t\bar{t}b\bar{b}$ cross section in the fits to different observables is below 5 (20)% in the phase space regions with at least three (four) b jets.

Table 5: Contributions of the considered sources of uncertainty to the total uncertainty in the inclusive cross sections. For each group of uncertainty sources, the impacts of the corresponding nuisance parameters on the total cross section are combined, taking into account their correlation in the fit. The numbers show relative uncertainties (in %). The statistical uncertainty is obtained as the difference, in quadrature, between the total uncertainty and the sum of all systematic uncertainties.

| | Relative uncertainty (%) | | | |
|---|---|---|---|---|
| Uncertainty source | 5j3b | 6j3b3l | 6j4b | 7j4b3l |
| Integrated luminosity | 1.6 | 1.6 | 2.0 | 1.8 |
| Pileup reweighting | 0.2 | 0.8 | 0.4 | 0.5 |
| Lepton and trigger | 1.1 | 0.9 | 1.9 | 1.8 |
| JES, JER | 2.1 | 1.6 | 3.5 | 5.7 |
| b tagging | 4.5 | 3.9 | 7.0 | 9.1 |
| $\mu_R$ and $\mu_F$ scales | 2.8 | 6.8 | 8.2 | 12 |
| Top quark $p_T$ modelling | 0.3 | 1.0 | 0.6 | 1.3 |
| PDF | 0.2 | 0.7 | 1.0 | 1.9 |
| PS scales | 2.8 | 2.7 | 2.4 | 1.5 |
| ME-PS matching ($h_{damp}$) | 0.4 | 0.9 | 1.3 | 2.8 |
| Underlying event | 0.4 | $<$0.1 | 0.4 | 0.4 |
| Colour reconnection | 1.1 | 1.5 | 1.9 | 4.5 |
| b quark fragmentation | 0.3 | 0.4 | 0.4 | 0.4 |
| Inclusive $t\bar{t}C$ cross section | 0.5 | 0.3 | 1.9 | 2.6 |
| MC statistical | 0.8 | 1.6 | 2.4 | 2.8 |
| Total systematic uncertainty | 6.0 | 8.7 | 13 | 17 |
| Statistical uncertainty | 0.6 | 1.2 | 2.2 | 3.3 |
| Total uncertainty | 6.0 | 8.8 | 13 | 17 |

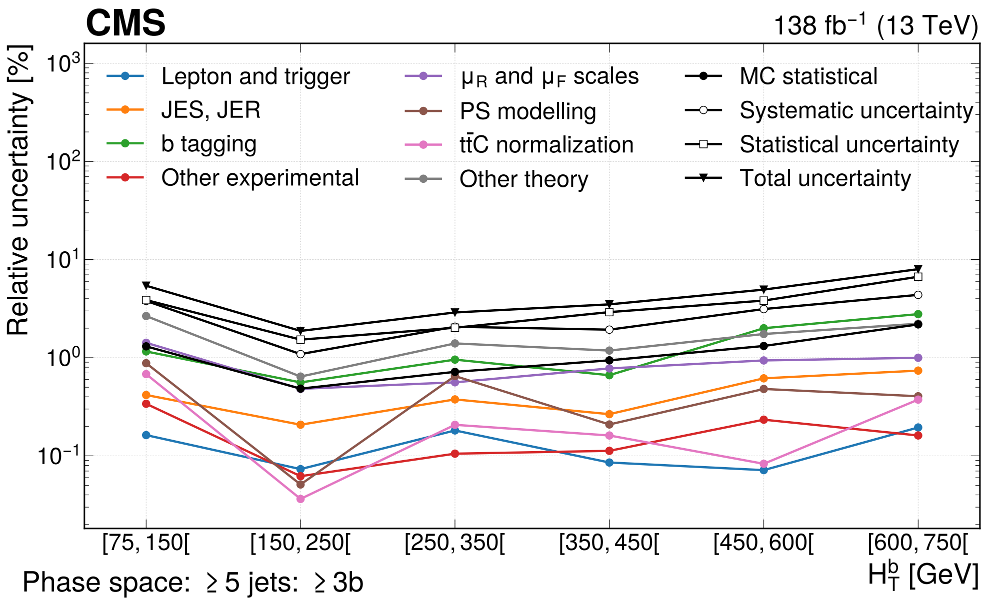


Figure 5: Effect of the considered sources of uncertainties on the measurement of the normalized differential cross section of the $H_T$ of b jets in the ≥5 jets: ≥3b phase space, obtained by combining the impacts of associated nuisance parameters according to Eq. (2). The ordering of the various sources is similar for other observables and in the other phase space regions. The last bin of the distribution is not shown, since it has no associated parameter of interest but is constrained by the other bins as described in Section 6.3. The category "other theory" includes b quark fragmentation, top quark $p_T$ modelling, PDF, $h_{damp}$, colour reconnection, and underlying event uncertainties. The category "other experimental" includes pileup and the integrated luminosity uncertainties.

# 8 Results

The results are obtained with the statistical procedures described in Section 6.3. Inclusive and differential cross section results are presented in Sections 8.1 and 8.2, respectively.

## 8.1 Inclusive cross sections

The inclusive $t\bar{t}b\bar{b}$ cross sections, measured in each of the fiducial phase space regions, are shown in Fig. 6 and listed in Table 6, along with the predictions obtained from the $t\bar{t}b\bar{b}$ generator setups described in Section 3. In each phase space, the representative observable for which we report the measured inclusive cross section is that for which the measured value is closest to the mean of all measured inclusive cross sections in order to provide a value representative of the ensemble of measurements. These observables are $|\eta(b_3)|$ in the 5j3b phase space, $H_T^{light}$ in the 6j3b3l phase space, $|\eta(b_2^{extra})|$ in the 6j4b phase space, and $|\Delta\phi(lj_1^{extra}, b_{soft})|$ in the 7j4b3l phase space. Their observed distributions at the detector level, combined for both lepton channels and all data-taking periods, are shown in Figs. 7 and 8 after the fits to data. The correlations between the parameters $\vec{\mu}$ in the fit of $|\eta(b_3)|$ in the 5j3b phase space are shown in Fig. 9. For the other representative observables, corresponding figures are shown in Appendix C. The inclusive cross section results for all observables are provided in the HEPData record for this analysis [46].

The measured cross sections in all phase space regions are larger than the theoretical predictions, as was also observed in previous measurements of the inclusive $t\bar{t}b\bar{b}$ cross section (with

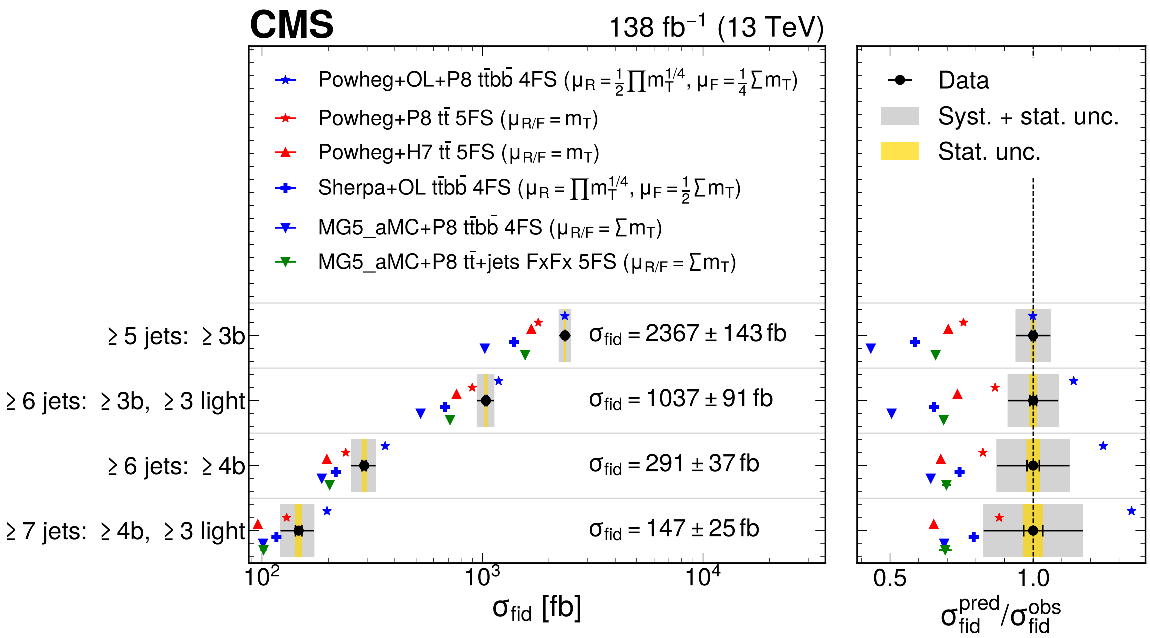


Figure 6: Measured inclusive cross sections for each considered phase space, compared to predictions from different $t\bar{t}b\bar{b}$ simulation approaches shown as coloured symbols. The predictions include uncertainties (horizontal bars) due to the limited number of simulated events. The blue colour is reserved for models using massive b quarks and NLO QCD $t\bar{t}b\bar{b}$ MEs, while red is used for the inclusive $t\bar{t}$ generators at NLO in QCD with massless b quarks. The right panel shows the ratios between the predicted and measured cross sections, with the black bars showing the relative uncertainties in the measurements.

Table 6: Measured and predicted inclusive cross sections in the four considered phase space regions (in fb).

| Fiducial phase space | 5j3b | 6j3b3l | 6j4b | 7j4b3l |
|---|---|---|---|---|
| Measured cross section | 2367 ± 142 (syst) ± 14 (stat) | 1037 ± 90 (syst) ± 12 (stat) | 291 ± 36 (syst) ± 6 (stat) | 147 ± 24 (syst) ± 5 (stat) |
| POWHEG+OL+P8 $t\bar{t}b\bar{b}$ 4FS | 2361 | 1183 | 361 | 197 |
| $\mu_R$ variation | +1161/−737 | +826/−433 | +183/−113 | +121/−67 |
| $\mu_F$ variation | +126 /−100 | +97 /−78 | +23 /−18 | +16 /−13 |
| POWHEG+P8 $t\bar{t}$ 5FS | 1791 | 899 | 240 | 129 |
| POWHEG+H7 $t\bar{t}$ 5FS | 1665 | 762 | 197 | 95 |
| SHERPA+OL $t\bar{t}b\bar{b}$ 4FS | 1391 | 677 | 216 | 116 |
| MG5_aMC+P8 $t\bar{t}b\bar{b}$ 4FS | 1024 | 524 | 187 | 101 |
| MG5_aMC+P8 $t\bar{t}$+jets FxFx 5FS | 1560 | 712 | 203 | 101 |

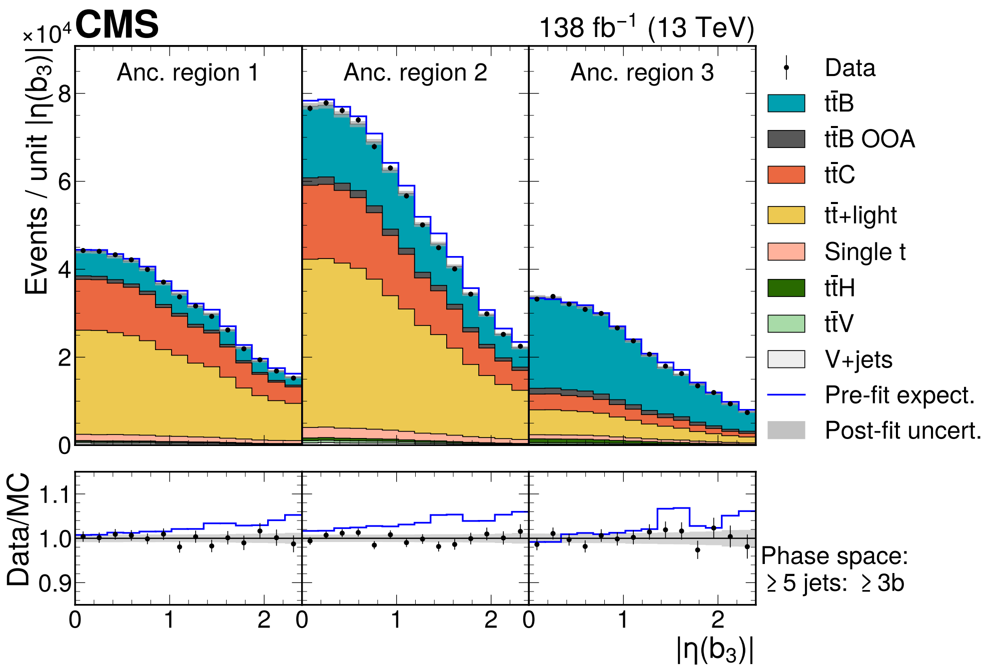


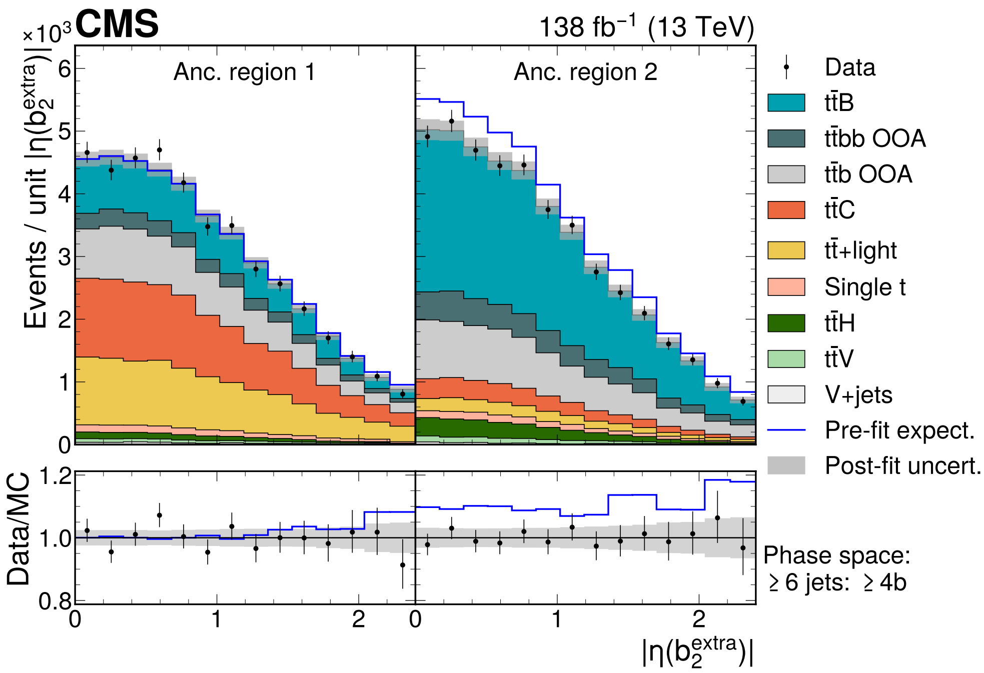


Figure 7: The $|\eta|$ of the third-hardest b jet in $p_{\mathrm{T}}$ ($|\eta(\mathrm{b}_3)|$) in the $\geq$5 jets: $\geq$3b phase space (upper) and the $|\eta|$ of the subleading additional b jet ($|\eta(\mathrm{b}_2^{\mathrm{extra}})|$) in the $\geq$6 jets: $\geq$4b phase space (lower) after the fit to data, shown for both lepton channels and all data periods combined. The distributions are shown separately for each ancillary region, as defined in Section 6.1. In the $\geq$5 jets: $\geq$3b ($\geq$6 jets: $\geq$4b ) phase space the ancillary regions are defined as $\leq$2, 2, and $\geq$3 ($\leq$3 and $\geq$3) tight b-tagged jets. The shaded bands include all uncertainties described in Section 7 after profiling the nuisance parameters in the fit, estimated by sampling the predicted yields from the fit covariance matrix. The blue line shows the sum of the predicted yields for all processes before the fit to data, using the nominal $\mathrm{t\bar{t}b\bar{b}}$ samples and its corresponding cross section for the signal. In the ratio panel the expected yields before the fit to data are shown relative to the predicted yields after the fit to data. The last bins contain the overflow.

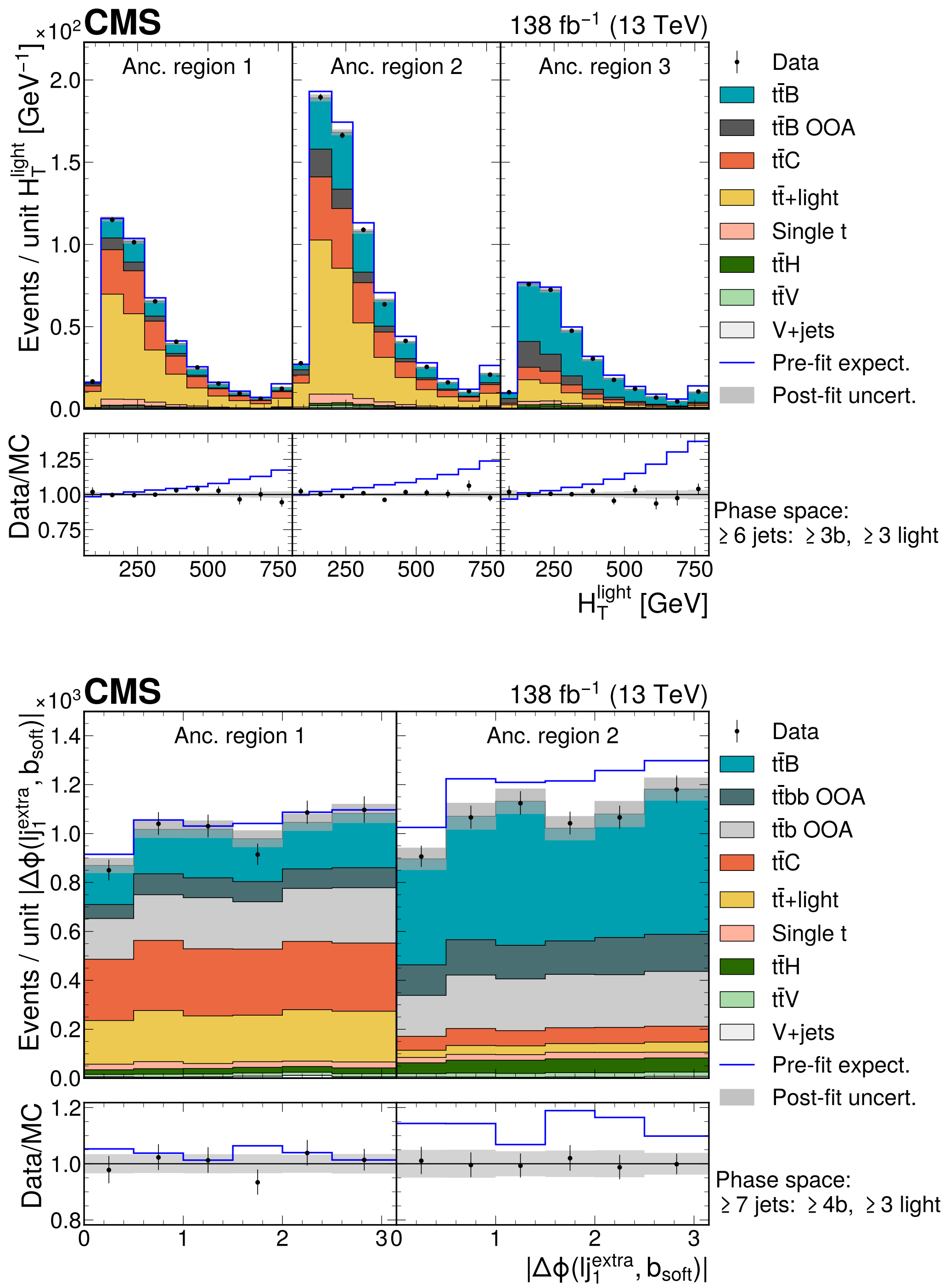


Figure 8: The $H_T$ of all light jets in the $\geq$6 jets: $\geq$3b, $\geq$3 light phase space (upper) and the azimuthal angle between the hardest remaining light jet and the softest b jet ($|\Delta\phi(\mathrm{lj}_1^{\mathrm{extra}}, \mathrm{b}_{\mathrm{soft}})|$) in the $\geq$7 jets: $\geq$4b, $\geq$3 light phase space (lower) after the fit to data, shown for both lepton channels and all data periods combined. The distributions are shown separately for each ancillary region, as defined in Section 6.1. In the $\geq$6 jets: $\geq$3b, $\geq$3 light ($\geq$7 jets: $\geq$4b, $\geq$3 light) phase space the ancillary regions are defined as $\leq$2, 2, and $\geq$3 ($\leq$3 and $\geq$3) tight b-tagged jets. The shaded bands include all uncertainties described in Section 7 after profiling the nuisance parameters in the fit, estimated by sampling the predicted yields from the fit covariance matrix. The blue line shows the sum of the predicted yields for all processes before the fit to data, using the nominal $\mathrm{t\bar{t}b\bar{b}}$ samples and its corresponding cross section for the signal. In the ratio panel the expected yields before the fit to data are shown relative to the predicted yields after the fit to data. The last bins contain the overflow.

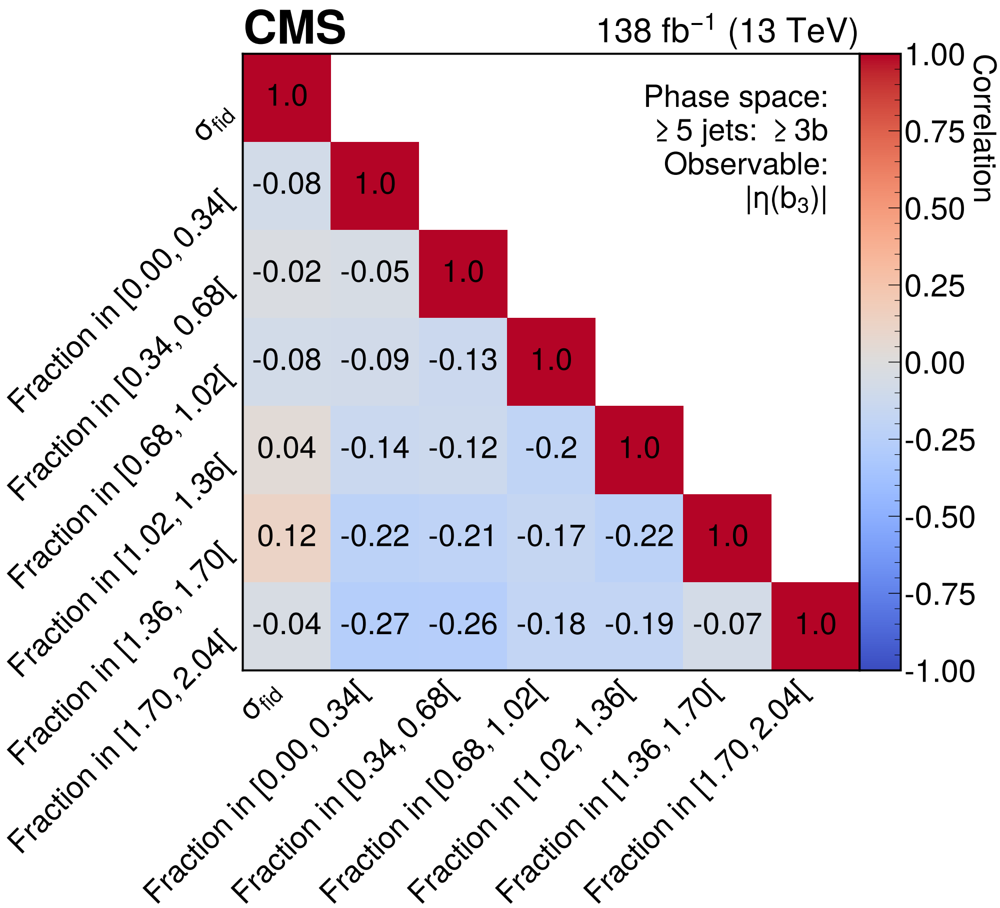


Figure 9: Correlations between the parameters of interest $\vec{\mu}$ in the fit for $|\eta(b_3)|$ in the $\geq$5 jets: $\geq$3b phase space.

somewhat different fiducial definitions) by the CMS [42–44] and ATLAS [39] Collaborations, with the notable exception of the POWHEG+OL+P8 $t\bar{t}b\bar{b}$ 4FS generator setup. The choice of reduced central $\mu_R$ and $\mu_F$ scales in the POWHEG+OL+P8 $t\bar{t}b\bar{b}$ 4FS sample, justified by the previous measurements and by studies of fixed-order NLO QCD corrections to the $t\bar{t}b\bar{b}j$ process [1], results in significantly larger cross sections in all phase space regions. This prediction agrees well with the measurement in the 5j3b phase space, but overestimates the cross section by 10–35% in the other phase space regions. Nevertheless, the POWHEG+OL+P8 $t\bar{t}b\bar{b}$ 4FS predictions agree with the measurements when considering their $\mu_R$ scale uncertainties of about 50%, estimated by varying the $\mu_R$ scale by a factor of two. When considering $\mu_R$ scale uncertainties in both the ME and in the PS, the POWHEG+P8 $t\bar{t}$ 5FS predictions agree with the measurements in the phase space regions targeting additional light radiation in $t\bar{t}b$ and $t\bar{t}b\bar{b}$ events.

## 8.2 Normalized differential cross sections

The normalized differential cross section is measured in four different fiducial phase space regions for 29 observables that use exclusively stable-particle level information without reference to any simulated event history, and eight observables targeting explicitly the b jets that do not originate from decaying top quarks. For each observable, customized bin sizes are chosen, depending on the resolution of the observables and the statistical uncertainty in the measured event yields.

The resulting normalized differential cross sections are shown in Fig. 10 for the observables of the 5j3b phase space, in Figs. 11–13 for the observables of the 6j4b phase space, for the observables targeting the b jets that do not originate from decaying top quarks in Figs. 14 and 15, and finally in Fig. 16 for the observables of the 6j3b3l and 7j4b3l phase space regions. The measurements are compared to six cross section predictions of the $\mathrm{t\bar{t}b\bar{b}}$ process, obtained at the particle level, produced with the different combinations of event generators and PSs introduced in Section 3. The various predictions are shown as symbols distinguished by colour and shape. It should be noted that predictions from SHERPA+OL $\mathrm{t\bar{t}b\bar{b}}$ 4FS cannot be compared to the observables related to the additional b jets, since that generator does not provide the necessary information (parton-level top quarks) to assign b jets to the decaying top quarks.

The compatibility of the predictions with the unfolded data in each of the phase space regions is quantified using $\chi^2$ tests, which are converted to $z$ scores [102], which quantify the $p$-value in terms of the equivalent number of standard deviations by which each theoretical prediction differs from the mean of a normal distribution centered at the normalized cross-section measurements. These are shown in Fig. 17 and as tables in Appendix E. The $\chi^2$ test statistics are computed using the predicted and measured normalized cross sections, as well as the estimated covariance between the bins of the unfolded distributions, but do not include the inclusive cross sections. No uncertainties in the predictions are considered in these tests. Varying levels of agreement between the predicted and measured distributions are observed, whereby no event generator setup describes all observables well since they each result in $z \geq 2$ for several observables.

In the 5j3b phase space (Fig. 10), with a few exceptions, none of the distributions are described well by any of the considered generator setups, quantified by the $z$ scores without any consideration of the uncertainties on the predictions. Most generator setups predict a higher number of inclusive jets than what is observed, with the exception of POWHEG+H7 $\mathrm{t\bar{t}}$ 5FS and MG5_aMC+P8 $\mathrm{t\bar{t}}$+jets FxFx 5FS showing better agreement. The b jet multiplicity distribution, which can be interpreted as a measure of the ratio between the cross sections of $\mathrm{t\bar{t}b\bar{b}}$ and $\mathrm{t\bar{t}b}$, is only well described by the inclusive POWHEG $\mathrm{t\bar{t}}$ simulations matched to PYTHIA or HERWIG. The NLO $\mathrm{t\bar{t}b\bar{b}}$ simulations all predict a higher ratio of events with at least four b jets over exactly three b jets. The $H_{\mathrm{T}}^{\mathrm{j}}$ distribution shows a significant trend towards higher values than what is observed in data for MG5_aMC+P8 $\mathrm{t\bar{t}b\bar{b}}$ 4FS, and towards lower values for POWHEG+H7 $\mathrm{t\bar{t}}$ 5FS, while the other generator setups better describe the distribution. The $H_{\mathrm{T}}^{\mathrm{b}}$ distribution shows a trend towards lower values in data compared to most predictions, with the exception of POWHEG+H7 $\mathrm{t\bar{t}}$ 5FS and SHERPA+OL $\mathrm{t\bar{t}b\bar{b}}$ 4FS. The predictions of the different simulations for $|\eta(\mathrm{b}_3)|$ are all very similar to each other and have $z$ scores around 2. All generator setups predict somewhat larger values of the $p_{\mathrm{T}}$ of the third b jet.

Observables which are not fully described by the NLO $\mathrm{t\bar{t}b\bar{b}}$ ME, such as observables related to the radiation of light jets, are expected to have strong dependencies on the $\mu_{\mathrm{R}}$ and $\mu_{\mathrm{F}}$ scale choices when described with a NLO $\mathrm{t\bar{t}b\bar{b}}$ ME simulation setup [2]. Hence, in Appendix D, the measured normalized differential cross sections of the $N_{\mathrm{jets}}$ and $H_{\mathrm{T}}^{\mathrm{j}}$ observables are compared with alternative $\mu_{\mathrm{R}}$ and $\mu_{\mathrm{F}}$ scale choices of the POWHEG+OL+P8 $\mathrm{t\bar{t}b\bar{b}}$ 4FS simulation approach. These comparisons show that increased $\mu_{\mathrm{R}}$ and $\mu_{\mathrm{F}}$ scales relative to the nominal scale choices (see Table 1) tend to better describe these observables.

The agreement between data and predictions is generally better in the 6j4b phase space (Figs. 11–13), at least in part due to the larger uncertainties in the measurements. With a few exceptions, the predictions between the various generator setups are also closer to each other than in the 5j3b phase space. $H_{\mathrm{T}}^{\mathrm{b}}$ and $H_{\mathrm{T}}^{\mathrm{j}}$ are generally modelled well, while for the POWHEG+H7

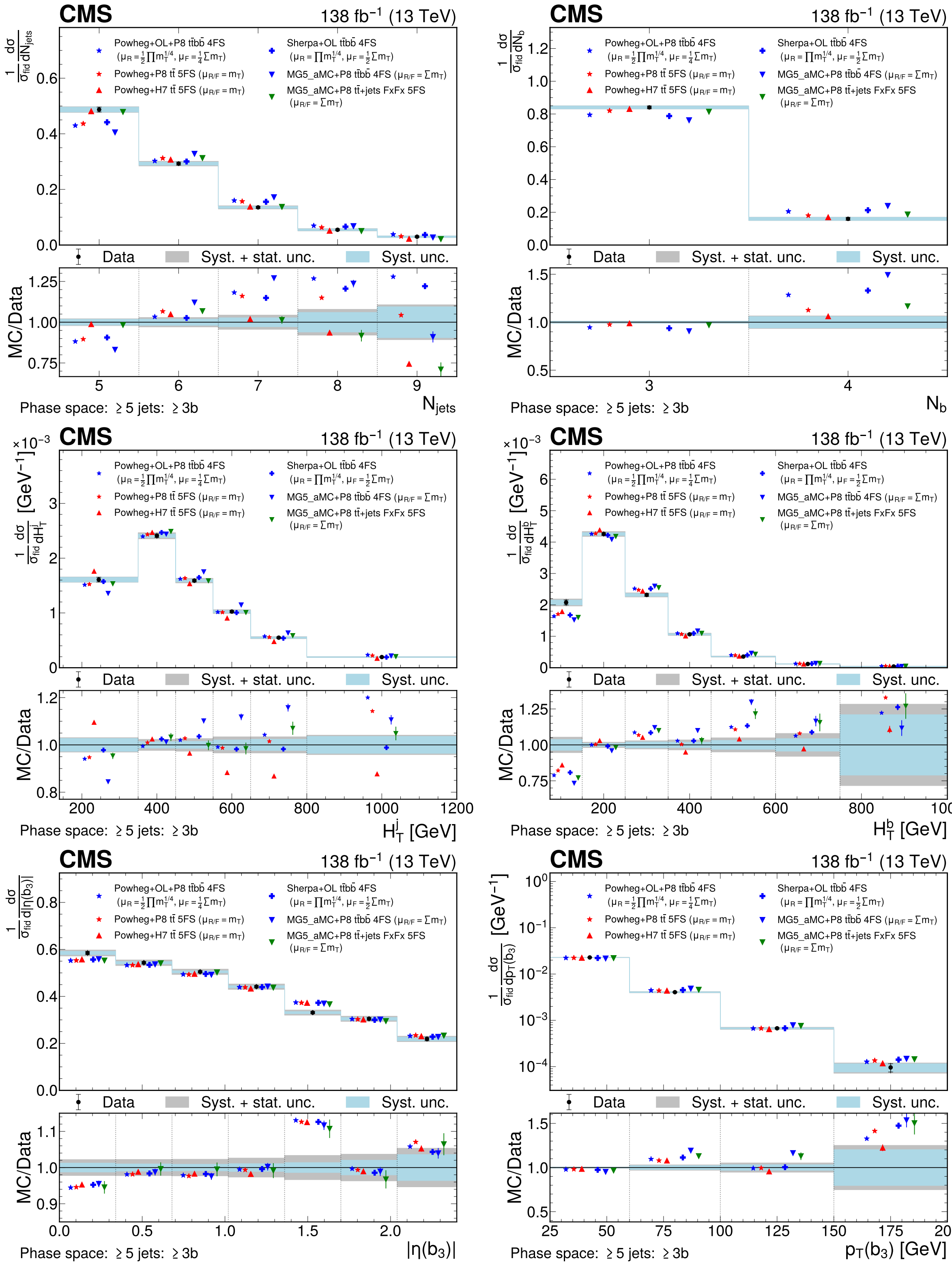


Figure 10: Predicted and observed normalized differential cross sections in the $\geq$5 jets: $\geq$3b fiducial phase space, for the inclusive jet multiplicity (upper left), the b jet multiplicity (upper right), the inclusive jet $H_{\mathrm{T}}$ (middle left, $H_{\mathrm{T}}^{\mathrm{j}}$), the $H_{\mathrm{T}}$ of b jets (middle right, $H_{\mathrm{T}}^{\mathrm{b}}$), the $|\eta|$ of the third b jet (lower left), and the $p_{\mathrm{T}}$ of the third b jet (lower right). The data are represented by points, with inner (outer) vertical bars indicating the systematic (total) uncertainties, also represented as blue (grey) bands. Cross section prediction obtained at the particle level from different simulation approaches are shown, including their statistical uncertainties, as coloured symbols with different shapes. For $N_{\text{jets}}$, $N_{\mathrm{b}}$, $H_{\mathrm{T}}^{\mathrm{j}}$, $H_{\mathrm{T}}^{\mathrm{b}}$, and $p_{\mathrm{T}}(\mathrm{b}_3)$, the last bins contain the overflow.

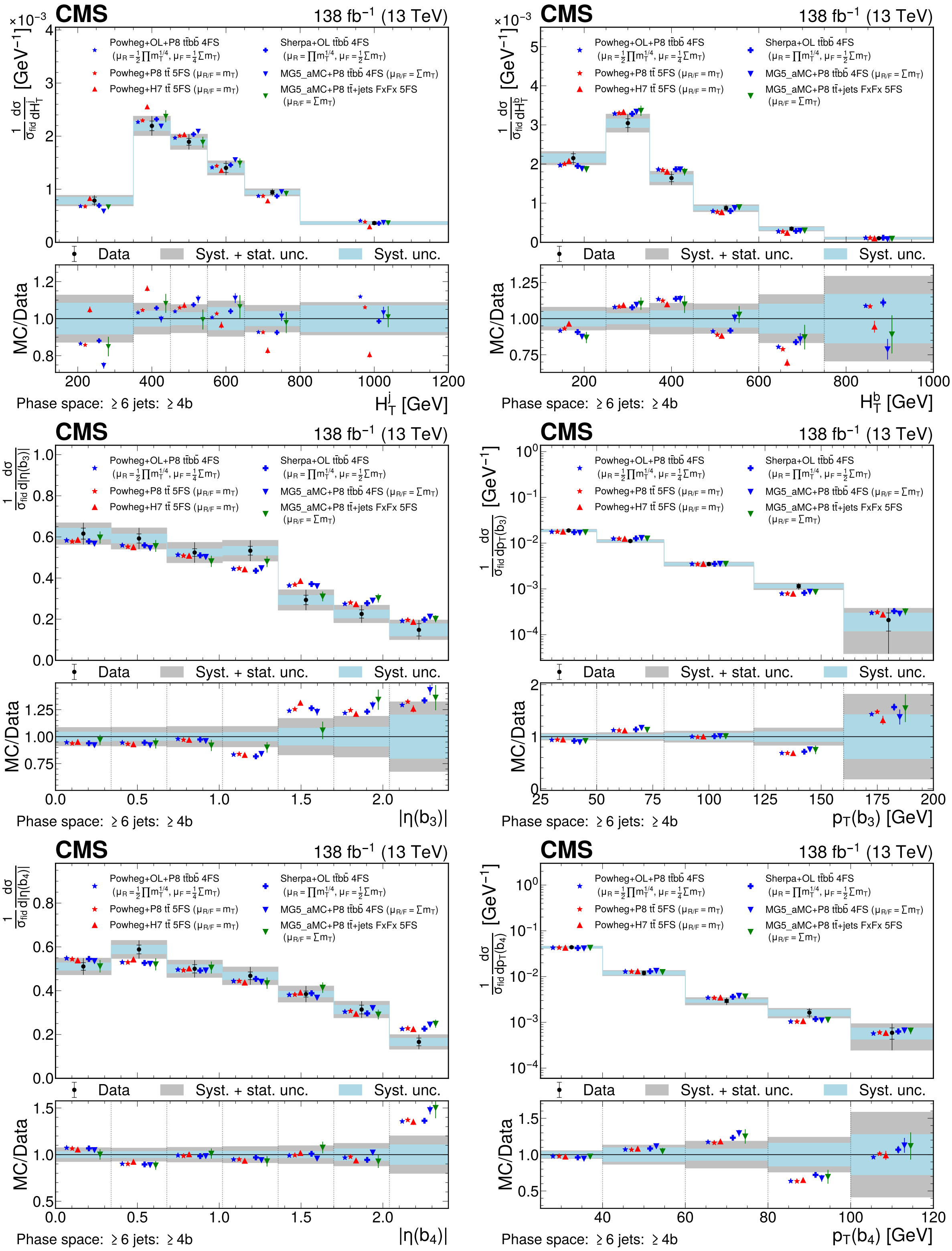


Figure 11: Predicted and observed normalized differential cross sections in the $\geq$6 jets: $\geq$4b fiducial phase space, for the inclusive jet $H_T$ (upper left), the $H_T$ of b jets (upper right), the $|\eta|$ of the third b jet (middle left), the $p_T$ of the third b jet (middle right), the $|\eta|$ of the fourth b jet (lower left), and the $p_T$ of the fourth b jet (lower right). The data are represented by points, with inner (outer) vertical bars indicating the systematic (total) uncertainties, also represented as blue (grey) bands. Cross section predictions obtained at the particle level from different simulation approaches are shown, including their statistical uncertainties, as coloured symbols with different shapes. For $H_T$ and $p_T$, the last bins contain the overflow.

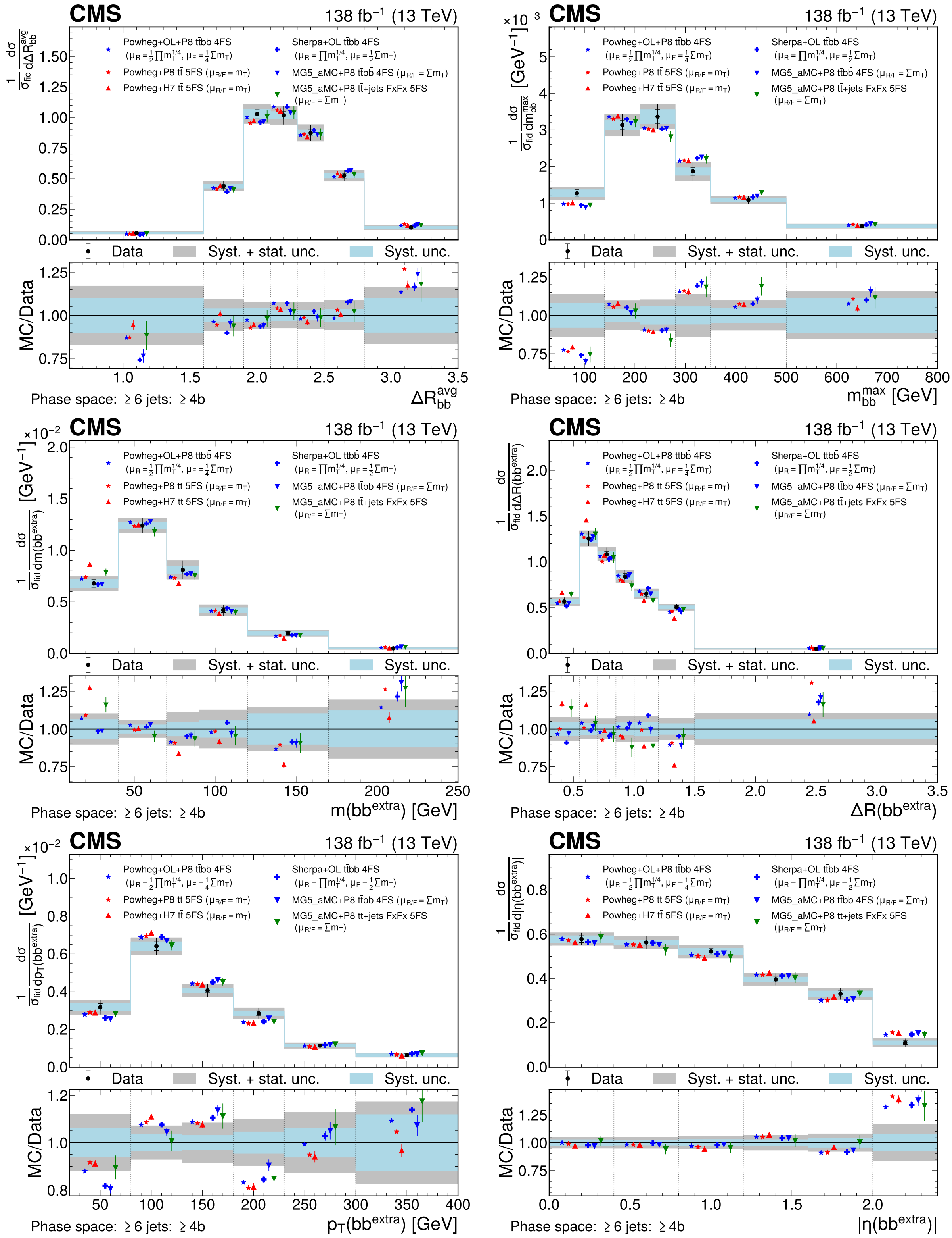

Figure 12: Predicted and observed normalized differential cross sections in the ≥6 jets: ≥4b fiducial phase space, for the average $\Delta R$ of all possible bb pairs (upper left), the largest invariant mass of any bb pair (upper right), the invariant mass (middle left), $\Delta R$ (middle right), $p_{\mathrm{T}}$ (lower left), and $|\eta|$ (lower right) of the extra b-jet pair. The data are represented by points, with inner (outer) vertical bars indicating the systematic (total) uncertainties, also represented as blue (grey) bands. Cross section predictions obtained at the particle level from different simulation approaches are shown, including their statistical uncertainties, as coloured symbols. For $m_{\mathrm{bb}}$ and $p_{\mathrm{T}}$, the last bins contain the overflow.

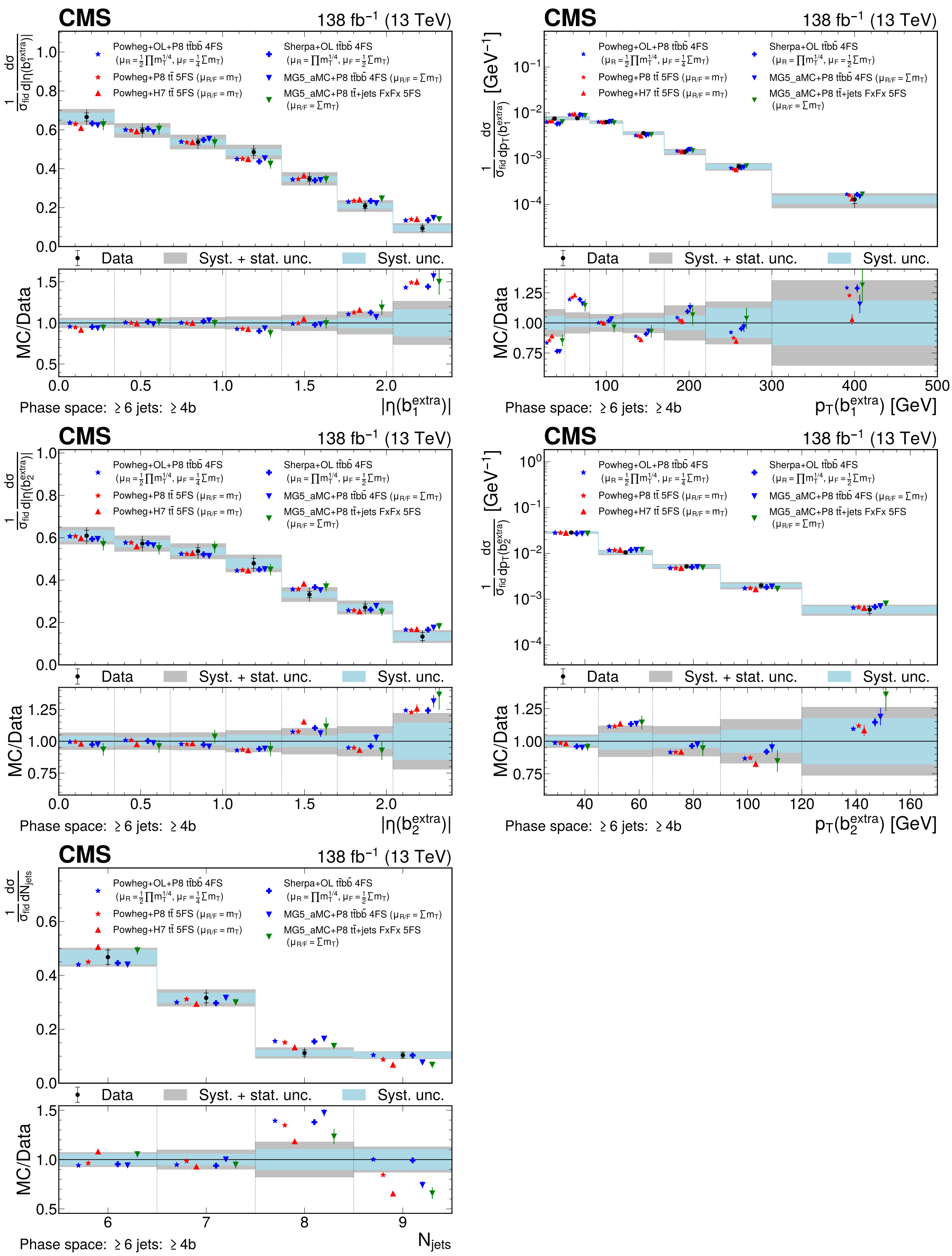


Figure 13: Predicted and observed normalized differential cross sections in the ≥6 jets: ≥4b fiducial phase space, for the $|\eta|$ (upper left) and $p_T$ (upper right) of the first extra b jet, the $|\eta|$ (middle left) and $p_T$ (middle right) of the second extra b jet, and the inclusive jet multiplicity (lower left). The data are represented by points, with inner (outer) vertical bars indicating the systematic (total) uncertainties, also represented as blue (grey) bands. Cross section predictions obtained at the particle level from different simulation approaches are shown, including their statistical uncertainties, as coloured symbols. For $N_{jets}$ and $p_T$, the last bins contain the overflow.

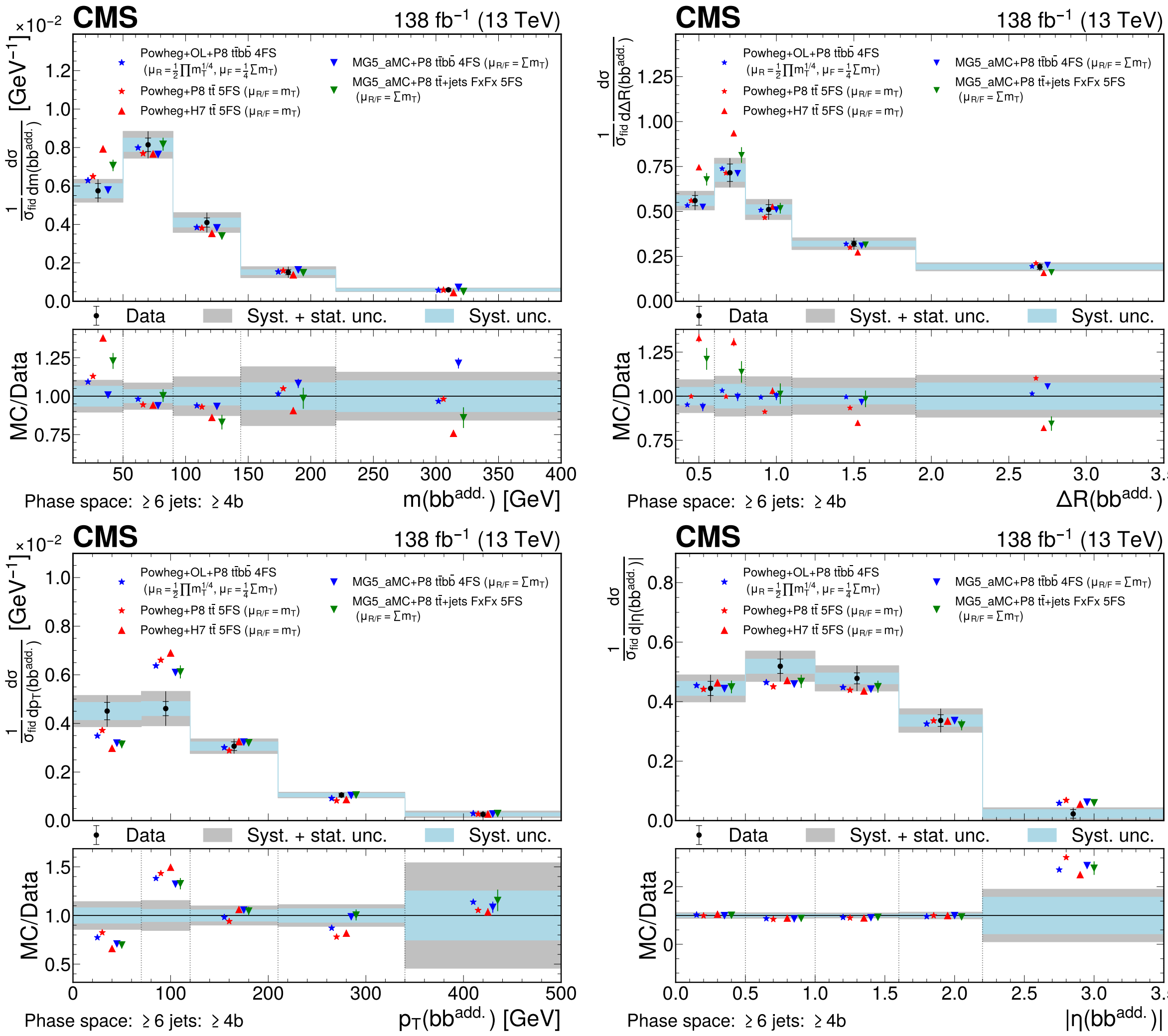


Figure 14: Predicted and observed normalized differential cross sections in the ≥6 jets: ≥4b fiducial phase space, for the invariant mass (upper left), $\Delta R$ (upper right), $p_{\mathrm{T}}$ (lower left), and $|\eta|$ (lower right) of the additional b-jet pair not originating from decaying top quarks. The data are represented by points, with inner (outer) vertical bars indicating the systematic (total) uncertainties, also represented as blue (grey) bands. Cross section predictions obtained at the particle level from different simulation approaches are shown, including their statistical uncertainties, as coloured symbols. For $m_{\mathrm{bb}}$ and $p_{\mathrm{T}}$, the last bins contain the overflow.

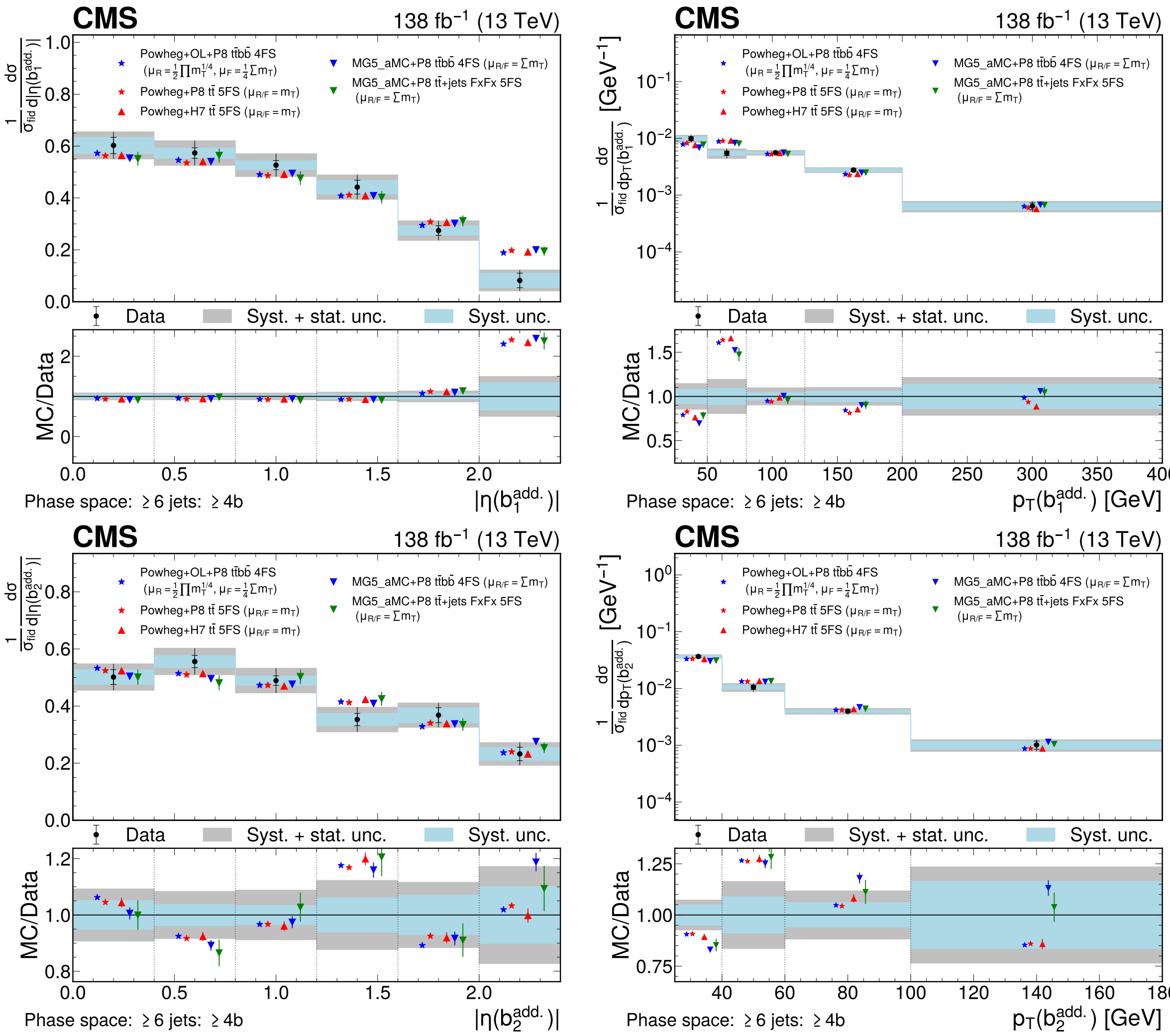

Figure 15: Predicted and observed normalized differential cross sections in the ≥6 jets: ≥4b fiducial phase space, for the $|\eta|$ (left) and $p_{\mathrm{T}}$ (right) of the first (upper row) and second (lower row) additional b of the b-jet pair not originating from decaying top quarks. The data are represented by points, with inner (outer) vertical bars indicating the systematic (total) uncertainties, also represented as blue (grey) bands. Cross section predictions obtained at the particle level from different simulation approaches are shown, including their statistical uncertainties, as coloured symbols. For $p_{\mathrm{T}}$, the last bins contain the overflow.

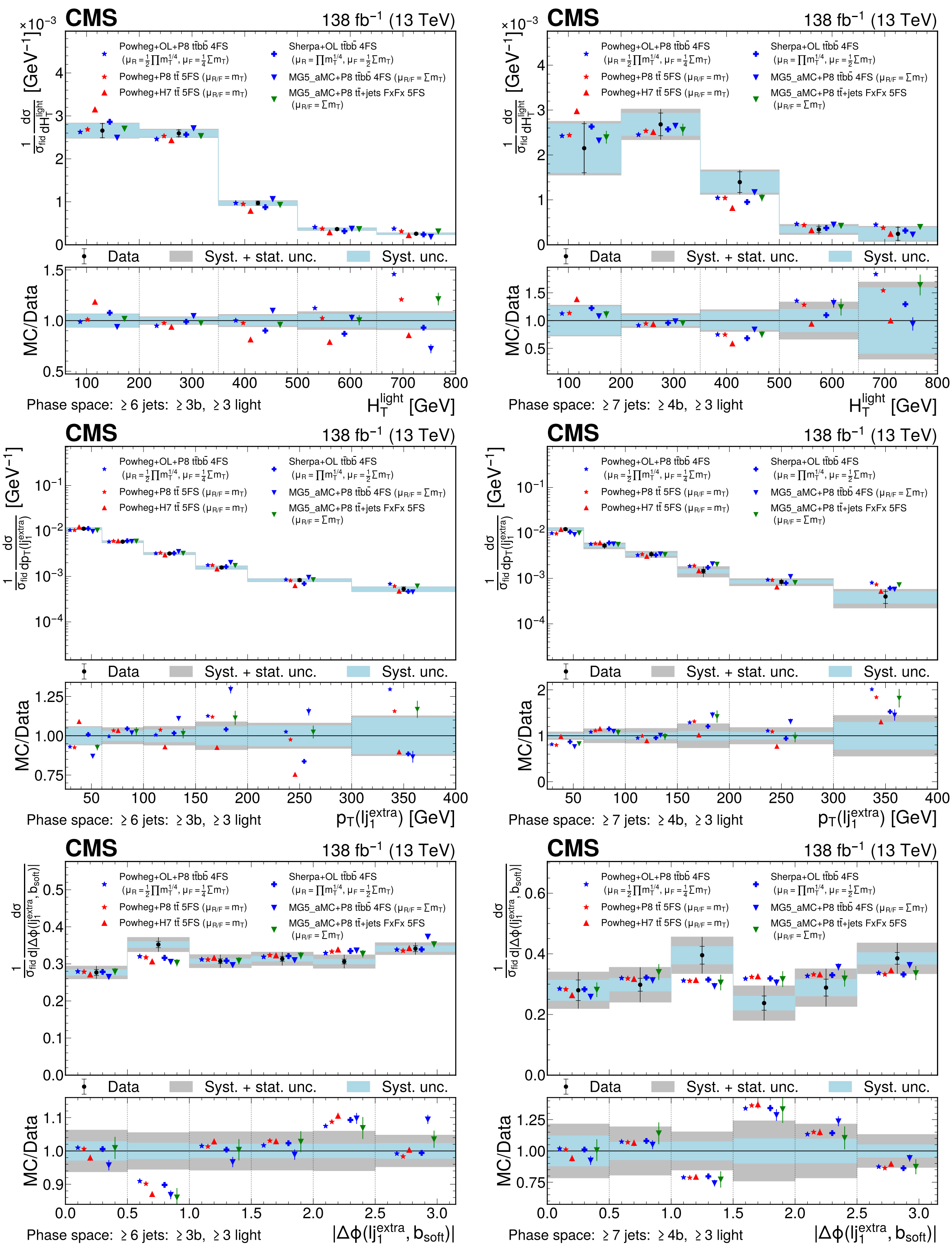


Figure 16: Predicted and observed normalized differential cross sections in the ≥6 jets: ≥3b, ≥3 light (left) and ≥7 jets: ≥4b, ≥3 light (right) fiducial phase space regions, for the $H_T$ of light jets (upper row), the $p_T$ of the extra light jet (middle row), and the $\Delta\phi$ between the extra light jet and the softest b jet (lower row). The data are represented by points, with inner (outer) vertical bars indicating the systematic (total) uncertainties, also represented as blue (grey) bands. Cross section predictions obtained at the particle level from different simulation approaches are shown, including their statistical uncertainties, as coloured symbols with different shapes. For $H_T$ and $p_T$, the last bins contain the overflow.

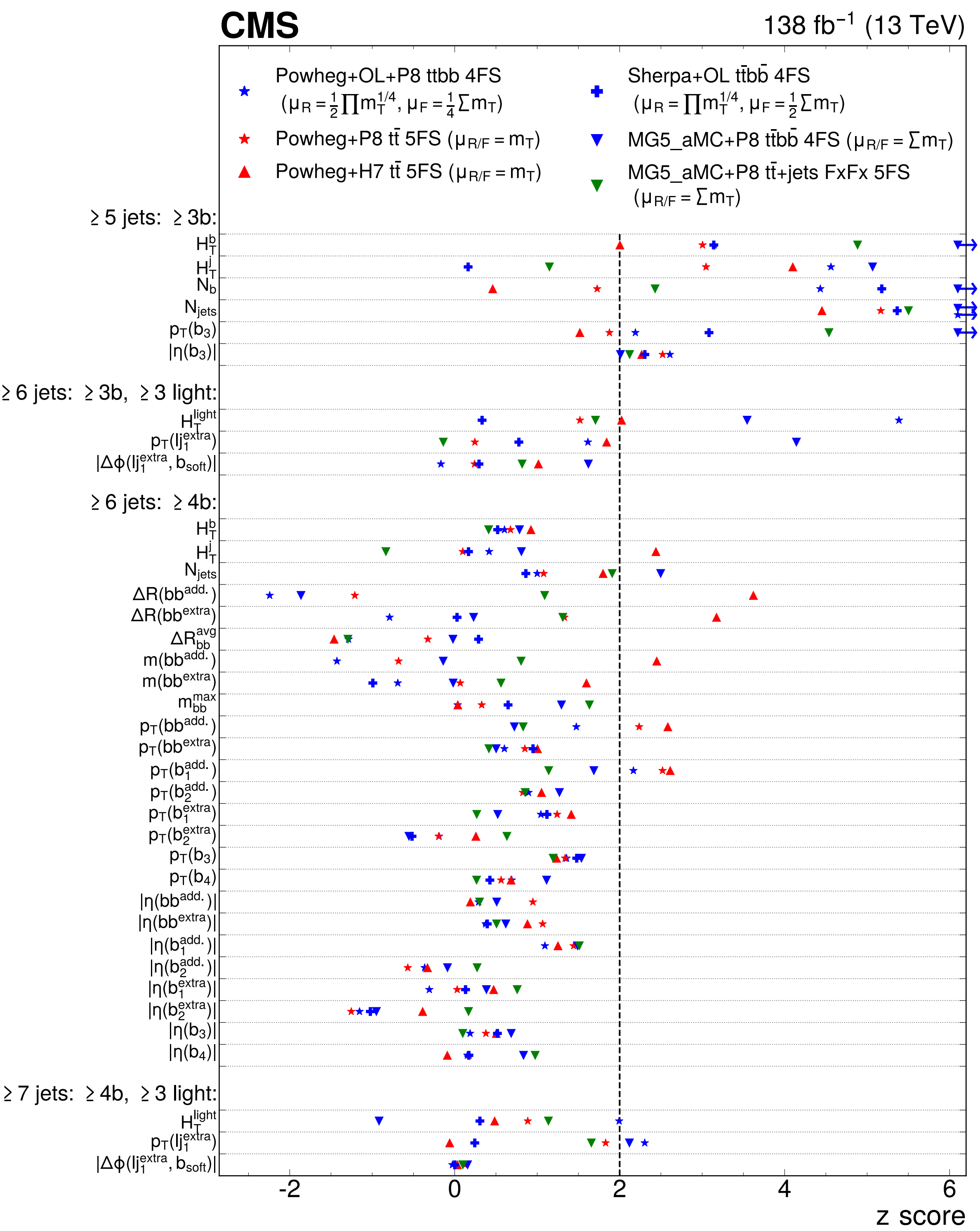


Figure 17: Observed $z$ score for each of the theoretical predictions, given the unfolded normalized differential cross sections and their covariances. A lower value indicates a better agreement between prediction and measurement. The dashed line at $z = 2$ indicates a $p$-value of 5%. Predictions for which the $z$ score exceeds the visible range of the figure are marked with arrows (→).

$t\bar{t}$ 5FS simulation a trend toward lower values is observed, similar to the 5j3b phase space. However, most generator setups underpredict the threshold region at low values of $H_T$. The predictions for $p_T(b_3)$, $|\eta(b_3)|$, $p_T(b_4)$, and $|\eta(b_4)|$ are generally compatible with the data, with only a slight trend visible in data towards more central (lower $|\eta|$) and softer (lower $p_T$) b jets. Similarly, predictions for the $p_T$ and $|\eta|$ for the extra b jets all describe the data well within the measurement uncertainties. The total number of jets is reasonably described by all predictions and does not show any clear trend.

The measured $\Delta R^{avg}_{bb}$ shows a small trend towards lower values for all simulation approaches, but is compatible with the data within the uncertainties of the measurement, as is the maximum invariant mass of any $b\bar{b}$ pair.

The observables related to the $bb^{extra}$ pair are modelled well by most of the generator setups, except for POWHEG+H7 $t\bar{t}$ 5FS, which predicts a softer $m(bb^{extra})$, and a smaller $\Delta R(bb^{extra})$. The variables related to the $bb^{add.}$ pair (Figs. 14–15), i.e. the b jets not part of the top quark decay chain, show similar behaviour, whereby $\Delta R(bb^{add.})$, $m(bb^{add.})$ and $p_T(bb^{add.})$ are not described by POWHEG+H7 $t\bar{t}$ 5FS. Predictions for the $p_T$ and $|\eta|$ of the individual additional b jets all tend to describe the data well.

In the 6j3b3l and 7j4b3l phase space regions (Fig. 16), the $H_T^{light}$ and $|\Delta\phi(lj_1^{extra}, b_{soft})|$ observables are modelled well by most generator setups, with only POWHEG+OL+P8 $t\bar{t}b\bar{b}$ 4FS predicting a higher $H_T^{light}$. With the exception of POWHEG+H7 $t\bar{t}$ 5FS, $p_T(lj_1^{extra})$ is observed to be softer than what is predicted by most generator setups. In Appendix D, the measured normalized differential cross sections of the $p_T(lj_1^{extra})$ and $H_T^{light}$ observables in the 6j3b3l phase space are compared with alternative $\mu_R$ and $\mu_F$ scale choices of the POWHEG+OL+P8 $t\bar{t}b\bar{b}$ 4FS simulation approach. These comparisons show that increased $\mu_R$ and $\mu_F$ scales relative to the nominal scale choices (see Table 1) tend to better describe these observables.

# 9 Summary

Measurements of inclusive and normalized differential cross sections of the associated production of top quark-antiquark and bottom quark-antiquark pairs, $t\bar{t}b\bar{b}$, for events containing an electron or a muon, have been presented. These measurements use proton-proton collision data recorded by the CMS detector at $\sqrt{s} = 13\,\text{TeV}$ and correspond to an integrated luminosity of $138\,\text{fb}^{-1}$.

The inclusive cross sections are measured in four fiducial phase space regions requiring different jet, b jet, and light jet multiplicities. With total uncertainties of 6–17%, depending on the phase space, these are the most precise measurements of the $t\bar{t}b\bar{b}$ cross section to date. The uncertainties are dominated by systematic sources, with the leading uncertainties originating from the calibration of the b tagging and of the jet energy scale, and from the choice of renormalization scale in the signal $t\bar{t}b\bar{b}$ and background $t\bar{t}$ processes. In most cases, the measured inclusive cross sections exceed the predictions with the chosen generator settings. The only exception is when using a particular choice of dynamic renormalization scale, $\mu_R = \frac{1}{2}\prod_{i=t,\bar{t},b,\bar{b}} m_{T,i}^{1/4}$, where $m_{T,i}^2 = m_i^2 + p_{T,i}^2$ are the transverse masses of top and bottom quarks.

Differential cross section measurements are performed as a function of several observables in the aforementioned phase space regions. These observables mainly target b jets as well as additional light jets produced in association with the top quark pairs. In the phase space containing events with at least six jets, of which at least four are b tagged, the additional b-jet radiation is probed with two different approaches. The first approach uses observables defined purely at the particle level, without any reference to the top quark decay chains, by selecting the two b jets with the smallest angular separation. The second approach uses explicitly the b jets at the generator level that do not originate from top quark decays and identifies those jets at the detector level with a neural network discriminant. The differential measurements have relative uncertainties in the range of 2–50%, depending on the phase space and the observable.

The results are compared to the predictions of several event generator setups, and it is found that none of them simultaneously describe all measured distributions in the various phase space regions. In the more inclusive phase space with five jets and three b jets, the agreement between data and predictions is generally poor, while in the phase space with six jets and four b jets, corresponding to the case in which the two additional b jets in $t\bar{t}b\bar{b}$ production are resolved, most predictions are compatible with the data within the larger experimental uncertainties. These measurements will help to further tune and refine the theoretical predictions and better assess the validity of the theoretical uncertainties estimated from the various $t\bar{t}b\bar{b}$ event generators.

## Acknowledgments

We congratulate our colleagues in the CERN accelerator departments for the excellent performance of the LHC and thank the technical and administrative staffs at CERN and at other CMS institutes for their contributions to the success of the CMS effort. In addition, we gratefully acknowledge the computing centres and personnel of the Worldwide LHC Computing Grid and other centres for delivering so effectively the computing infrastructure essential to our analyses. Finally, we acknowledge the enduring support for the construction and operation of the LHC, the CMS detector, and the supporting computing infrastructure provided by the following funding agencies: SC (Armenia), BMBWF and FWF (Austria); FNRS and FWO (Belgium); CNPq, CAPES, FAPERJ, FAPERGS, and FAPESP (Brazil); MES and BNSF (Bulgaria); CERN; CAS, MoST, and NSFC (China); MINCIENCIAS (Colombia); MSES and CSF (Croatia); RIF (Cyprus); SENESCYT (Ecuador); MoER, ERC PUT and ERDF (Estonia); Academy of Finland, MEC, and HIP (Finland); CEA and CNRS/IN2P3 (France); SRNSF (Georgia); BMBF, DFG, and HGF (Germany); GSRI (Greece); NKFIH (Hungary); DAE and DST (India); IPM (Iran); SFI (Ireland); INFN (Italy); MSIP and NRF (Republic of Korea); MES (Latvia); LAS (Lithuania); MOE and UM (Malaysia); BUAP, CINVESTAV, CONACYT, LNS, SEP, and UASLP-FAI (Mexico); MOS (Montenegro); MBIE (New Zealand); PAEC (Pakistan); MES and NSC (Poland); FCT (Portugal); MESTD (Serbia); MCIN/AEI and PCTI (Spain); MOSTR (Sri Lanka); Swiss Funding Agencies (Switzerland); MST (Taipei); MHESI and NSTDA (Thailand); TUBITAK and TENMAK (Turkey); NASU (Ukraine); STFC (United Kingdom); DOE and NSF (USA).

Individuals have received support from the Marie-Curie programme and the European Research Council and Horizon 2020 Grant, contract Nos. 675440, 724704, 752730, 758316, 765710, 824093, and COST Action CA16108 (European Union); the Leventis Foundation; the Alfred P. Sloan Foundation; the Alexander von Humboldt Foundation; the Science Committee, project no. 22rl-037 (Armenia); the Belgian Federal Science Policy Office; the Fonds pour la Formation à la Recherche dans l'Industrie et dans l'Agriculture (FRIA-Belgium); the Agentschap voor Innovatie door Wetenschap en Technologie (IWT-Belgium); the F.R.S.-FNRS and FWO (Belgium) under the "Excellence of Science – EOS" – be.h project n. 30820817; the Beijing Municipal Science & Technology Commission, No. Z191100007219010 and Fundamental Research Funds for the Central Universities (China); the Ministry of Education, Youth and Sports (MEYS) of the Czech Republic; the Shota Rustaveli National Science Foundation, grant FR-22-985 (Georgia);

the Deutsche Forschungsgemeinschaft (DFG), under Germany's Excellence Strategy – EXC 2121 "Quantum Universe" – 390833306, and under project number 400140256 - GRK2497; the Hellenic Foundation for Research and Innovation (HFRI), Project Number 2288 (Greece); the Hungarian Academy of Sciences, the New National Excellence Program - ÚNKP, the NKFIH research grants K 124845, K 124850, K 128713, K 128786, K 129058, K 131991, K 133046, K 138136, K 143460, K 143477, 2020-2.2.1-ED-2021-00181, and TKP2021-NKTA-64 (Hungary); the Council of Science and Industrial Research, India; the Latvian Council of Science; the Ministry of Education and Science, project no. 2022/WK/14, and the National Science Center, contracts Opus 2021/41/B/ST2/01369 and 2021/43/B/ST2/01552 (Poland); the Fundação para a Ciência e a Tecnologia, grant CEECIND/01334/2018 (Portugal); the National Priorities Research Program by Qatar National Research Fund; MCIN/AEI/10.13039/501100011033, ERDF "a way of making Europe", and the Programa Estatal de Fomento de la Investigación Científica y Técnica de Excelencia María de Maeztu, grant MDM-2017-0765 and Programa Severo Ochoa del Principado de Asturias (Spain); the Chulalongkorn Academic into Its 2nd Century Project Advancement Project, and the National Science, Research and Innovation Fund via the Program Management Unit for Human Resources & Institutional Development, Research and Innovation, grant B05F650021 (Thailand); the Kavli Foundation; the Nvidia Corporation; the SuperMicro Corporation; the Welch Foundation, contract C-1845; and the Weston Havens Foundation (USA).

## References

[1] F. Buccioni, S. Kallweit, S. Pozzorini, and M. F. Zoller, "NLO QCD predictions for $\mathrm{t\bar{t}b\bar{b}}$ production in association with a light jet at the LHC", *JHEP* **12** (2019) 015, doi:10.1007/JHEP12(2019)015, arXiv:1907.13624.

[2] T. Ježo, J. M. Lindert, N. Moretti, and S. Pozzorini, "New NLOPS predictions for $\mathrm{t\bar{t}}+\mathrm{b}$-jet production at the LHC", *Eur. Phys. J. C* **78** (2018) 502, doi:10.1140/epjc/s10052-018-5956-0, arXiv:1802.00426.

[3] ATLAS Collaboration, "Search for the standard model Higgs boson decaying into $\mathrm{b\bar{b}}$ produced in association with top quarks decaying hadronically in pp collisions at $\sqrt{s}=8\,\mathrm{TeV}$ with the ATLAS detector", *JHEP* **05** (2016) 160, doi:10.1007/JHEP05(2016)160, arXiv:1604.03812.

[4] ATLAS Collaboration, "Search for the standard model Higgs boson produced in association with top quarks and decaying into a $\mathrm{b\bar{b}}$ pair in pp collisions at $\sqrt{s}=13\,\mathrm{TeV}$ with the ATLAS detector", *Phys. Rev. D* **97** (2018) 072016, doi:10.1103/PhysRevD.97.072016, arXiv:1712.08895.

[5] ATLAS Collaboration, "Observation of Higgs boson production in association with a top quark pair at the LHC with the ATLAS detector", *Phys. Lett. B* **784** (2018) 173, doi:10.1016/j.physletb.2018.07.035, arXiv:1806.00425.

[6] CMS Collaboration, "Search for $\mathrm{t\bar{t}H}$ production in the all-jet final state in proton-proton collisions at $\sqrt{s}=13\,\mathrm{TeV}$", *JHEP* **06** (2018) 101, doi:10.1007/JHEP06(2018)101, arXiv:1803.06986.

[7] CMS Collaboration, "Observation of $\mathrm{t\bar{t}H}$ production", *Phys. Rev. Lett.* **120** (2018) 231801, doi:10.1103/PhysRevLett.120.231801, arXiv:1804.02610.

[8] CMS Collaboration, "Search for $t\bar{t}H$ production in the $H \to b\bar{b}$ decay channel with leptonic $t\bar{t}$ decays in proton-proton collisions at $\sqrt{s} = 13$ TeV", *JHEP* **03** (2019) 026, doi:10.1007/JHEP03(2019)026, arXiv:1804.03682.

[9] ATLAS Collaboration, "Search for four-top-quark production in the single-lepton and opposite-sign dilepton final states in pp collisions at $\sqrt{s} = 13$ TeV with the ATLAS detector", *Phys. Rev. D* **99** (2019) 052009, doi:10.1103/PhysRevD.99.052009, arXiv:1811.02305.

[10] ATLAS Collaboration, "Evidence for $t\bar{t}t\bar{t}$ production in the multilepton final state in proton-proton collisions at $\sqrt{s} = 13$ TeV with the ATLAS detector", *Eur. Phys. J. C* **80** (2020) 1085, doi:10.1140/epjc/s10052-020-08509-3, arXiv:2007.14858.

[11] ATLAS Collaboration, "Measurement of the $t\bar{t}t\bar{t}$ production cross section in pp collisions at $\sqrt{s} = 13$ TeV with the ATLAS detector", *JHEP* **11** (2021) 118, doi:10.1007/JHEP11(2021)118, arXiv:2106.11683.

[12] CMS Collaboration, "Search for standard model production of four top quarks in the lepton+jets channel in pp collisions at $\sqrt{s} = 8$ TeV", *JHEP* **11** (2014) 154, doi:10.1007/JHEP11(2014)154, arXiv:1409.7339.

[13] CMS Collaboration, "Search for standard model production of four top quarks with same-sign and multilepton final states in proton-proton collisions at $\sqrt{s} = 13$ TeV", *Eur. Phys. J. C* **78** (2018) 140, doi:10.1140/epjc/s10052-018-5607-5, arXiv:1710.10614.

[14] CMS Collaboration, "Search for standard model production of four top quarks in proton-proton collisions at $\sqrt{s} = 13$ TeV", *Phys. Lett. B* **772** (2017) 336, doi:10.1016/j.physletb.2017.06.064, arXiv:1702.06164.

[15] CMS Collaboration, "Search for the production of four top quarks in the single-lepton and opposite-sign dilepton final states in proton-proton collisions at $\sqrt{s} = 13$ TeV", *JHEP* **11** (2019) 082, doi:10.1007/JHEP11(2019)082, arXiv:1906.02805.

[16] CMS Collaboration, "Search for production of four top quarks in final states with same-sign or multiple leptons in proton-proton collisions at $\sqrt{s} = 13$ TeV", *Eur. Phys. J. C* **80** (2020) 75, doi:10.1140/epjc/s10052-019-7593-7, arXiv:1908.06463.

[17] CMS Collaboration, "Evidence for four-top quark production in proton-proton collisions at $\sqrt{s} = 13$ TeV", *Phys. Lett. B* **844** (2023) 138076, doi:10.1016/j.physletb.2023.138076, arXiv:2303.03864.

[18] ATLAS Collaboration, "Observation of four-top-quark production in the multilepton final state with the ATLAS detector", *Eur. Phys. J. C* **83** (2023) 496, doi:10.1140/epjc/s10052-023-11573-0, arXiv:2303.15061.

[19] CMS Collaboration, "Observation of four top quark production in proton-proton collisions at $\sqrt{s} = 13$ TeV", 2023. arXiv:2305.13439. Submitted to *Phys. Lett. B*.

[20] Q.-H. Cao, S.-L. Chen, and Y. Liu, "Probing Higgs width and top quark Yukawa coupling from $t\bar{t}H$ and $t\bar{t}t\bar{t}$ productions", *Phys. Rev. D* **95** (2017) 053004, doi:10.1103/PhysRevD.95.053004, arXiv:1602.01934.

[21] Q.-H. Cao et al., "Limiting top quark-Higgs boson interaction and Higgs-boson width from multitop productions", *Phys. Rev. D* **99** (2019) 113003, doi:10.1103/PhysRevD.99.113003, arXiv:1901.04567.

[22] M. Worek, "Next-to-leading order QCD corrections to $t\bar{t}b\bar{b}$ production at the LHC", in *Proc. 33rd Int. Conf. of Theoretical Physics on Matter to the Deepest: Ustroń, Poland, September 11–16, 2009*. 2009. arXiv:0910.4080. [Acta Phys. Pol. B 40 (2009) 2937].

[23] G. Bevilacqua et al., "Assault on the NLO wishlist: $pp \rightarrow t\bar{t}b\bar{b}$", *JHEP* **09** (2009) 109, doi:10.1088/1126-6708/2009/09/109, arXiv:0907.4723.

[24] A. Bredenstein, A. Denner, S. Dittmaier, and S. Pozzorini, "NLO QCD corrections to $pp \rightarrow t\bar{t}b\bar{b} + X$ at the LHC", *Phys. Rev. Lett.* **103** (2009) 012002, doi:10.1103/PhysRevLett.103.012002, arXiv:0905.0110.

[25] A. Bredenstein, A. Denner, S. Dittmaier, and S. Pozzorini, "NLO QCD corrections to $t\bar{t}b\bar{b}$ production at the LHC: 2. Full hadronic results", *JHEP* **03** (2010) 021, doi:10.1007/JHEP03(2010)021, arXiv:1001.4006.

[26] M. Worek, "On the next-to-leading order QCD *K*-factor for $t\bar{t}b\bar{b}$ production at the Tevatron", *JHEP* **02** (2012) 043, doi:10.1007/JHEP02(2012)043, arXiv:1112.4325.

[27] A. Denner, J.-N. Lang, and M. Pellen, "Full NLO QCD corrections to off-shell $t\bar{t}b\bar{b}$ production", *Phys. Rev. D* **104** (2021) 056018, doi:10.1103/PhysRevD.104.056018, arXiv:2008.00918.

[28] G. Bevilacqua et al., "$t\bar{t}b\bar{b}$ at the LHC: on the size of corrections and b-jet definitions", *JHEP* **08** (2021) 008, doi:10.1007/JHEP08(2021)008, arXiv:2105.08404.

[29] S. Höche et al., "Next-to-leading order QCD predictions for top-quark pair production with up to two jets merged with a parton shower", *Phys. Lett. B* **748** (2015) 74, doi:10.1016/j.physletb.2015.06.060, arXiv:1402.6293.

[30] M. V. Garzelli, A. Kardos, and Z. Trócsányi, "Hadroproduction of $t\bar{t}b\bar{b}$ final states at LHC: predictions at NLO accuracy matched with parton shower", *JHEP* **03** (2015) 083, doi:10.1007/JHEP03(2015)083, arXiv:1408.0266.

[31] S. Höche et al., "Next-to-leading order QCD predictions for top-quark pair production with up to three jets", *Eur. Phys. J. C* **77** (2017) 145, doi:10.1140/epjc/s10052-017-4715-y, arXiv:1607.06934.

[32] J. Alwall et al., "The automated computation of tree-level and next-to-leading order differential cross sections, and their matching to parton shower simulations", *JHEP* **07** (2014) 079, doi:10.1007/JHEP07(2014)079, arXiv:1405.0301.

[33] R. Frederix and S. Frixione, "Merging meets matching in MC@NLO", *JHEP* **12** (2012) 061, doi:10.1007/JHEP12(2012)061, arXiv:1209.6215.

[34] S. Frixione, P. Nason, and G. Ridolfi, "A positive-weight next-to-leading-order Monte Carlo for heavy flavour hadroproduction", *JHEP* **09** (2007) 126, doi:10.1088/1126-6708/2007/09/126, arXiv:0707.3088.

[35] F. Cascioli et al., "NLO matching for $t\bar{t}b\bar{b}$ production with massive b-quarks", *Phys. Lett. B* **734** (2014) 210, doi:10.1016/j.physletb.2014.05.040, arXiv:1309.5912.

[36] G. Bevilacqua, M. V. Garzelli, and A. Kardos, "$t\bar{t}b\bar{b}$ hadroproduction with massive bottom quarks with POWHEL", 2017. arXiv:1709.06915.

[37] ATLAS Collaboration, "Study of heavy-flavor quarks produced in association with top-quark pairs at $\sqrt{s} = 7$ TeV using the ATLAS detector", *Phys. Rev. D* **89** (2014) 072012, doi:10.1103/PhysRevD.89.072012, arXiv:1304.6386.

[38] ATLAS Collaboration, "Measurements of fiducial cross-sections for $t\bar{t}$ production with one or two additional b-jets in pp collisions at $\sqrt{s} = 8$ TeV using the ATLAS detector", *Eur. Phys. J. C* **76** (2016) 11, doi:10.1140/epjc/s10052-015-3852-4, arXiv:1508.06868.

[39] ATLAS Collaboration, "Measurements of inclusive and differential fiducial cross-sections of $t\bar{t}$ production with additional heavy-flavour jets in proton-proton collisions at $\sqrt{s} = 13$ TeV with the ATLAS detector", *JHEP* **04** (2019) 046, doi:10.1007/JHEP04(2019)046, arXiv:1811.12113.

[40] CMS Collaboration, "Measurement of $t\bar{t}$ production with additional jet activity, including b quark jets, in the dilepton decay channel using pp collisions at $\sqrt{s} = 8$ TeV", *Eur. Phys. J. C* **76** (2016) 379, doi:10.1140/epjc/s10052-016-4105-x, arXiv:1510.03072.

[41] CMS Collaboration, "Measurement of the cross section ratio $\sigma_{t\bar{t}b\bar{b}}/\sigma_{t\bar{t}jj}$ in pp collisions at $\sqrt{s} = 8$ TeV", *Phys. Lett. B* **746** (2015) 132, doi:10.1016/j.physletb.2015.04.060, arXiv:1411.5621.

[42] CMS Collaboration, "Measurements of $t\bar{t}$ cross sections in association with b jets and inclusive jets and their ratio using dilepton final states in pp collisions at $\sqrt{s} = 13$ TeV", *Phys. Lett. B* **776** (2018) 355, doi:10.1016/j.physletb.2017.11.043, arXiv:1705.10141.

[43] CMS Collaboration, "Measurement of the $t\bar{t}b\bar{b}$ production cross section in the all-jet final state in pp collisions at $\sqrt{s} = 13$ TeV", *Phys. Lett. B* **803** (2020) 135285, doi:10.1016/j.physletb.2020.135285, arXiv:1909.05306.

[44] CMS Collaboration, "Measurement of the cross section for $t\bar{t}$ production with additional jets and b jets in pp collisions at $\sqrt{s} = 13$ TeV", *JHEP* **07** (2020) 125, doi:10.1007/JHEP07(2020)125, arXiv:2003.06467.

[45] CMS Collaboration, "First measurement of the cross section for top quark pair production with additional charm jets using dileptonic final states in pp collisions at $\sqrt{s} = 13$ TeV", *Phys. Lett. B* **820** (2021) 136565, doi:10.1016/j.physletb.2021.136565, arXiv:2012.09225.

[46] HEPData record for this analysis, 2023. doi:10.17182/hepdata.138416.

[47] CMS Collaboration, "The CMS experiment at the CERN LHC", *JINST* **3** (2008) S08004, doi:10.1088/1748-0221/3/08/S08004.

[48] CMS Tracker Group, "The CMS Phase-1 pixel detector upgrade", *JINST* **16** (2021) P02027, doi:10.1088/1748-0221/16/02/P02027, arXiv:2012.14304.

[49] CMS Collaboration, "Performance of the CMS Level-1 trigger in proton-proton collisions at $\sqrt{s} = 13\,\text{TeV}$", *JINST* **15** (2020) P10017, doi:10.1088/1748-0221/15/10/P10017, arXiv:2006.10165.

[50] CMS Collaboration, "The CMS trigger system", *JINST* **12** (2017) P01020, doi:10.1088/1748-0221/12/01/P01020, arXiv:1609.02366.

[51] T. Sjöstrand et al., "An introduction to PYTHIA 8.2", *Comput. Phys. Commun.* **191** (2015) 159, doi:10.1016/j.cpc.2015.01.024, arXiv:1410.3012.

[52] GEANT4 Collaboration, "GEANT4—a simulation toolkit", *Nucl. Instrum. Meth. A* **506** (2003) 250, doi:10.1016/S0168-9002(03)01368-8.

[53] T. Ježo and P. Nason, "On the treatment of resonances in next-to-leading order calculations matched to a parton shower", *JHEP* **12** (2015) 065, doi:10.1007/JHEP12(2015)065, arXiv:1509.09071.

[54] F. Buccioni et al., "OPENLOOPS 2", *Eur. Phys. J. C* **79** (2019) 866, doi:10.1140/epjc/s10052-019-7306-2, arXiv:1907.13071.

[55] M. Bähr et al., "HERWIG++ physics and manual", *Eur. Phys. J. C* **58** (2008) 639, doi:10.1140/epjc/s10052-008-0798-9, arXiv:0803.0883.

[56] J. Bellm et al., "HERWIG 7.0/HERWIG++ 3.0 release note", *Eur. Phys. J. C* **76** (2016) 196, doi:10.1140/epjc/s10052-016-4018-8, arXiv:1512.01178.

[57] CMS Collaboration, "Development and validation of HERWIG 7 tunes from CMS underlying-event measurements", *Eur. Phys. J. C* **81** (2021) 312, doi:10.1140/epjc/s10052-021-08949-5, arXiv:2011.03422.

[58] T. Gleisberg et al., "Event generation with SHERPA 1.1", *JHEP* **02** (2009) 007, doi:10.1088/1126-6708/2009/02/007, arXiv:0811.4622.

[59] M. Czakon and A. Mitov, "TOP++: A program for the calculation of the top-pair cross-section at hadron colliders", *Comput. Phys. Commun.* **185** (2014) 2930, doi:10.1016/j.cpc.2014.06.021, arXiv:1112.5675.

[60] N. Kidonakis, "Top quark production", in *Proc. Helmholtz International Summer School on Physics of Heavy Quarks and Hadrons (HQ 2013): Dubna, Russa, July 15–28, 2013.* 2013. arXiv:1311.0283. [DESY-PROC-2013-03]. doi:10.3204/DESY-PROC-2013-03/Kidonakis.

[61] P. Nason, "A new method for combining NLO QCD with shower Monte Carlo algorithms", *JHEP* **11** (2004) 040, doi:10.1088/1126-6708/2004/11/040, arXiv:hep-ph/0409146.

[62] S. Frixione, P. Nason, and C. Oleari, "Matching NLO QCD computations with parton shower simulations: the POWHEG method", *JHEP* **11** (2007) 070, doi:10.1088/1126-6708/2007/11/070, arXiv:0709.2092.

[63] S. Alioli, P. Nason, C. Oleari, and E. Re, "A general framework for implementing NLO calculations in shower Monte Carlo programs: the POWHEG BOX", *JHEP* **06** (2010) 043, doi:10.1007/JHEP06(2010)043, arXiv:1002.2581.

[64] S. Alioli, P. Nason, C. Oleari, and E. Re, "NLO single-top production matched with shower in POWHEG: $s$- and $t$-channel contributions", *JHEP* **09** (2009) 111, doi:10.1088/1126-6708/2009/09/111, arXiv:0907.4076. [Erratum: doi:10.1007/JHEP02(2010)011].

[65] E. Re, "Single-top W$t$-channel production matched with parton showers using the POWHEG method", *Eur. Phys. J. C* **71** (2011) 1547, doi:10.1140/epjc/s10052-011-1547-z, arXiv:1009.2450.

[66] H. B. Hartanto, B. Jäger, L. Reina, and D. Wackeroth, "Higgs boson production in association with top quarks in the POWHEG BOX", *Phys. Rev. D* **91** (2015) 094003, doi:10.1103/PhysRevD.91.094003, arXiv:1501.04498.

[67] P. Artoisenet, R. Frederix, O. Mattelaer, and R. Rietkerk, "Automatic spin-entangled decays of heavy resonances in Monte Carlo simulations", *JHEP* **03** (2013) 015, doi:10.1007/JHEP03(2013)015, arXiv:1212.3460.

[68] J. Alwall et al., "Comparative study of various algorithms for the merging of parton showers and matrix elements in hadronic collisions", *Eur. Phys. J. C* **53** (2008) 473, doi:10.1140/epjc/s10052-007-0490-5, arXiv:0706.2569.

[69] NNPDF Collaboration, "Parton distributions for the LHC run II", *JHEP* **04** (2015) 040, doi:10.1007/JHEP04(2015)040, arXiv:1410.8849.

[70] CMS Collaboration, "Extraction and validation of a new set of CMS PYTHIA 8 tunes from underlying-event measurements", *Eur. Phys. J. C* **80** (2020) 4, doi:10.1140/epjc/s10052-019-7499-4, arXiv:1903.12179.

[71] Y. Li and F. Petriello, "Combining QCD and electroweak corrections to dilepton production in the framework of the FEWZ simulation code", *Phys. Rev. D* **86** (2012) 094034, doi:10.1103/PhysRevD.86.094034, arXiv:1208.5967.

[72] CMS Collaboration, "Particle-flow reconstruction and global event description with the CMS detector", *JINST* **12** (2017) P10003, doi:10.1088/1748-0221/12/10/P10003, arXiv:1706.04965.

[73] CMS Collaboration, "Technical proposal for the Phase-II upgrade of the Compact Muon Solenoid", CMS Technical Proposal CERN-LHCC-2015-010, CMS-TDR-15-02, 2015.

[74] CMS Collaboration, "Electron and photon reconstruction and identification with the CMS experiment at the CERN LHC", *JINST* **16** (2021) P05014, doi:10.1088/1748-0221/16/05/P05014, arXiv:2012.06888.

[75] CMS Collaboration, "Performance of the CMS muon detector and muon reconstruction with proton-proton collisions at $\sqrt{s} = 13\,\text{TeV}$", *JINST* **13** (2018) P06015, doi:10.1088/1748-0221/13/06/P06015, arXiv:1804.04528.

[76] CMS Collaboration, "Pileup mitigation at CMS in 13 TeV data", *JINST* **15** (2020) P09018, doi:10.1088/1748-0221/15/09/P09018, arXiv:2003.00503.

[77] M. Cacciari, G. P. Salam, and G. Soyez, "The anti-$k_{\mathrm{T}}$ jet clustering algorithm", *JHEP* **04** (2008) 063, doi:10.1088/1126-6708/2008/04/063, arXiv:0802.1189.

[78] M. Cacciari, G. P. Salam, and G. Soyez, "FASTJET user manual", *Eur. Phys. J. C* **72** (2012) 1896, doi:10.1140/epjc/s10052-012-1896-2, arXiv:1111.6097.

[79] CMS Collaboration, "Jet energy scale and resolution in the CMS experiment in pp collisions at 8 TeV", *JINST* **12** (2017) P02014, doi:10.1088/1748-0221/12/02/P02014, arXiv:1607.03663.

[80] CMS Collaboration, "Identification of heavy-flavour jets with the CMS detector in pp collisions at 13 TeV", *JINST* **13** (2018) P05011, doi:10.1088/1748-0221/13/05/P05011, arXiv:1712.07158.

[81] E. Bols et al., "Jet flavour classification using DEEPJET", *JINST* **15** (2020) P12012, doi:10.1088/1748-0221/15/12/P12012, arXiv:2008.10519.

[82] CMS Collaboration, "Performance summary of AK4 jet b tagging with data from proton-proton collisions at 13 TeV with the CMS detector", CMS Detector Performance Note CMS-DP-2023-005, 2023.

[83] M. Cacciari and G. P. Salam, "Pileup subtraction using jet areas", *Phys. Lett. B* **659** (2008) 119, doi:10.1016/j.physletb.2007.09.077, arXiv:0707.1378.

[84] CMS Collaboration, "Simulation of the silicon strip tracker pre-amplifier in early 2016 data", CMS Detector Performance Note CMS-DP-2020-045, 2020.

[85] Y. LeCun et al., "Handwritten digit recognition with a back-propagation network", in *Proc. 2nd Int. Conf. on Advances in Neural Information Processing Systems (NIPS'89): Denver CO, USA, November 27–30, 1989*, p. 396. 1989.

[86] S. Hochreiter and J. Schmidhuber, "Long short-term memory", *Neural Comput.* **9** (1997) 1735, doi:10.1162/neco.1997.9.8.1735.

[87] F. Chollet et al., "KERAS: Deep learning for humans". Software available at https://github.com/keras-team/keras, 2023. More information at http://keras.io (accessed 2023-09-19).

[88] M. Abadi et al., "TENSORFLOW: large-scale machine learning on heterogeneous distributed systems", 2016. arXiv:1603.04467.

[89] D. P. Kingma and J. Ba, "ADAM: a method for stochastic optimization", in *Proc. 3rd Int. Conf. on Learning Representations (ICLR 2015): San Diego CA, USA, May 7–9, 2015*. 2015. arXiv:1412.6980.

[90] N. Srivastava et al., "Dropout: a simple way to prevent neural networks from overfitting", *J. Mach. Learn. Res.* **15** (2014) 1929.

[91] S. Wertz, "SMOOFIT: a package for smooth binned likelihood fits". Software available at https://gitlab.cern.ch/swertz/smoofit, 2022. More information at https://smoofit.readthedocs.io (accessed 2023-09-19).

[92] J. Bradbury et al., "JAX: AUTOGRAD and XLA". Software available at https://github.com/google/jax, 2023. More information at http://jax.readthedocs.io (accessed 2023-09-19).

[93] CMS Collaboration, "Precision luminosity measurement in proton-proton collisions at $\sqrt{s} = 13$ TeV in 2015 and 2016 at CMS", *Eur. Phys. J. C* **81** (2021) 800, doi:10.1140/epjc/s10052-021-09538-2, arXiv:2104.01927.

[94] CMS Collaboration, "CMS luminosity measurement for the 2017 data-taking period at $\sqrt{s} = 13$ TeV", CMS Physics Analysis Summary CMS-PAS-LUM-17-004, 2018.

[95] CMS Collaboration, "CMS luminosity measurement for the 2018 data-taking period at $\sqrt{s} = 13$ TeV", CMS Physics Analysis Summary CMS-PAS-LUM-18-002, 2019.

[96] M. Czakon et al., "Top-pair production at the LHC through NNLO QCD and NLO EW", *JHEP* **10** (2017) 186, doi:10.1007/JHEP10(2017)186, arXiv:1705.04105.

[97] S. Argyropoulos and T. Sjöstrand, "Effects of color reconnection on $t\bar{t}$ final states at the LHC", *JHEP* **11** (2014) 043, doi:10.1007/JHEP11(2014)043, arXiv:1407.6653.

[98] J. R. Christiansen and P. Z. Skands, "String formation beyond leading colour", *JHEP* **08** (2015) 003, doi:10.1007/JHEP08(2015)003, arXiv:1505.01681.

[99] ATLAS Collaboration, "Measurement of b-quark fragmentation properties in jets using the decay $B^{\pm} \to J/\psi K^{\pm}$ in pp collisions at $\sqrt{s} = 13$ TeV with the ATLAS detector", *JHEP* **12** (2021) 131, doi:10.1007/JHEP12(2021)131, arXiv:2108.11650.

[100] R. J. Barlow and C. Beeston, "Fitting using finite Monte Carlo samples", *Comput. Phys. Commun.* **77** (1993) 219, doi:10.1016/0010-4655(93)90005-W.

[101] J. S. Conway, "Incorporating nuisance parameters in likelihoods for multisource spectra", in *Proc. 2011 Workshop on Statistical Issues Related to Discovery Claims in Search Experiments and Unfolding (PHYSTAT 2011): Geneva, Switzerland, January 17–20, 2011.* 2011. arXiv:1103.0354. doi:10.5170/CERN-2011-006.115.

[102] R. D. Cousins, J. T. Linnemann, and J. Tucker, "Evaluation of three methods for calculating statistical significance when incorporating a systematic uncertainty into a test of the background-only hypothesis for a Poisson process", *Nucl. Instrum. Meth. A* **595** (2008) 480, doi:10.1016/j.nima.2008.07.086, arXiv:physics/0702156.

# A Leading nuisance parameter impacts

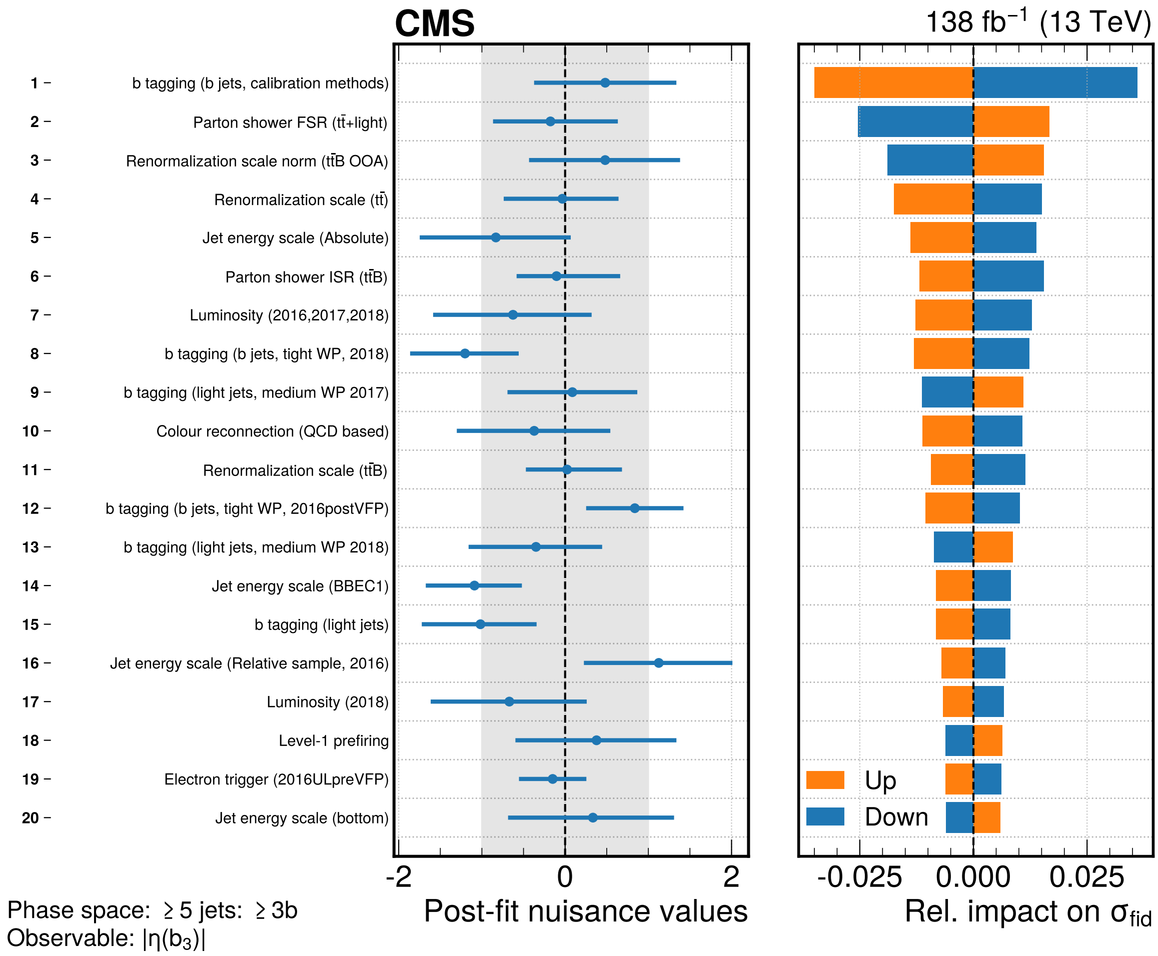


Figure A.1: Post-fit nuisance parameter values and relative impacts on the fiducial cross section, for the fit of $|\eta|$ of the b jet with third-highest $p_{\mathrm{T}}$ in the $\geq$5 jets: $\geq$3b phase space. The nuisance parameters are defined such that the prefit value is zero with unity uncertainty.

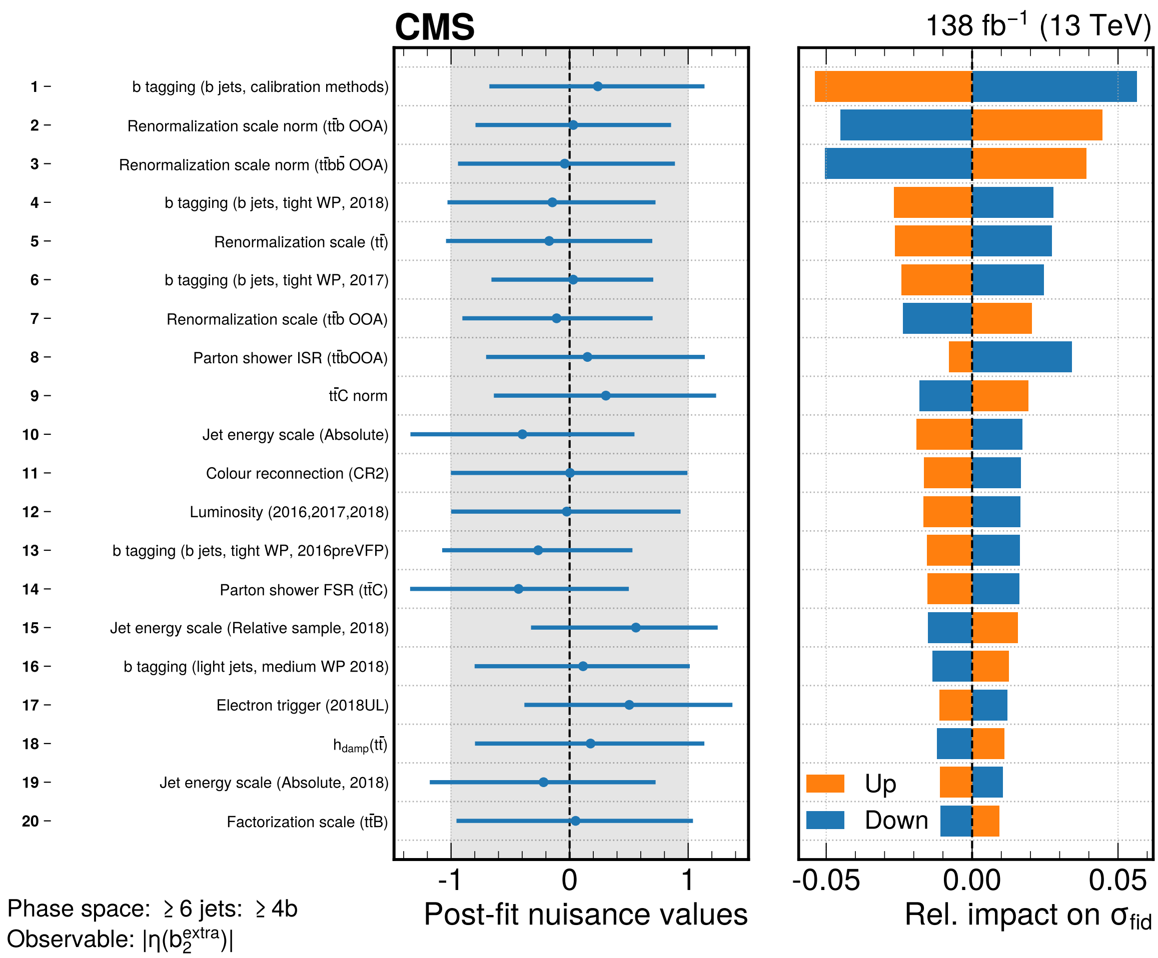


Figure A.2: Post-fit nuisance parameter values and relative impacts on the fiducial cross section, for the fit of $|\eta|$ of the subleading extra b jet in the $\geq$6 jets: $\geq$4b phase space. The nuisance parameters are defined such that the prefit value is zero with unity uncertainty.

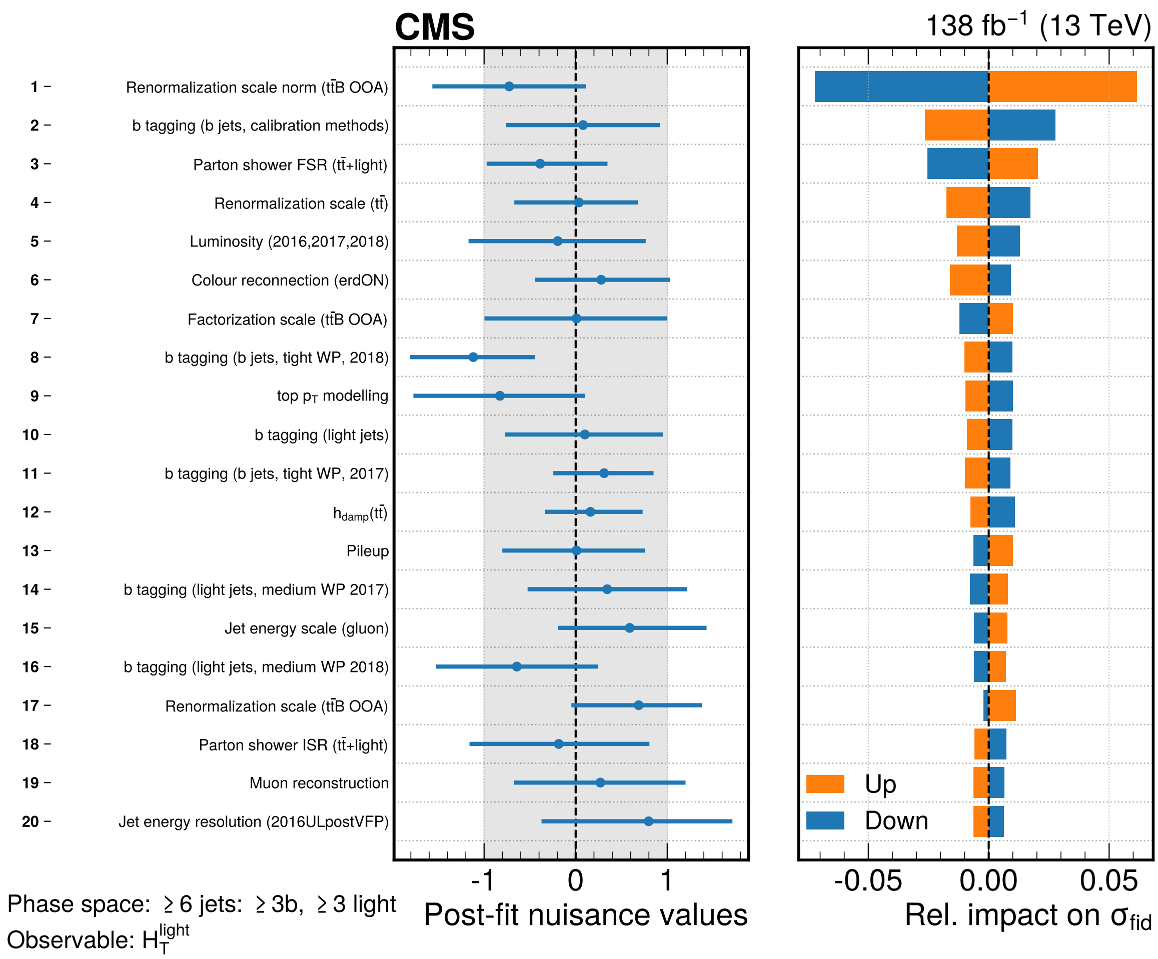


Figure A.3: Post-fit nuisance parameter values and relative impacts on the fiducial cross section, for the fit of $H_T$ of light jets in the $\geq$6 jets: $\geq$3b, $\geq$3 light phase space. The nuisance parameters are defined such that the prefit value is zero with unity uncertainty.

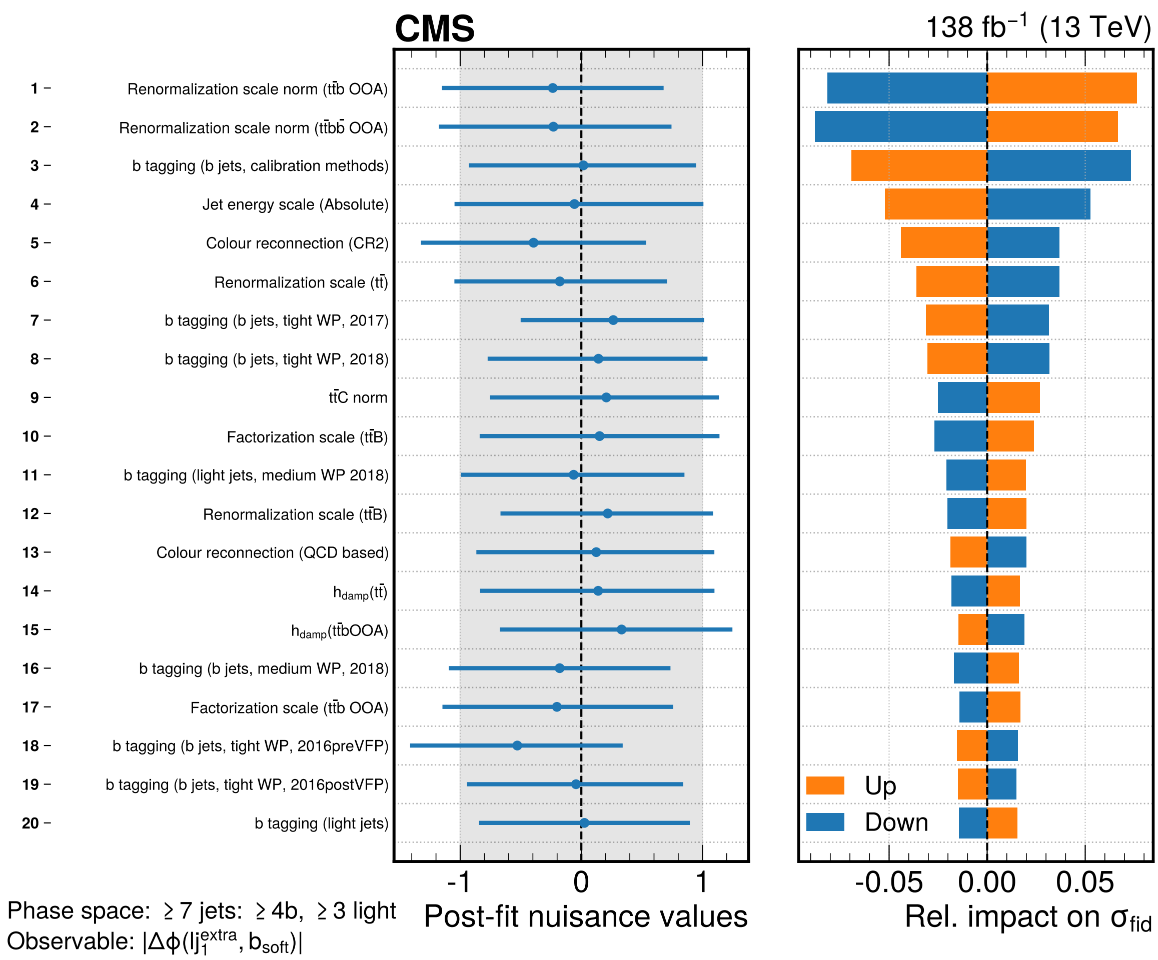


Figure A.4: Post-fit nuisance parameter values and relative impacts on the fiducial cross section, for the fit of $\Delta\phi$ between leading light jet and softest b jet in the $\geq$7 jets: $\geq$4b, $\geq$3 light phase space. The nuisance parameters are defined such that the prefit value is zero with unity uncertainty.

# B Groups of impacts

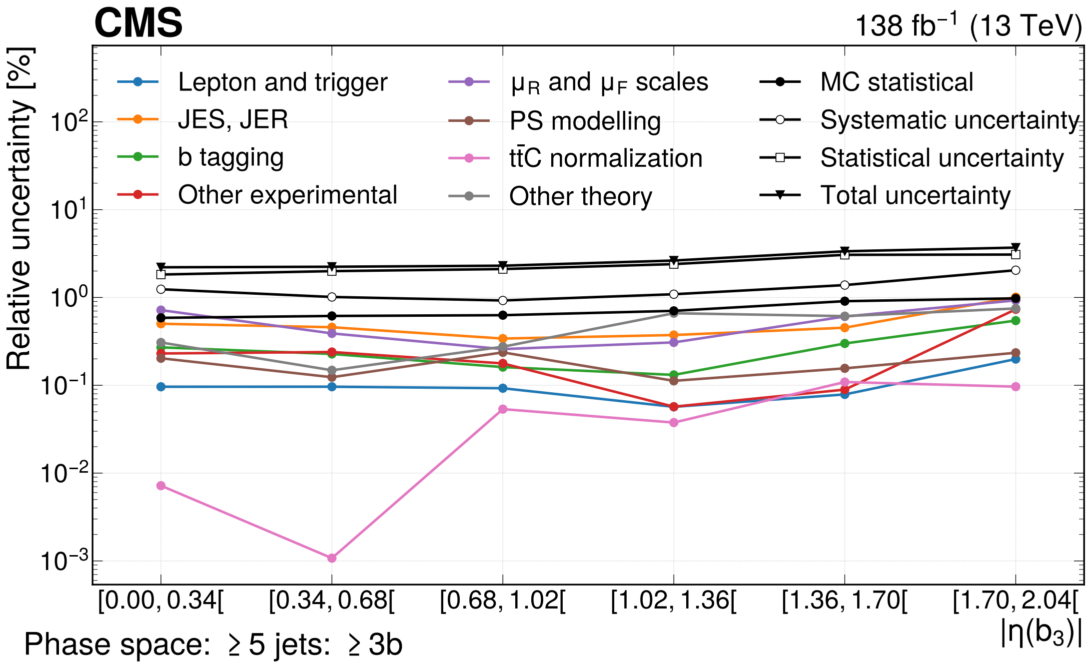


Figure B.1: Effect of the considered sources of uncertainties on the measurement of the normalized differential cross section of the $|\eta|$ of the b jet with third-highest $p_T$ in the $\geq$5 jets: $\geq$3b phase space, obtained by combining the impacts of associated nuisance parameters. The last bin of the distribution is not shown, since it has no associated parameter of interest but is constrained by the other bins. The category "other theory" includes b quark fragmentation, top quark $p_T$ modelling, PDF, $h_{damp}$, colour reconnection, and underlying event uncertainties. The category "other experimental" includes pileup and the integrated luminosity uncertainties.

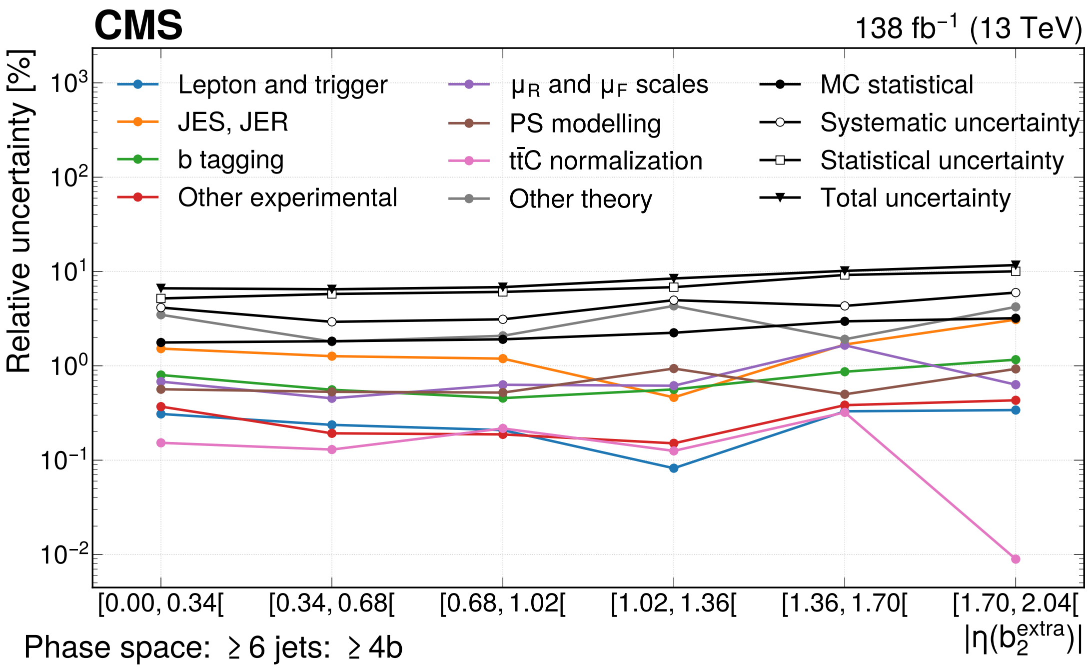


Figure B.2: Effect of the considered sources of uncertainties on the measurement of the normalized differential cross section of the $|\eta|$ of the subleading extra b jet in the ≥6 jets: ≥4b phase space, obtained by combining the impacts of associated nuisance parameters. The last bin of the distribution is not shown, since it has no associated parameter of interest but is constrained by the other bins. The category "other theory" includes b quark fragmentation, top quark $p_T$ modelling, PDF, $h_{damp}$, colour reconnection, and underlying event uncertainties. The category "other experimental" includes pileup and the integrated luminosity uncertainties.

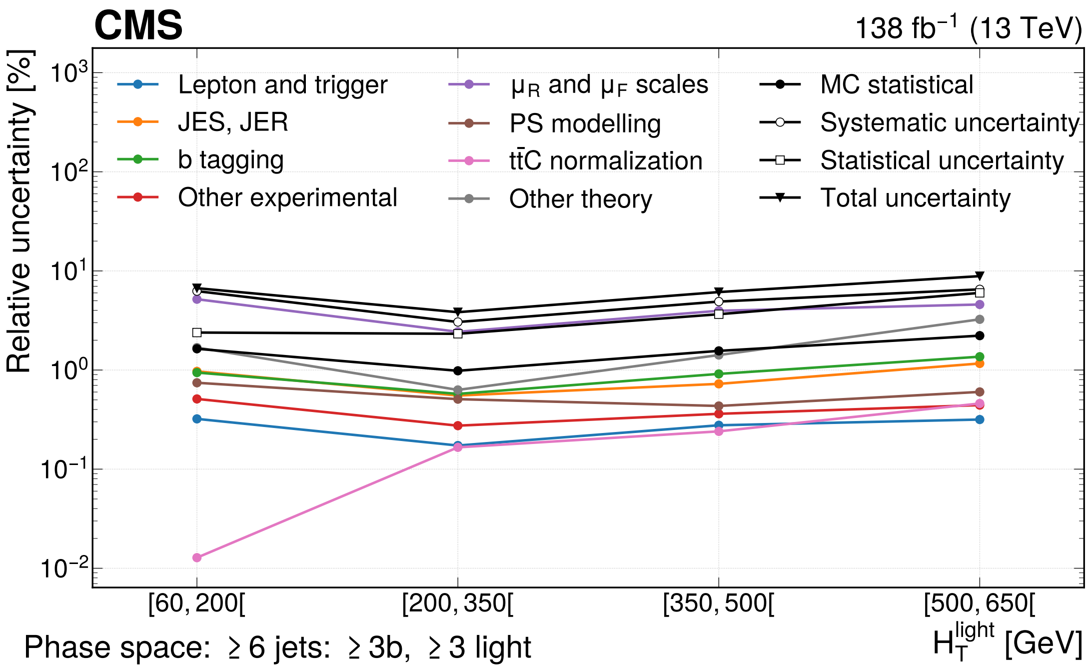


Figure B.3: Effect of the considered sources of uncertainties on the measurement of the normalized differential cross section of the $H_T$ of light jets in the ≥6 jets: ≥3b, ≥3 light phase space, obtained by combining the impacts of associated nuisance parameters. The last bin of the distribution is not shown, since it has no associated parameter of interest but is constrained by the other bins. The category "other theory" includes b quark fragmentation, top quark $p_T$ modelling, PDF, $h_{damp}$, colour reconnection, and underlying event uncertainties. The category "other experimental" includes pileup and the integrated luminosity uncertainties.

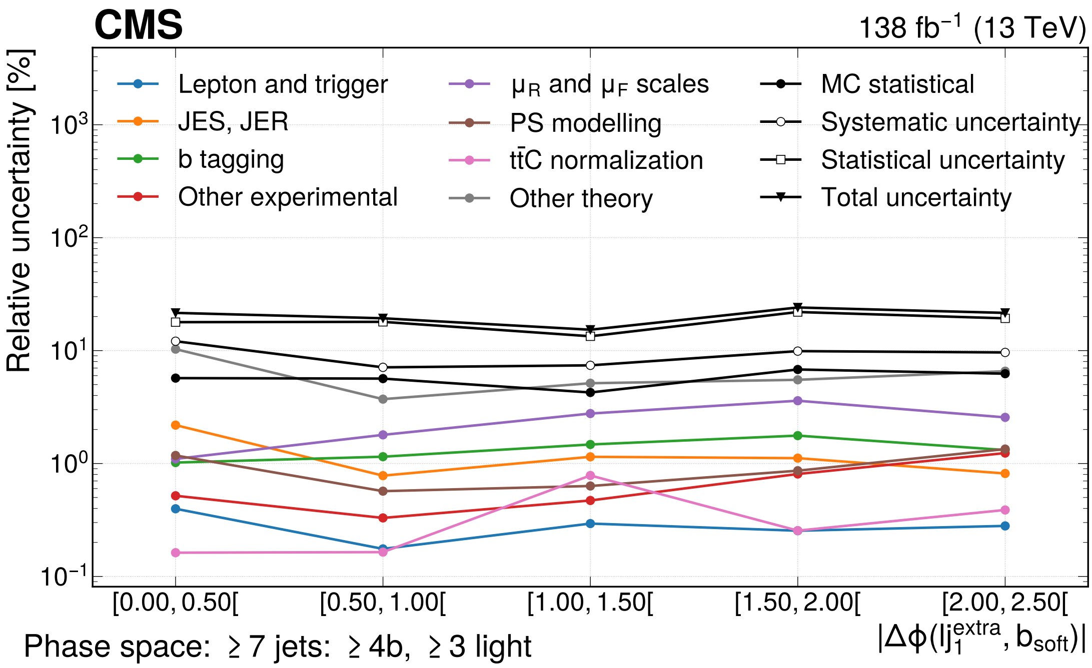


Figure B.4: Effect of the considered sources of uncertainties on the measurement of the normalized differential cross section of the $\Delta\phi$ between leading light jet and softest b jet in the ≥7 jets: ≥4b, ≥3 light phase space, obtained by combining the impacts of associated nuisance parameters. The last bin of the distribution is not shown, since it has no associated parameter of interest but is constrained by the other bins. The category "other theory" includes b quark fragmentation, top quark $p_T$ modelling, PDF, $h_{damp}$, colour reconnection, and underlying event uncertainties. The category "other experimental" includes pileup and the integrated luminosity uncertainties.

## C Correlation of POIs

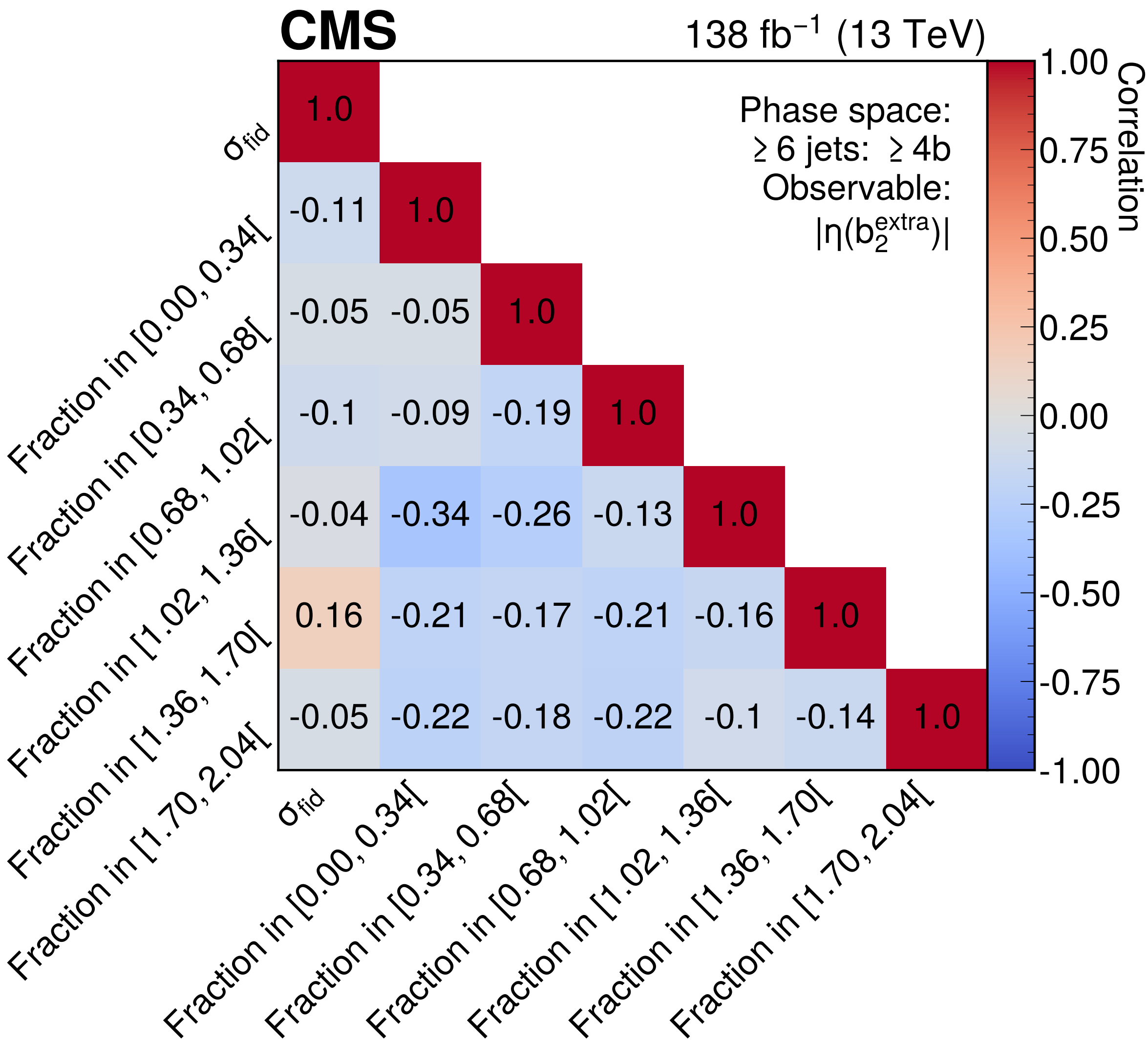


Figure C.1: Correlations between the parameters of interest $\vec{\mu}$ in the fit of the $|\eta|$ of the subleading extra b jet in the ≥6 jets: ≥4b phase space.

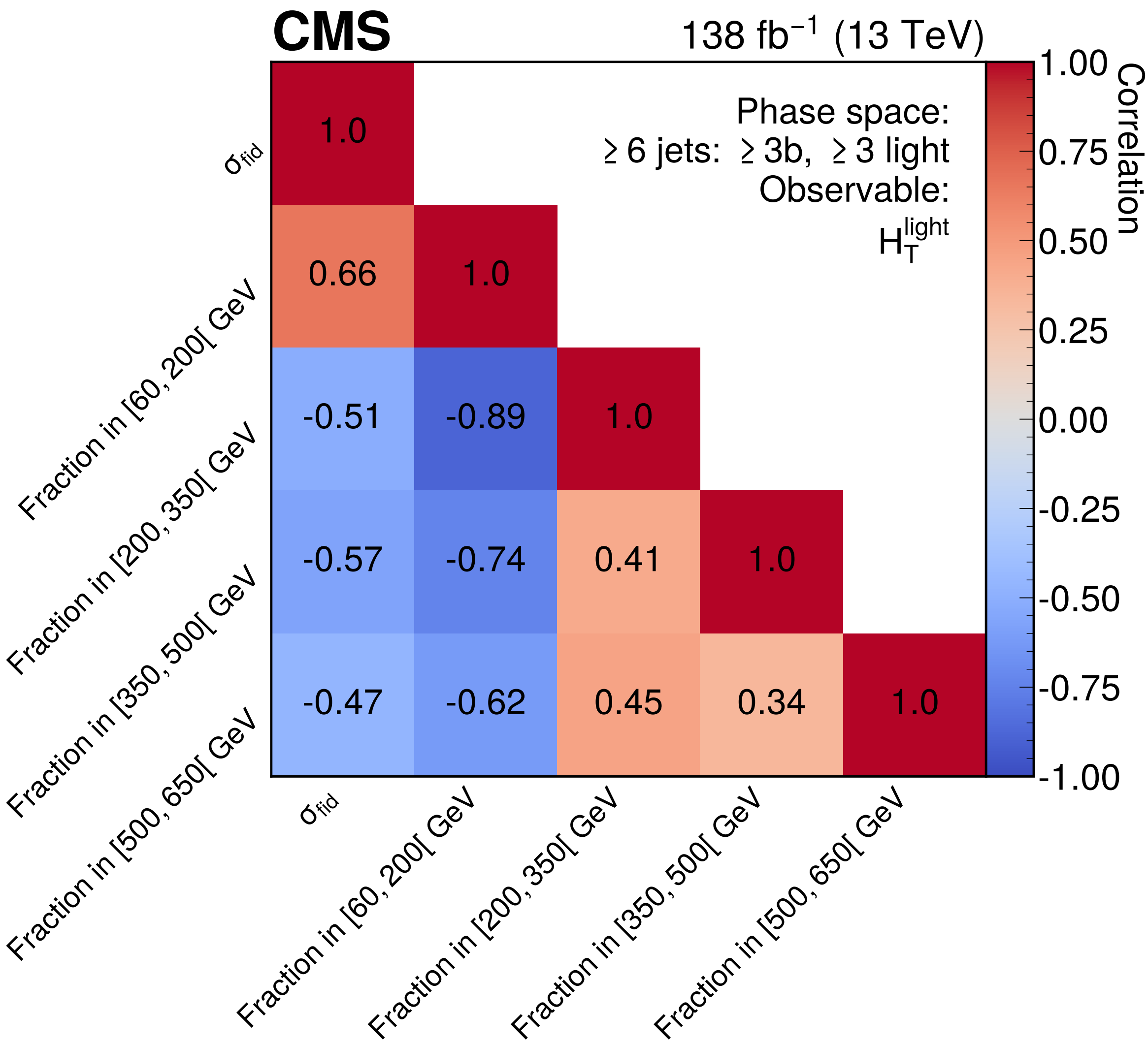


Figure C.2: Correlations between the parameters of interest $\vec{\mu}$ in the fit of the $H_T$ of light jets in the ≥6 jets: ≥3b, ≥3 light phase space.

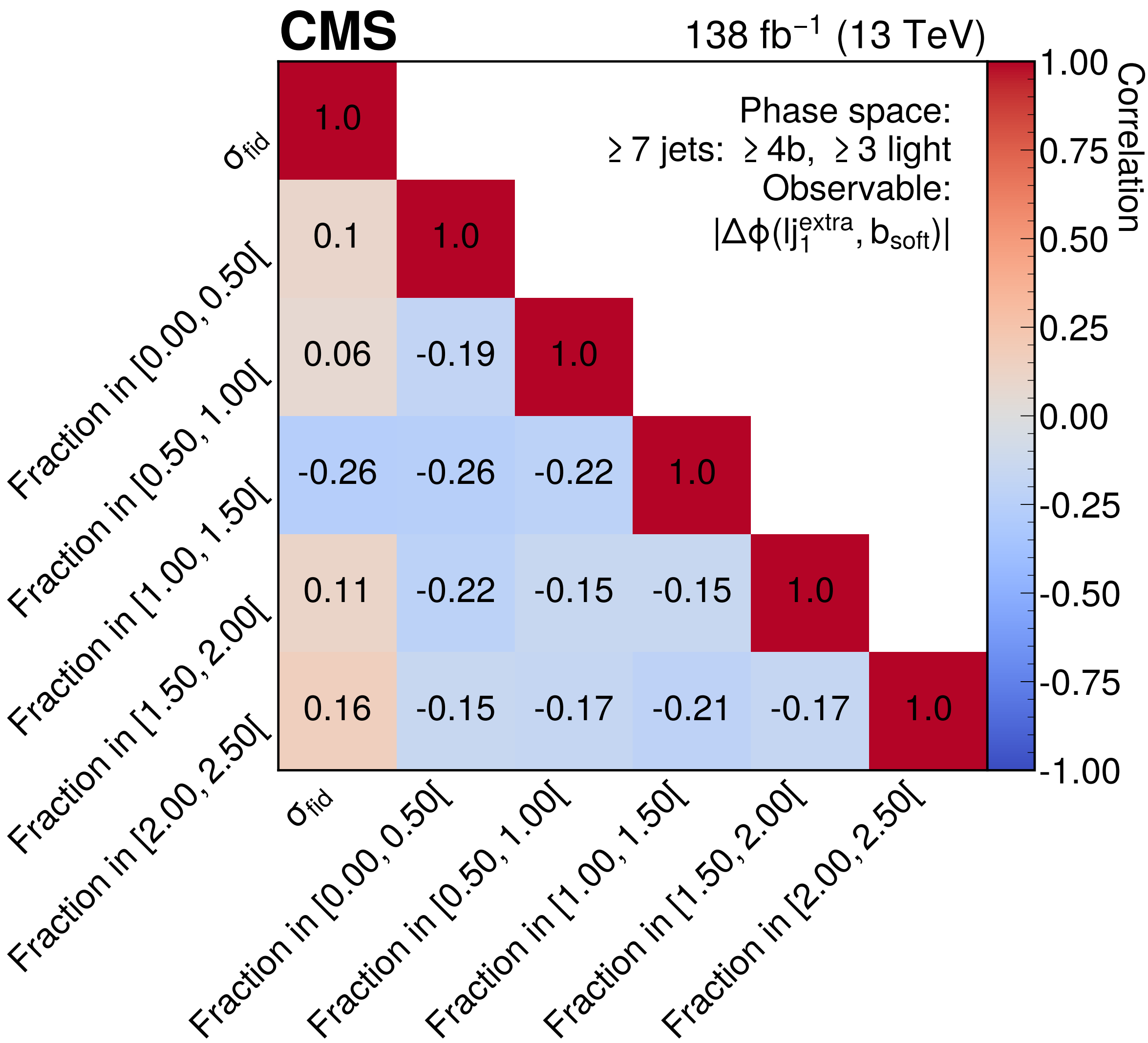


Figure C.3: Correlations between the parameters of interest $\vec{\mu}$ in the fit of the $\Delta\phi$ between leading light jet and softest b jet in the ≥7 jets: ≥4b, ≥3 light phase space.

# D Variation of renormalization and factorization scales

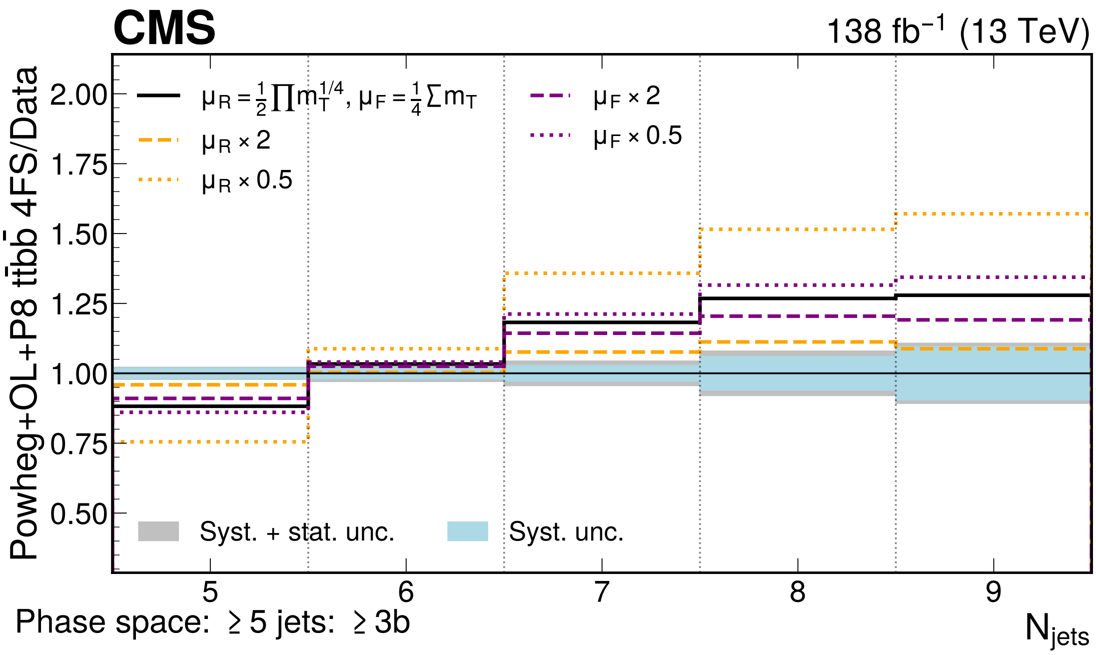


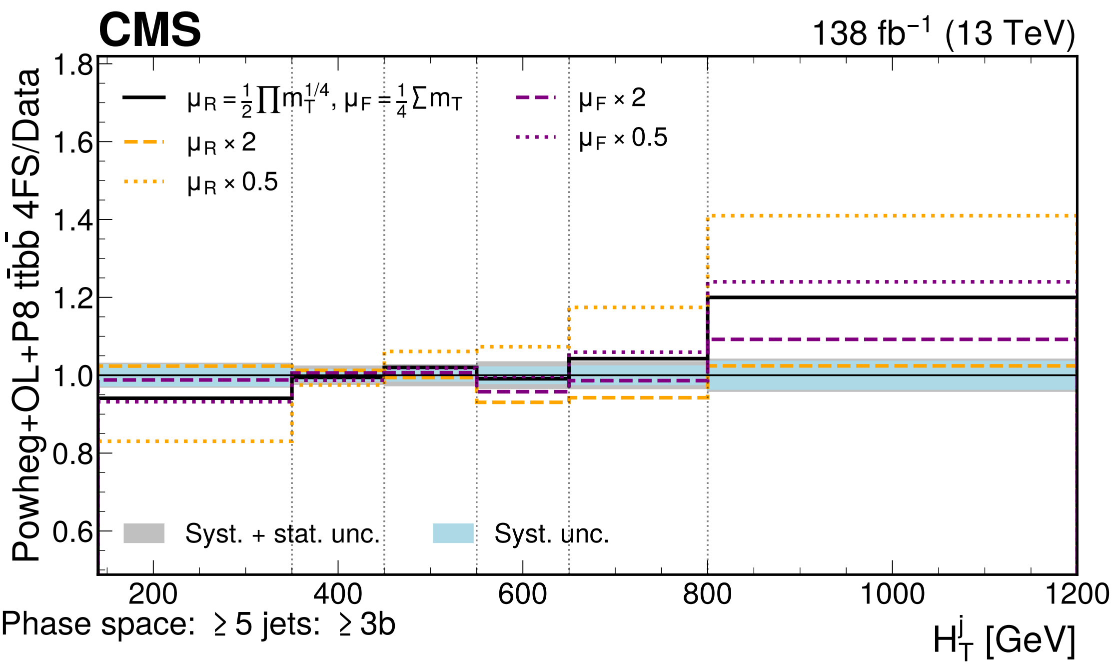


Figure D.1: Ratio of normalized differential cross section predictions of the POWHEG+OL+P8 $t\bar{t}b\bar{b}$ 4FS modeling approach with different $\mu_R$ and $\mu_F$ scale settings relative to the measured normalized differential cross sections for the number of jets (upper) and $H_T$ of jets (lower) in the ≥5 jets: ≥3b phase space. The systematic (total) uncertainties of the measurement are represented as grey (blue) bands. Variations of the $\mu_R$ ($\mu_F$) scale relative to the nominal scale setting are shown in orange (purple). The last bin in the distributions contains the overflow.

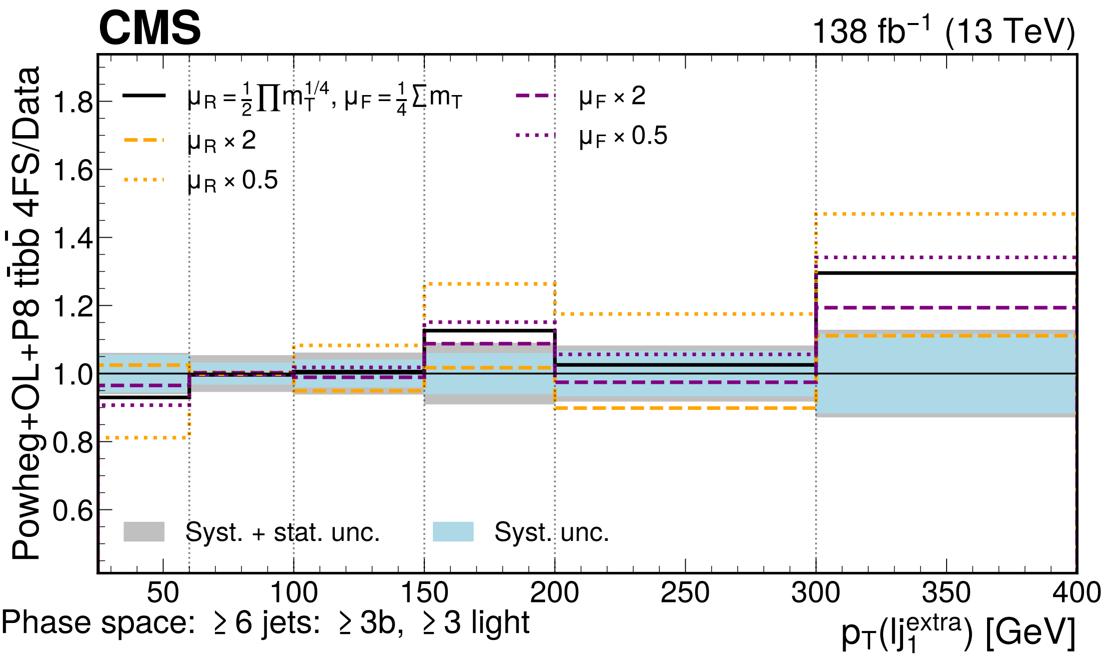


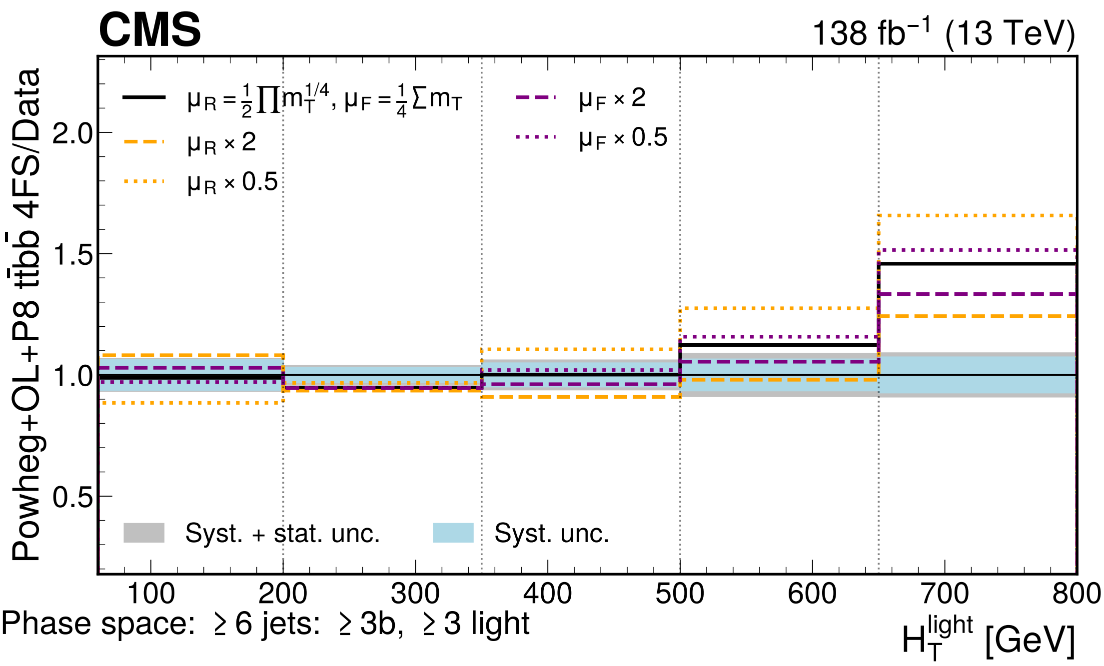


Figure D.2: Ratio of normalized differential cross section predictions of the POWHEG+OL+P8 $t\bar{t}b\bar{b}$ 4FS modeling approach with different $\mu_R$ and $\mu_F$ scale settings relative to the measured normalized differential cross sections for the extra light jet (upper) and $H_T$ of light jets (lower) in the ≥6 jets: ≥3b, ≥3 light phase space. The systematic (total) uncertainties of the measurement are represented as grey (blue) bands. The systematic (total) uncertainties of the measurement are represented as grey (blue) bands. Variations of the $\mu_R$ ($\mu_F$) scale relative to the nominal scale setting are shown in orange (purple). The last bin in the distributions contains the overflow.

# E Normalized differential cross section compatibility

Table E.1: Observed $z$ score for each of the theoretical predictions in the 5j3b phase space, given the unfolded data and covariance matrix. For the determination of the $z$ score, only the measurement uncertainties are considered.

| | Observed $z$ score | | | | | |
|---|---|---|---|---|---|---|
| 5j3b phase space | $H_T^b$ | $H_T^j$ | $N_b$ | $N_{jets}$ | $p_T(b_3)$ | $\|\eta(b_3)\|$ |
| MG5_aMC+P8 $t\bar{t}$+jets FxFx 5FS | 4.88 | 1.15 | 2.43 | 5.50 | 4.54 | 2.12 |
| MG5_aMC+P8 $t\bar{t}b\bar{b}$ 4FS | >6 | 5.07 | >6 | >6 | >6 | 2.01 |
| POWHEG+H7 $t\bar{t}$ 5FS | 2.00 | 4.10 | 0.46 | 4.45 | 1.53 | 2.27 |
| POWHEG+OL+P8 $t\bar{t}b\bar{b}$ 4FS | 3.14 | 4.56 | 4.43 | >6 | 2.19 | 2.61 |
| POWHEG+P8 $t\bar{t}$ 5FS | 3.01 | 3.05 | 1.73 | 5.17 | 1.88 | 2.52 |
| SHERPA+OL $t\bar{t}b\bar{b}$ 4FS | 3.14 | 0.16 | 5.18 | 5.37 | 3.08 | 2.31 |

Table E.2: Observed $z$ score for each of the theoretical predictions in the 6j4b phase space, given the unfolded data and covariance matrix. For the determination of the $z$ score, only the measurement uncertainties are considered.

| | Observed $z$ score | | | | | | | | |
|---|---|---|---|---|---|---|---|---|---|
| 6j4b phase space | $H_T^b$ | $H_T^j$ | $N_{jets}$ | $\Delta R_{bb}^{avg}$ | $m_{bb}^{max}$ | $p_T(b_3)$ | $p_T(b_4)$ | $\|\eta(b_3)\|$ | $\|\eta(b_4)\|$ |
| MG5_aMC+P8 $t\bar{t}$+jets FxFx 5FS | 0.41 | −0.83 | 1.91 | −1.30 | 1.63 | 1.19 | 0.27 | 0.10 | 0.98 |
| MG5_aMC+P8 $t\bar{t}b\bar{b}$ 4FS | 0.79 | 0.81 | 2.50 | −0.02 | 1.30 | 1.54 | 1.11 | 0.69 | 0.83 |
| POWHEG+H7 $t\bar{t}$ 5FS | 0.92 | 2.44 | 1.80 | −1.46 | 0.04 | 1.24 | 0.68 | 0.50 | −0.09 |
| POWHEG+OL+P8 $t\bar{t}b\bar{b}$ 4FS | 0.60 | 0.42 | 1.00 | −1.29 | 0.04 | 1.36 | 0.69 | 0.19 | 0.15 |
| POWHEG+P8 $t\bar{t}$ 5FS | 0.68 | 0.10 | 1.08 | −0.33 | 0.34 | 1.34 | 0.56 | 0.38 | 0.18 |
| SHERPA+OL $t\bar{t}b\bar{b}$ 4FS | 0.52 | 0.17 | 0.86 | 0.29 | 0.65 | 1.48 | 0.43 | 0.52 | 0.17 |

Table E.3: Observed $z$ score for each of the theoretical predictions in the 6j4b phase space of the observables related to the $bb^{extra}$ pair, given the unfolded data and covariance matrix. For the determination of the $z$ score, only the measurement uncertainties are considered.

| | Observed $z$ score | | | | | | | |
|---|---|---|---|---|---|---|---|---|
| 6j4b phase space | $\Delta R(bb^{extra})$ | $m(bb^{extra})$ | $p_T(bb^{extra})$ | $p_T(b_1^{extra})$ | $p_T(b_2^{extra})$ | $\|\eta(b_1^{extra})\|$ | $\|\eta(b_2^{extra})\|$ | $\|\eta(bb^{extra})\|$ |
| MG5_aMC+P8 $t\bar{t}$+jets FxFx 5FS | 1.31 | 0.56 | 0.42 | 0.27 | 0.63 | 0.76 | 0.17 | 0.51 |
| MG5_aMC+P8 $t\bar{t}b\bar{b}$ 4FS | 0.23 | −0.02 | 0.50 | 0.52 | −0.56 | 0.38 | −0.95 | 0.62 |
| POWHEG+H7 $t\bar{t}$ 5FS | 3.17 | 1.60 | 1.00 | 1.41 | 0.26 | 0.47 | −0.39 | 0.88 |
| POWHEG+OL+P8 $t\bar{t}b\bar{b}$ 4FS | −0.79 | −0.69 | 0.60 | 1.05 | −0.19 | −0.31 | −1.15 | 0.38 |
| POWHEG+P8 $t\bar{t}$ 5FS | 1.33 | 0.07 | 0.85 | 1.24 | −0.19 | 0.03 | −1.25 | 1.07 |
| SHERPA+OL $t\bar{t}b\bar{b}$ 4FS | 0.03 | −0.99 | 0.95 | 1.12 | −0.52 | 0.13 | −1.02 | 0.40 |

Table E.4: Observed $z$ score for each of the theoretical predictions in the 6j4b phase space of the observables related to the $bb^{add.}$ pair, given the unfolded data and covariance matrix. For the determination of the $z$ score, only the measurement uncertainties are considered.

| | Observed $z$ score | | | | | | | |
|---|---|---|---|---|---|---|---|---|
| 6j4b phase space | $\Delta R(bb^{add.})$ | $m(bb^{add.})$ | $p_T(bb^{add.})$ | $p_T(b_1^{add.})$ | $p_T(b_2^{add.})$ | $\|\eta(bb^{add.})\|$ | $\|\eta(b_1^{add.})\|$ | $\|\eta(b_2^{add.})\|$ |
| MG5_aMC+P8 $t\bar{t}$+jets FxFx 5FS | 1.09 | 0.81 | 0.83 | 1.14 | 0.86 | 0.30 | 1.51 | 0.27 |
| MG5_aMC+P8 $t\bar{t}b\bar{b}$ 4FS | −1.86 | −0.14 | 0.72 | 1.69 | 1.27 | 0.51 | 1.49 | −0.09 |
| POWHEG+H7 $t\bar{t}$ 5FS | 3.62 | 2.45 | 2.58 | 2.61 | 1.05 | 0.19 | 1.25 | −0.33 |
| POWHEG+OL+P8 $t\bar{t}b\bar{b}$ 4FS | −2.24 | −1.43 | 1.48 | 2.17 | 0.90 | 0.29 | 1.09 | −0.36 |
| POWHEG+P8 $t\bar{t}$ 5FS | −1.21 | −0.68 | 2.24 | 2.52 | 0.83 | 0.95 | 1.44 | −0.57 |

Table E.5: Observed $z$ score for each of the theoretical predictions in the 6j3b3l phase space, given the unfolded data and covariance matrix. For the determination of the $z$ score, only the measurement uncertainties are considered.

| | Observed $z$ score | | |
|---|---|---|---|
| 6j3b3l phase space | $H_T^{light}$ | $p_T(lj_1^{extra})$ | $\|\Delta\phi(lj_1^{extra}, b_{soft})\|$ |
| MG5_aMC+P8 $t\bar{t}$+jets FxFx 5FS | 1.71 | −0.14 | 0.81 |
| MG5_aMC+P8 $t\bar{t}b\bar{b}$ 4FS | 3.55 | 4.14 | 1.62 |
| POWHEG+H7 $t\bar{t}$ 5FS | 2.02 | 1.84 | 1.03 |
| POWHEG+OL+P8 $t\bar{t}b\bar{b}$ 4FS | 5.39 | 1.62 | −0.17 |
| POWHEG+P8 $t\bar{t}$ 5FS | 1.52 | 0.24 | 0.24 |
| SHERPA+OL $t\bar{t}b\bar{b}$ 4FS | 0.33 | 0.78 | 0.30 |

Table E.6: Observed $z$ score for each of the theoretical predictions in the 7j4b3l phase space, given the unfolded data and covariance matrix. For the determination of the $z$ score, only the measurement uncertainties are considered.

| | Observed $z$ score | | |
|---|---|---|---|
| 7j4b3l phase space | $H_T^{light}$ | $p_T(lj_1^{extra})$ | $\|\Delta\phi(lj_1^{extra}, b_{soft})\|$ |
| MG5_aMC+P8 $t\bar{t}$+jets FxFx 5FS | 1.14 | 1.66 | 0.10 |
| MG5_aMC+P8 $t\bar{t}b\bar{b}$ 4FS | −0.92 | 2.12 | 0.16 |
| POWHEG+H7 $t\bar{t}$ 5FS | 0.49 | −0.06 | 0.03 |
| POWHEG+OL+P8 $t\bar{t}b\bar{b}$ 4FS | 2.00 | 2.30 | −0.03 |
| POWHEG+P8 $t\bar{t}$ 5FS | 0.89 | 1.83 | 0.13 |
| SHERPA+OL $t\bar{t}b\bar{b}$ 4FS | 0.31 | 0.24 | 0.00 |

# F The CMS Collaboration

**Yerevan Physics Institute, Yerevan, Armenia**
A. Hayrapetyan, A. Tumasyan[1]

**Institut für Hochenergiephysik, Vienna, Austria**
W. Adam, J.W. Andrejkovic, T. Bergauer, S. Chatterjee, K. Damanakis, M. Dragicevic, A. Escalante Del Valle, P.S. Hussain, M. Jeitler[2], N. Krammer, D. Liko, I. Mikulec, J. Schieck[2], R. Schöfbeck, D. Schwarz, M. Sonawane, S. Templ, W. Waltenberger, C.-E. Wulz[2]

**Universiteit Antwerpen, Antwerpen, Belgium**
M.R. Darwish[3], T. Janssen, P. Van Mechelen

**Vrije Universiteit Brussel, Brussel, Belgium**
E.S. Bols, J. D'Hondt, S. Dansana, A. De Moor, M. Delcourt, H. El Faham, S. Lowette, I. Makarenko, A. Morton, D. Müller, A.R. Sahasransu, S. Tavernier, M. Tytgat[4], S. Van Putte, D. Vannerom

**Université Libre de Bruxelles, Bruxelles, Belgium**
B. Clerbaux, G. De Lentdecker, L. Favart, D. Hohov, J. Jaramillo, A. Khalilzadeh, K. Lee, M. Mahdavikhorrami, A. Malara, S. Paredes, L. Pétré, N. Postiau, L. Thomas, M. Vanden Bemden, C. Vander Velde, P. Vanlaer

**Ghent University, Ghent, Belgium**
M. De Coen, D. Dobur, Y. Hong, J. Knolle, L. Lambrecht, G. Mestdach, C. Rendón, A. Samalan, K. Skovpen, N. Van Den Bossche, L. Wezenbeek

**Université Catholique de Louvain, Louvain-la-Neuve, Belgium**
A. Benecke, G. Bruno, C. Caputo, C. Delaere, I.S. Donertas, A. Giammanco, K. Jaffel, Sa. Jain, V. Lemaitre, J. Lidrych, P. Mastrapasqua, K. Mondal, T.T. Tran, S. Wertz

**Centro Brasileiro de Pesquisas Fisicas, Rio de Janeiro, Brazil**
G.A. Alves, E. Coelho, C. Hensel, T. Menezes De Oliveira, A. Moraes, P. Rebello Teles, M. Soeiro

**Universidade do Estado do Rio de Janeiro, Rio de Janeiro, Brazil**
W.L. Aldá Júnior, M. Alves Gallo Pereira, M. Barroso Ferreira Filho, H. Brandao Malbouisson, W. Carvalho, J. Chinellato[5], E.M. Da Costa, G.G. Da Silveira[6], D. De Jesus Damiao, S. Fonseca De Souza, J. Martins[7], C. Mora Herrera, K. Mota Amarilo, L. Mundim, H. Nogima, A. Santoro, S.M. Silva Do Amaral, A. Sznajder, M. Thiel, A. Vilela Pereira

**Universidade Estadual Paulista, Universidade Federal do ABC, São Paulo, Brazil**
C.A. Bernardes[6], L. Calligaris, T.R. Fernandez Perez Tomei, E.M. Gregores, P.G. Mercadante, S.F. Novaes, B. Orzari, Sandra S. Padula

**Institute for Nuclear Research and Nuclear Energy, Bulgarian Academy of Sciences, Sofia, Bulgaria**
A. Aleksandrov, G. Antchev, R. Hadjiiska, P. Iaydjiev, M. Misheva, M. Shopova, G. Sultanov

**University of Sofia, Sofia, Bulgaria**
A. Dimitrov, T. Ivanov, L. Litov, B. Pavlov, P. Petkov, A. Petrov, E. Shumka

**Instituto De Alta Investigación, Universidad de Tarapacá, Casilla 7 D, Arica, Chile**
S. Keshri, S. Thakur

**Beihang University, Beijing, China**
T. Cheng, Q. Guo, T. Javaid, M. Mittal, L. Yuan

**Department of Physics, Tsinghua University, Beijing, China**
G. Bauer[8], Z. Hu, K. Yi[8,9]

**Institute of High Energy Physics, Beijing, China**
G.M. Chen[10], H.S. Chen[10], M. Chen[10], F. Iemmi, C.H. Jiang, A. Kapoor, H. Liao, Z.-A. Liu[11], F. Monti, R. Sharma, J.N. Song[11], J. Tao, J. Wang, H. Zhang

**State Key Laboratory of Nuclear Physics and Technology, Peking University, Beijing, China**
A. Agapitos, Y. Ban, A. Levin, C. Li, Q. Li, X. Lyu, Y. Mao, S.J. Qian, X. Sun, D. Wang, H. Yang, C. Zhou

**Sun Yat-Sen University, Guangzhou, China**
Z. You

**University of Science and Technology of China, Hefei, China**
N. Lu

**Institute of Modern Physics and Key Laboratory of Nuclear Physics and Ion-beam Application (MOE) - Fudan University, Shanghai, China**
X. Gao[12], D. Leggat, H. Okawa, Y. Zhang

**Zhejiang University, Hangzhou, Zhejiang, China**
Z. Lin, C. Lu, M. Xiao

**Universidad de Los Andes, Bogota, Colombia**
C. Avila, D.A. Barbosa Trujillo, A. Cabrera, C. Florez, J. Fraga, J.A. Reyes Vega

**Universidad de Antioquia, Medellin, Colombia**
J. Mejia Guisao, F. Ramirez, M. Rodriguez, J.D. Ruiz Alvarez

**University of Split, Faculty of Electrical Engineering, Mechanical Engineering and Naval Architecture, Split, Croatia**
D. Giljanovic, N. Godinovic, D. Lelas, A. Sculac

**University of Split, Faculty of Science, Split, Croatia**
M. Kovac, T. Sculac

**Institute Rudjer Boskovic, Zagreb, Croatia**
P. Bargassa, V. Brigljevic, B.K. Chitroda, D. Ferencek, S. Mishra, A. Starodumov[13], T. Susa

**University of Cyprus, Nicosia, Cyprus**
A. Attikis, K. Christoforou, S. Konstantinou, J. Mousa, C. Nicolaou, F. Ptochos, P.A. Razis, H. Rykaczewski, H. Saka, A. Stepennov

**Charles University, Prague, Czech Republic**
M. Finger, M. Finger Jr., A. Kveton

**Escuela Politecnica Nacional, Quito, Ecuador**
E. Ayala

**Universidad San Francisco de Quito, Quito, Ecuador**

E. Carrera Jarrin

**Academy of Scientific Research and Technology of the Arab Republic of Egypt, Egyptian Network of High Energy Physics, Cairo, Egypt**
H. Abdalla[14], Y. Assran[15,16]

**Center for High Energy Physics (CHEP-FU), Fayoum University, El-Fayoum, Egypt**
M.A. Mahmoud, Y. Mohammed

**National Institute of Chemical Physics and Biophysics, Tallinn, Estonia**
R.K. Dewanjee[17], K. Ehataht, M. Kadastik, T. Lange, S. Nandan, C. Nielsen, J. Pata, M. Raidal, L. Tani, C. Veelken

**Department of Physics, University of Helsinki, Helsinki, Finland**
H. Kirschenmann, K. Osterberg, M. Voutilainen

**Helsinki Institute of Physics, Helsinki, Finland**
S. Bharthuar, E. Brücken, F. Garcia, J. Havukainen, K.T.S. Kallonen, M.S. Kim, R. Kinnunen, T. Lampén, K. Lassila-Perini, S. Lehti, T. Lindén, M. Lotti, L. Martikainen, M. Myllymäki, M.m. Rantanen, H. Siikonen, E. Tuominen, J. Tuominiemi

**Lappeenranta-Lahti University of Technology, Lappeenranta, Finland**
P. Luukka, H. Petrow, T. Tuuva[†]

**IRFU, CEA, Université Paris-Saclay, Gif-sur-Yvette, France**
M. Besancon, F. Couderc, M. Dejardin, D. Denegri, J.L. Faure, F. Ferri, S. Ganjour, P. Gras, G. Hamel de Monchenault, V. Lohezic, J. Malcles, J. Rander, A. Rosowsky, M.Ö. Sahin, A. Savoy-Navarro[18], P. Simkina, M. Titov

**Laboratoire Leprince-Ringuet, CNRS/IN2P3, Ecole Polytechnique, Institut Polytechnique de Paris, Palaiseau, France**
C. Baldenegro Barrera, F. Beaudette, A. Buchot Perraguin, P. Busson, A. Cappati, C. Charlot, F. Damas, O. Davignon, G. Falmagne, B.A. Fontana Santos Alves, S. Ghosh, A. Gilbert, R. Granier de Cassagnac, A. Hakimi, B. Harikrishnan, L. Kalipoliti, G. Liu, J. Motta, M. Nguyen, C. Ochando, L. Portales, R. Salerno, U. Sarkar, J.B. Sauvan, Y. Sirois, A. Tarabini, E. Vernazza, A. Zabi, A. Zghiche

**Université de Strasbourg, CNRS, IPHC UMR 7178, Strasbourg, France**
J.-L. Agram[19], J. Andrea, D. Apparu, D. Bloch, J.-M. Brom, E.C. Chabert, C. Collard, S. Falke, U. Goerlach, C. Grimault, R. Haeberle, A.-C. Le Bihan, M.A. Sessini, P. Van Hove

**Institut de Physique des 2 Infinis de Lyon (IP2I ), Villeurbanne, France**
S. Beauceron, B. Blancon, G. Boudoul, N. Chanon, J. Choi, D. Contardo, P. Depasse, C. Dozen[20], H. El Mamouni, J. Fay, S. Gascon, M. Gouzevitch, C. Greenberg, G. Grenier, B. Ille, I.B. Laktineh, M. Lethuillier, L. Mirabito, S. Perries, M. Vander Donckt, P. Verdier, J. Xiao

**Georgian Technical University, Tbilisi, Georgia**
I. Lomidze, T. Toriashvili[21], Z. Tsamalaidze[13]

**RWTH Aachen University, I. Physikalisches Institut, Aachen, Germany**
V. Botta, L. Feld, K. Klein, M. Lipinski, D. Meuser, A. Pauls, N. Röwert, M. Teroerde

**RWTH Aachen University, III. Physikalisches Institut A, Aachen, Germany**
S. Diekmann, A. Dodonova, N. Eich, D. Eliseev, F. Engelke, M. Erdmann, P. Fackeldey, B. Fischer, T. Hebbeker, K. Hoepfner, F. Ivone, A. Jung, M.y. Lee, L. Mastrolorenzo, M. Merschmeyer, A. Meyer, S. Mukherjee, D. Noll, A. Novak, F. Nowotny, A. Pozdnyakov, Y. Rath, W. Redjeb, F. Rehm, H. Reithler, V. Sarkisovi, A. Schmidt, S.C. Schuler, A. Sharma, A. Stein, F. Torres Da Silva De Araujo[22], L. Vigilante, S. Wiedenbeck, S. Zaleski

**RWTH Aachen University, III. Physikalisches Institut B, Aachen, Germany**
C. Dziwok, G. Flügge, W. Haj Ahmad[23], T. Kress, A. Nowack, O. Pooth, A. Stahl, T. Ziemons, A. Zotz

**Deutsches Elektronen-Synchrotron, Hamburg, Germany**
H. Aarup Petersen, M. Aldaya Martin, J. Alimena, S. Amoroso, Y. An, S. Baxter, M. Bayatmakou, H. Becerril Gonzalez, O. Behnke, A. Belvedere, S. Bhattacharya, F. Blekman[24], K. Borras[25], D. Brunner, A. Campbell, A. Cardini, C. Cheng, F. Colombina, S. Consuegra Rodríguez, G. Correia Silva, M. De Silva, G. Eckerlin, D. Eckstein, L.I. Estevez Banos, O. Filatov, E. Gallo[24], A. Geiser, A. Giraldi, G. Greau, V. Guglielmi, M. Guthoff, A. Hinzmann, A. Jafari[26], L. Jeppe, N.Z. Jomhari, B. Kaech, M. Kasemann, H. Kaveh, C. Kleinwort, R. Kogler, M. Komm, D. Krücker, W. Lange, D. Leyva Pernia, K. Lipka[27], W. Lohmann[28], R. Mankel, I.-A. Melzer-Pellmann, M. Mendizabal Morentin, J. Metwally, A.B. Meyer, G. Milella, A. Mussgiller, A. Nürnberg, Y. Otarid, D. Pérez Adán, E. Ranken, A. Raspereza, B. Ribeiro Lopes, J. Rübenach, A. Saggio, M. Scham[29,25], V. Scheurer, S. Schnake[25], P. Schütze, C. Schwanenberger[24], M. Shchedrolosiev, R.E. Sosa Ricardo, L.P. Sreelatha Pramod, D. Stafford, F. Vazzoler, A. Ventura Barroso, R. Walsh, Q. Wang, Y. Wen, K. Wichmann, L. Wiens[25], C. Wissing, S. Wuchterl, Y. Yang, A. Zimermmane Castro Santos

**University of Hamburg, Hamburg, Germany**
A. Albrecht, S. Albrecht, M. Antonello, S. Bein, L. Benato, M. Bonanomi, P. Connor, M. Eich, K. El Morabit, Y. Fischer, A. Fröhlich, C. Garbers, E. Garutti, A. Grohsjean, M. Hajheidari, J. Haller, H.R. Jabusch, G. Kasieczka, P. Keicher, R. Klanner, W. Korcari, T. Kramer, V. Kutzner, F. Labe, J. Lange, A. Lobanov, C. Matthies, A. Mehta, L. Moureaux, M. Mrowietz, A. Nigamova, Y. Nissan, A. Paasch, K.J. Pena Rodriguez, T. Quadfasel, B. Raciti, M. Rieger, D. Savoiu, J. Schindler, P. Schleper, M. Schröder, J. Schwandt, M. Sommerhalder, H. Stadie, G. Steinbrück, A. Tews, M. Wolf

**Karlsruher Institut fuer Technologie, Karlsruhe, Germany**
S. Brommer, M. Burkart, E. Butz, T. Chwalek, A. Dierlamm, A. Droll, N. Faltermann, M. Giffels, A. Gottmann, F. Hartmann[30], M. Horzela, U. Husemann, M. Klute, R. Koppenhöfer, M. Link, A. Lintuluoto, S. Maier, S. Mitra, M. Mormile, Th. Müller, M. Neukum, M. Oh, E. Pfeffer, G. Quast, K. Rabbertz, I. Shvetsov, H.J. Simonis, N. Trevisani, R. Ulrich, J. van der Linden, R.F. Von Cube, M. Wassmer, S. Wieland, F. Wittig, R. Wolf, S. Wunsch, X. Zuo

**Institute of Nuclear and Particle Physics (INPP), NCSR Demokritos, Aghia Paraskevi, Greece**
G. Anagnostou, P. Assiouras, G. Daskalakis, A. Kyriakis, A. Papadopoulos[30], A. Stakia

**National and Kapodistrian University of Athens, Athens, Greece**

D. Karasavvas, P. Kontaxakis, G. Melachroinos, A. Panagiotou, I. Papavergou, I. Paraskevas, N. Saoulidou, K. Theofilatos, E. Tziaferi, K. Vellidis, I. Zisopoulos

**National Technical University of Athens, Athens, Greece**
G. Bakas, T. Chatzistavrou, G. Karapostoli, K. Kousouris, I. Papakrivopoulos, E. Siamarkou, G. Tsipolitis, A. Zacharopoulou

**University of Ioánnina, Ioánnina, Greece**
K. Adamidis, I. Bestintzanos, I. Evangelou, C. Foudas, P. Gianneios, C. Kamtsikis, P. Katsoulis, P. Kokkas, P.G. Kosmoglou Kioseoglou, N. Manthos, I. Papadopoulos, J. Strologas

**MTA-ELTE Lendület CMS Particle and Nuclear Physics Group, Eötvös Loránd University, Budapest, Hungary**
M. Csanád, K. Farkas, M.M.A. Gadallah[31], Á. Kadlecsik, P. Major, K. Mandal, G. Pásztor, A.J. Rádl[32], G.I. Veres

**Wigner Research Centre for Physics, Budapest, Hungary**
M. Bartók[33], C. Hajdu, D. Horvath[34,35], F. Sikler, V. Veszpremi

**Institute of Nuclear Research ATOMKI, Debrecen, Hungary**
G. Bencze, S. Czellar, J. Karancsi[33], J. Molnar, Z. Szillasi

**Institute of Physics, University of Debrecen, Debrecen, Hungary**
P. Raics, B. Ujvari[36], G. Zilizi

**Karoly Robert Campus, MATE Institute of Technology, Gyongyos, Hungary**
T. Csorgo[32], F. Nemes[32], T. Novak

**Panjab University, Chandigarh, India**
J. Babbar, S. Bansal, S.B. Beri, V. Bhatnagar, G. Chaudhary, S. Chauhan, N. Dhingra[37], R. Gupta, A. Kaur, A. Kaur, H. Kaur, M. Kaur, S. Kumar, P. Kumari, M. Meena, K. Sandeep, T. Sheokand, J.B. Singh[38], A. Singla

**University of Delhi, Delhi, India**
A. Ahmed, A. Bhardwaj, A. Chhetri, B.C. Choudhary, A. Kumar, M. Naimuddin, K. Ranjan, S. Saumya

**Saha Institute of Nuclear Physics, HBNI, Kolkata, India**
S. Baradia, S. Barman[39], S. Bhattacharya, D. Bhowmik, S. Dutta, S. Dutta, B. Gomber[40], P. Palit, G. Saha, B. Sahu[40], S. Sarkar

**Indian Institute of Technology Madras, Madras, India**
P.K. Behera, S.C. Behera, S. Chatterjee, P. Jana, P. Kalbhor, J.R. Komaragiri[41], D. Kumar[41], M. Mohammad Mobassir Ameen, L. Panwar[41], R. Pradhan, P.R. Pujahari, N.R. Saha, A. Sharma, A.K. Sikdar, S. Verma

**Tata Institute of Fundamental Research-A, Mumbai, India**
T. Aziz, I. Das, S. Dugad, M. Kumar, G.B. Mohanty, P. Suryadevara

**Tata Institute of Fundamental Research-B, Mumbai, India**
A. Bala, S. Banerjee, R.M. Chatterjee, M. Guchait, S. Karmakar, S. Kumar, G. Majumder, K. Mazumdar, S. Mukherjee, A. Thachayath

**National Institute of Science Education and Research, An OCC of Homi Bhabha National Institute, Bhubaneswar, Odisha, India**

S. Bahinipati[42], A.K. Das, C. Kar, D. Maity[43], P. Mal, T. Mishra, V.K. Muraleedharan Nair Bindhu[43], K. Naskar[43], A. Nayak[43], P. Sadangi, P. Saha, S.K. Swain, S. Varghese[43], D. Vats[43]

**Indian Institute of Science Education and Research (IISER), Pune, India**
A. Alpana, S. Dube, B. Kansal, A. Laha, A. Rastogi, S. Sharma

**Isfahan University of Technology, Isfahan, Iran**
H. Bakhshiansohi[44], E. Khazaie, M. Zeinali[45]

**Institute for Research in Fundamental Sciences (IPM), Tehran, Iran**
S. Chenarani[46], S.M. Etesami, M. Khakzad, M. Mohammadi Najafabadi

**University College Dublin, Dublin, Ireland**
M. Grunewald

**INFN Sezione di Bari[a], Università di Bari[b], Politecnico di Bari[c], Bari, Italy**
M. Abbrescia[a,b], R. Aly[a,c,47], A. Colaleo[a], D. Creanza[a,c], B. D' Anzi[a,b], N. De Filippis[a,c], M. De Palma[a,b], A. Di Florio[a,c], W. Elmetenawee[a,b,47], L. Fiore[a], G. Iaselli[a,c], G. Maggi[a,c], M. Maggi[a], I. Margjeka[a,b], V. Mastrapasqua[a,b], S. My[a,b], S. Nuzzo[a,b], A. Pellecchia[a,b], A. Pompili[a,b], G. Pugliese[a,c], R. Radogna[a], G. Ramirez-Sanchez[a,c], D. Ramos[a], A. Ranieri[a], L. Silvestris[a], F.M. Simone[a,b], Ü. Sözbilir[a], A. Stamerra[a], R. Venditti[a], P. Verwilligen[a], A. Zaza[a,b]

**INFN Sezione di Bologna[a], Università di Bologna[b], Bologna, Italy**
G. Abbiendi[a], C. Battilana[a,b], L. Borgonovi[a], R. Campanini[a,b], P. Capiluppi[a,b], A. Castro[a,b], F.R. Cavallo[a], M. Cuffiani[a,b], G.M. Dallavalle[a], T. Diotalevi[a,b], F. Fabbri[a], A. Fanfani[a,b], D. Fasanella[a,b], P. Giacomelli[a], L. Giommi[a,b], C. Grandi[a], L. Guiducci[a,b], S. Lo Meo[a,48], L. Lunerti[a,b], S. Marcellini[a], G. Masetti[a], F.L. Navarria[a,b], A. Perrotta[a], F. Primavera[a,b], A.M. Rossi[a,b], T. Rovelli[a,b], G.P. Siroli[a,b]

**INFN Sezione di Catania[a], Università di Catania[b], Catania, Italy**
S. Costa[a,b,49], A. Di Mattia[a], R. Potenza[a,b], A. Tricomi[a,b,49], C. Tuve[a,b]

**INFN Sezione di Firenze[a], Università di Firenze[b], Firenze, Italy**
G. Barbagli[a], G. Bardelli[a,b], B. Camaiani[a,b], A. Cassese[a], R. Ceccarelli[a], V. Ciulli[a,b], C. Civinini[a], R. D'Alessandro[a,b], E. Focardi[a,b], G. Latino[a,b], P. Lenzi[a,b], M. Lizzo[a,b], M. Meschini[a], S. Paoletti[a], A. Papanastassiou[a,b], G. Sguazzoni[a], L. Viliani[a]

**INFN Laboratori Nazionali di Frascati, Frascati, Italy**
L. Benussi, S. Bianco, S. Meola[50], D. Piccolo

**INFN Sezione di Genova[a], Università di Genova[b], Genova, Italy**
P. Chatagnon[a], F. Ferro[a], E. Robutti[a], S. Tosi[a,b]

**INFN Sezione di Milano-Bicocca[a], Università di Milano-Bicocca[b], Milano, Italy**
A. Benaglia[a], G. Boldrini[a], F. Brivio[a], F. Cetorelli[a], F. De Guio[a,b], M.E. Dinardo[a,b], P. Dini[a], S. Gennai[a], A. Ghezzi[a,b], P. Govoni[a,b], L. Guzzi[a], M.T. Lucchini[a,b], M. Malberti[a], S. Malvezzi[a], A. Massironi[a], D. Menasce[a], L. Moroni[a], M. Paganoni[a,b], D. Pedrini[a], B.S. Pinolini[a], S. Ragazzi[a,b], N. Redaelli[a], T. Tabarelli de Fatis[a,b], D. Zuolo[a]

**INFN Sezione di Napoli[a], Università di Napoli 'Federico II'[b], Napoli, Italy; Università della Basilicata[c], Potenza, Italy; Università G. Marconi[d], Roma, Italy**
S. Buontempo[a], A. Cagnotta[a,b], F. Carnevali[a,b], N. Cavallo[a,c], A. De Iorio[a,b], F. Fabozzi[a,c], A.O.M. Iorio[a,b], L. Lista[a,b,51], P. Paolucci[a,30], B. Rossi[a], C. Sciacca[a,b]

**INFN Sezione di Padova[a], Università di Padova[b], Padova, Italy; Università di Trento[c], Trento, Italy**
R. Ardino[a], P. Azzi[a], N. Bacchetta[a,52], D. Bisello[a,b], P. Bortignon[a], A. Bragagnolo[a,b], R. Carlin[a,b], P. Checchia[a], T. Dorigo[a], F. Gasparini[a,b], U. Gasparini[a,b], G. Grosso[a], L. Layer[a,53], E. Lusiani[a], M. Margoni[a,b], A.T. Meneguzzo[a,b], M. Migliorini[a,b], J. Pazzini[a,b], P. Ronchese[a,b], R. Rossin[a,b], F. Simonetto[a,b], G. Strong[a], M. Tosi[a,b], A. Triossi[a,b], S. Ventura[a], H. Yarar[a,b], M. Zanetti[a,b], P. Zotto[a,b], A. Zucchetta[a,b], G. Zumerle[a,b]

**INFN Sezione di Pavia[a], Università di Pavia[b], Pavia, Italy**
S. Abu Zeid[a,54], C. Aimè[a,b], A. Braghieri[a], S. Calzaferri[a,b], D. Fiorina[a,b], P. Montagna[a,b], V. Re[a], C. Riccardi[a,b], P. Salvini[a], I. Vai[a,b], P. Vitulo[a,b]

**INFN Sezione di Perugia[a], Università di Perugia[b], Perugia, Italy**
S. Ajmal[a,b], P. Asenov[a,55], G.M. Bilei[a], D. Ciangottini[a,b], L. Fanò[a,b], M. Magherini[a,b], G. Mantovani[a,b], V. Mariani[a,b], M. Menichelli[a], F. Moscatelli[a,55], A. Piccinelli[a,b], M. Presilla[a,b], A. Rossi[a,b], A. Santocchia[a,b], D. Spiga[a], T. Tedeschi[a,b]

**INFN Sezione di Pisa[a], Università di Pisa[b], Scuola Normale Superiore di Pisa[c], Pisa, Italy; Università di Siena[d], Siena, Italy**
P. Azzurri[a], G. Bagliesi[a], R. Bhattacharya[a], L. Bianchini[a,b], T. Boccali[a], E. Bossini[a], D. Bruschini[a,c], R. Castaldi[a], M.A. Ciocci[a,b], M. Cipriani[a,b], V. D'Amante[a,d], R. Dell'Orso[a], S. Donato[a], A. Giassi[a], F. Ligabue[a,c], D. Matos Figueiredo[a], A. Messineo[a,b], M. Musich[a,b], F. Palla[a], S. Parolia[a], A. Rizzi[a,b], G. Rolandi[a,c], S. Roy Chowdhury[a], T. Sarkar[a], A. Scribano[a], P. Spagnolo[a], R. Tenchini[a,b], G. Tonelli[a,b], N. Turini[a,d], A. Venturi[a], P.G. Verdini[a]

**INFN Sezione di Roma[a], Sapienza Università di Roma[b], Roma, Italy**
P. Barria[a], M. Campana[a,b], F. Cavallari[a], L. Cunqueiro Mendez[a,b], D. Del Re[a,b], E. Di Marco[a], M. Diemoz[a], F. Errico[a,b], E. Longo[a,b], P. Meridiani[a], J. Mijuskovic[a,b], G. Organtini[a,b], F. Pandolfi[a], R. Paramatti[a,b], C. Quaranta[a,b], S. Rahatlou[a,b], C. Rovelli[a], F. Santanastasio[a,b], L. Soffi[a], R. Tramontano[a,b]

**INFN Sezione di Torino[a], Università di Torino[b], Torino, Italy; Università del Piemonte Orientale[c], Novara, Italy**
N. Amapane[a,b], R. Arcidiacono[a,c], S. Argiro[a,b], M. Arneodo[a,c], N. Bartosik[a], R. Bellan[a,b], A. Bellora[a,b], C. Biino[a], N. Cartiglia[a], M. Costa[a,b], R. Covarelli[a,b], N. Demaria[a], L. Finco[a], M. Grippo[a,b], B. Kiani[a,b], F. Legger[a], F. Luongo[a,b], C. Mariotti[a], S. Maselli[a], A. Mecca[a,b], E. Migliore[a,b], M. Monteno[a], R. Mulargia[a], M.M. Obertino[a,b], G. Ortona[a], L. Pacher[a,b], N. Pastrone[a], M. Pelliccioni[a], M. Ruspa[a,c], F. Siviero[a,b], V. Sola[a,b], A. Solano[a,b], D. Soldi[a,b], A. Staiano[a], C. Tarricone[a,b], M. Tornago[a,b], D. Trocino[a], G. Umoret[a,b], A. Vagnerini[a,b], E. Vlasov[a,b]

**INFN Sezione di Trieste[a], Università di Trieste[b], Trieste, Italy**

S. Belforte[a], V. Candelise[a,b], M. Casarsa[a], F. Cossutti[a], K. De Leo[a,b], G. Della Ricca[a,b]

**Kyungpook National University, Daegu, Korea**
S. Dogra, J. Hong, C. Huh, B. Kim, D.H. Kim, J. Kim, H. Lee, S.W. Lee, C.S. Moon, Y.D. Oh, S.I. Pak, M.S. Ryu, S. Sekmen, Y.C. Yang

**Chonnam National University, Institute for Universe and Elementary Particles, Kwangju, Korea**
G. Bak, P. Gwak, H. Kim, D.H. Moon

**Hanyang University, Seoul, Korea**
E. Asilar, D. Kim, T.J. Kim, J.A. Merlin, J. Park, J. Song

**Korea University, Seoul, Korea**
S. Choi, S. Han, B. Hong, K. Lee, K.S. Lee, J. Park, S.K. Park, J. Yoo

**Kyung Hee University, Department of Physics, Seoul, Korea**
J. Goh

**Sejong University, Seoul, Korea**
H. S. Kim, Y. Kim, S. Lee

**Seoul National University, Seoul, Korea**
J. Almond, J.H. Bhyun, J. Choi, S. Jeon, W. Jun, J. Kim, J.S. Kim, S. Ko, H. Kwon, H. Lee, J. Lee, J. Lee, S. Lee, B.H. Oh, S.B. Oh, H. Seo, U.K. Yang, I. Yoon

**University of Seoul, Seoul, Korea**
W. Jang, D.Y. Kang, Y. Kang, S. Kim, B. Ko, J.S.H. Lee, Y. Lee, I.C. Park, Y. Roh, I.J. Watson, S. Yang

**Yonsei University, Department of Physics, Seoul, Korea**
S. Ha, H.D. Yoo

**Sungkyunkwan University, Suwon, Korea**
M. Choi, M.R. Kim, H. Lee, Y. Lee, I. Yu

**College of Engineering and Technology, American University of the Middle East (AUM), Dasman, Kuwait**
T. Beyrouthy, Y. Maghrbi

**Riga Technical University, Riga, Latvia**
K. Dreimanis, A. Gaile, G. Pikurs, A. Potrebko, M. Seidel, V. Veckalns[56]

**University of Latvia (LU), Riga, Latvia**
N.R. Strautnieks

**Vilnius University, Vilnius, Lithuania**
M. Ambrozas, A. Juodagalvis, A. Rinkevicius, G. Tamulaitis

**National Centre for Particle Physics, Universiti Malaya, Kuala Lumpur, Malaysia**
N. Bin Norjoharuddeen, I. Yusuff[57], Z. Zolkapli

**Universidad de Sonora (UNISON), Hermosillo, Mexico**
J.F. Benitez, A. Castaneda Hernandez, H.A. Encinas Acosta, L.G. Gallegos Maríñez, M. León Coello, J.A. Murillo Quijada, A. Sehrawat, L. Valencia Palomo

**Centro de Investigacion y de Estudios Avanzados del IPN, Mexico City, Mexico**

G. Ayala, H. Castilla-Valdez, E. De La Cruz-Burelo, I. Heredia-De La Cruz[58], R. Lopez-Fernandez, C.A. Mondragon Herrera, D.A. Perez Navarro, A. Sánchez Hernández

**Universidad Iberoamericana, Mexico City, Mexico**
C. Oropeza Barrera, M. Ramírez García

**Benemerita Universidad Autonoma de Puebla, Puebla, Mexico**
I. Bautista, I. Pedraza, H.A. Salazar Ibarguen, C. Uribe Estrada

**University of Montenegro, Podgorica, Montenegro**
I. Bubanja, N. Raicevic

**University of Canterbury, Christchurch, New Zealand**
P.H. Butler

**National Centre for Physics, Quaid-I-Azam University, Islamabad, Pakistan**
A. Ahmad, M.I. Asghar, A. Awais, M.I.M. Awan, H.R. Hoorani, W.A. Khan

**AGH University of Krakow, Faculty of Computer Science, Electronics and Telecommunications, Krakow, Poland**
V. Avati, L. Grzanka, M. Malawski

**National Centre for Nuclear Research, Swierk, Poland**
H. Bialkowska, M. Bluj, B. Boimska, M. Górski, M. Kazana, M. Szleper, P. Zalewski

**Institute of Experimental Physics, Faculty of Physics, University of Warsaw, Warsaw, Poland**
K. Bunkowski, K. Doroba, A. Kalinowski, M. Konecki, J. Krolikowski, A. Muhammad

**Warsaw University of Technology, Warsaw, Poland**
K. Pozniak, W. Zabolotny

**Laboratório de Instrumentação e Física Experimental de Partículas, Lisboa, Portugal**
M. Araujo, D. Bastos, C. Beirão Da Cruz E Silva, A. Boletti, M. Bozzo, P. Faccioli, M. Gallinaro, J. Hollar, N. Leonardo, T. Niknejad, M. Pisano, J. Seixas, J. Varela

**Faculty of Physics, University of Belgrade, Belgrade, Serbia**
P. Adzic, P. Milenovic

**VINCA Institute of Nuclear Sciences, University of Belgrade, Belgrade, Serbia**
M. Dordevic, J. Milosevic, V. Rekovic

**Centro de Investigaciones Energéticas Medioambientales y Tecnológicas (CIEMAT), Madrid, Spain**
M. Aguilar-Benitez, J. Alcaraz Maestre, M. Barrio Luna, Cristina F. Bedoya, M. Cepeda, M. Cerrada, N. Colino, B. De La Cruz, A. Delgado Peris, D. Fernández Del Val, J.P. Fernández Ramos, J. Flix, M.C. Fouz, O. Gonzalez Lopez, S. Goy Lopez, J.M. Hernandez, M.I. Josa, J. León Holgado, D. Moran, C. M. Morcillo Perez, Á. Navarro Tobar, C. Perez Dengra, A. Pérez-Calero Yzquierdo, J. Puerta Pelayo, I. Redondo, D.D. Redondo Ferrero, L. Romero, S. Sánchez Navas, L. Urda Gómez, J. Vazquez Escobar, C. Willmott

**Universidad Autónoma de Madrid, Madrid, Spain**
J.F. de Trocóniz

**Universidad de Oviedo, Instituto Universitario de Ciencias y Tecnologías Espaciales de Asturias (ICTEA), Oviedo, Spain**
B. Alvarez Gonzalez, J. Cuevas, J. Fernandez Menendez, S. Folgueras, I. Gonzalez Caballero, J.R. González Fernández, E. Palencia Cortezon, C. Ramón Álvarez, V. Rodríguez Bouza, A. Soto Rodríguez, A. Trapote, C. Vico Villalba, P. Vischia

**Instituto de Física de Cantabria (IFCA), CSIC-Universidad de Cantabria, Santander, Spain**
S. Bhowmik, S. Blanco Fernández, J.A. Brochero Cifuentes, I.J. Cabrillo, A. Calderon, J. Duarte Campderros, M. Fernandez, C. Fernandez Madrazo, G. Gomez, C. Lasaosa García, C. Martinez Rivero, P. Martinez Ruiz del Arbol, F. Matorras, P. Matorras Cuevas, E. Navarrete Ramos, J. Piedra Gomez, C. Prieels, L. Scodellaro, I. Vila, J.M. Vizan Garcia

**University of Colombo, Colombo, Sri Lanka**
M.K. Jayananda, B. Kailasapathy[59], D.U.J. Sonnadara, D.D.C. Wickramarathna

**University of Ruhuna, Department of Physics, Matara, Sri Lanka**
W.G.D. Dharmaratna[60], K. Liyanage, N. Perera, N. Wickramage

**CERN, European Organization for Nuclear Research, Geneva, Switzerland**
D. Abbaneo, C. Amendola, E. Auffray, G. Auzinger, J. Baechler, D. Barney, A. Bermúdez Martínez, M. Bianco, B. Bilin, A.A. Bin Anuar, A. Bocci, E. Brondolin, C. Caillol, T. Camporesi, G. Cerminara, N. Chernyavskaya, D. d'Enterria, A. Dabrowski, A. David, A. De Roeck, M.M. Defranchis, M. Deile, M. Dobson, F. Fallavollita[61], L. Forthomme, G. Franzoni, W. Funk, S. Giani, D. Gigi, K. Gill, F. Glege, L. Gouskos, M. Haranko, J. Hegeman, V. Innocente, T. James, P. Janot, J. Kieseler, S. Laurila, P. Lecoq, E. Leutgeb, C. Lourenço, B. Maier, L. Malgeri, M. Mannelli, A.C. Marini, F. Meijers, S. Mersi, E. Meschi, V. Milosevic, F. Moortgat, M. Mulders, S. Orfanelli, F. Pantaleo, M. Peruzzi, A. Petrilli, G. Petrucciani, A. Pfeiffer, M. Pierini, D. Piparo, H. Qu, D. Rabady, G. Reales Gutiérrez, M. Rovere, H. Sakulin, S. Scarfi, M. Selvaggi, A. Sharma, K. Shchelina, P. Silva, P. Sphicas[62], A.G. Stahl Leiton, A. Steen, S. Summers, D. Treille, P. Tropea, A. Tsirou, D. Walter, J. Wanczyk[63], K.A. Wozniak[64], P. Zehetner, P. Zejdl, W.D. Zeuner

**Paul Scherrer Institut, Villigen, Switzerland**
T. Bevilacqua[65], L. Caminada[65], A. Ebrahimi, W. Erdmann, R. Horisberger, Q. Ingram, H.C. Kaestli, D. Kotlinski, C. Lange, M. Missiroli[65], L. Noehte[65], T. Rohe

**ETH Zurich - Institute for Particle Physics and Astrophysics (IPA), Zurich, Switzerland**
T.K. Aarrestad, K. Androsov[63], M. Backhaus, A. Calandri, C. Cazzaniga, K. Datta, A. De Cosa, G. Dissertori, M. Dittmar, M. Donegà, F. Eble, M. Galli, K. Gedia, F. Glessgen, C. Grab, D. Hits, W. Lustermann, A.-M. Lyon, R.A. Manzoni, M. Marchegiani, L. Marchese, C. Martin Perez, A. Mascellani[63], F. Nessi-Tedaldi, F. Pauss, V. Perovic, S. Pigazzini, M.G. Ratti, M. Reichmann, C. Reissel, T. Reitenspiess, B. Ristic, F. Riti, D. Ruini, D.A. Sanz Becerra, R. Seidita, J. Steggemann[63], D. Valsecchi, R. Wallny

**Universität Zürich, Zurich, Switzerland**
C. Amsler[66], P. Bärtschi, C. Botta, D. Brzhechko, M.F. Canelli, K. Cormier, A. De Wit, R. Del Burgo, J.K. Heikkilä, M. Huwiler, W. Jin, A. Jofrehei, B. Kilminster, S. Leontsinis, S.P. Liechti, A. Macchiolo, P. Meiring,

V.M. Mikuni, U. Molinatti, I. Neutelings, A. Reimers, P. Robmann, S. Sanchez Cruz, K. Schweiger, M. Senger, Y. Takahashi

**National Central University, Chung-Li, Taiwan**
C. Adloff[67], C.M. Kuo, W. Lin, P.K. Rout, P.C. Tiwari[41], S.S. Yu

**National Taiwan University (NTU), Taipei, Taiwan**
L. Ceard, Y. Chao, K.F. Chen, P.s. Chen, Z.g. Chen, W.-S. Hou, T.h. Hsu, Y.w. Kao, R. Khurana, G. Kole, Y.y. Li, R.-S. Lu, E. Paganis, A. Psallidas, X.f. Su, J. Thomas-Wilsker, H.y. Wu, E. Yazgan

**High Energy Physics Research Unit, Department of Physics, Faculty of Science, Chulalongkorn University, Bangkok, Thailand**
C. Asawatangtrakuldee, N. Srimanobhas, V. Wachirapusitanand

**Çukurova University, Physics Department, Science and Art Faculty, Adana, Turkey**
D. Agyel, F. Boran, Z.S. Demiroglu, F. Dolek, I. Dumanoglu[68], E. Eskut, Y. Guler[69], E. Gurpinar Guler[69], C. Isik, O. Kara, A. Kayis Topaksu, U. Kiminsu, G. Onengut, K. Ozdemir[70], A. Polatoz, B. Tali[71], U.G. Tok, S. Turkcapar, E. Uslan, I.S. Zorbakir

**Middle East Technical University, Physics Department, Ankara, Turkey**
K. Ocalan[72], M. Yalvac[73]

**Bogazici University, Istanbul, Turkey**
B. Akgun, I.O. Atakisi, E. Gülmez, M. Kaya[74], O. Kaya[75], S. Tekten[76]

**Istanbul Technical University, Istanbul, Turkey**
A. Cakir, K. Cankocak[68], Y. Komurcu, S. Sen[77]

**Istanbul University, Istanbul, Turkey**
O. Aydilek, S. Cerci[71], V. Epshteyn, B. Hacisahinoglu, I. Hos[78], B. Isildak[79], B. Kaynak, S. Ozkorucuklu, O. Potok, H. Sert, C. Simsek, D. Sunar Cerci[71], C. Zorbilmez

**Institute for Scintillation Materials of National Academy of Science of Ukraine, Kharkiv, Ukraine**
A. Boyaryntsev, B. Grynyov

**National Science Centre, Kharkiv Institute of Physics and Technology, Kharkiv, Ukraine**
L. Levchuk

**University of Bristol, Bristol, United Kingdom**
D. Anthony, J.J. Brooke, A. Bundock, F. Bury, E. Clement, D. Cussans, H. Flacher, M. Glowacki, J. Goldstein, H.F. Heath, L. Kreczko, B. Krikler, S. Paramesvaran, S. Seif El Nasr-Storey, V.J. Smith, N. Stylianou[80], K. Walkingshaw Pass, R. White

**Rutherford Appleton Laboratory, Didcot, United Kingdom**
A.H. Ball, K.W. Bell, A. Belyaev[81], C. Brew, R.M. Brown, D.J.A. Cockerill, C. Cooke, K.V. Ellis, K. Harder, S. Harper, M.-L. Holmberg[82], Sh. Jain, J. Linacre, K. Manolopoulos, D.M. Newbold, E. Olaiya, D. Petyt, T. Reis, G. Salvi, T. Schuh, C.H. Shepherd-Themistocleous, I.R. Tomalin, T. Williams

**Imperial College, London, United Kingdom**
R. Bainbridge, P. Bloch, C.E. Brown, O. Buchmuller, V. Cacchio, C.A. Carrillo Mon-

toya, G.S. Chahal[83], D. Colling, J.S. Dancu, P. Dauncey, G. Davies, J. Davies, M. Della Negra, S. Fayer, G. Fedi, G. Hall, M.H. Hassanshahi, A. Howard, G. Iles, M. Knight, J. Langford, L. Lyons, A.-M. Magnan, S. Malik, A. Martelli, M. Mieskolainen, J. Nash[84], M. Pesaresi, B.C. Radburn-Smith, A. Richards, A. Rose, C. Seez, R. Shukla, A. Tapper, K. Uchida, G.P. Uttley, L.H. Vage, T. Virdee[30], M. Vojinovic, N. Wardle, D. Winterbottom

**Brunel University, Uxbridge, United Kingdom**
K. Coldham, J.E. Cole, A. Khan, P. Kyberd, I.D. Reid

**Baylor University, Waco, Texas, USA**
S. Abdullin, A. Brinkerhoff, B. Caraway, J. Dittmann, K. Hatakeyama, J. Hiltbrand, A.R. Kanuganti, B. McMaster, M. Saunders, S. Sawant, C. Sutantawibul, M. Toms[85], J. Wilson

**Catholic University of America, Washington, DC, USA**
R. Bartek, A. Dominguez, C. Huerta Escamilla, A.E. Simsek, R. Uniyal, A.M. Vargas Hernandez

**The University of Alabama, Tuscaloosa, Alabama, USA**
R. Chudasama, S.I. Cooper, S.V. Gleyzer, C.U. Perez, P. Rumerio[86], E. Usai, C. West, R. Yi

**Boston University, Boston, Massachusetts, USA**
A. Akpinar, A. Albert, D. Arcaro, C. Cosby, Z. Demiragli, C. Erice, E. Fontanesi, D. Gastler, J. Rohlf, K. Salyer, D. Sperka, D. Spitzbart, I. Suarez, A. Tsatsos, S. Yuan

**Brown University, Providence, Rhode Island, USA**
G. Benelli, X. Coubez[25], D. Cutts, M. Hadley, U. Heintz, J.M. Hogan[87], T. Kwon, G. Landsberg, K.T. Lau, D. Li, J. Luo, S. Mondal, M. Narain[†], N. Pervan, S. Sagir[88], F. Simpson, W.Y. Wong, X. Yan, W. Zhang

**University of California, Davis, Davis, California, USA**
S. Abbott, J. Bonilla, C. Brainerd, R. Breedon, M. Calderon De La Barca Sanchez, M. Chertok, M. Citron, J. Conway, P.T. Cox, R. Erbacher, G. Haza, F. Jensen, O. Kukral, G. Mocellin, M. Mulhearn, D. Pellett, B. Regnery, W. Wei, Y. Yao, F. Zhang

**University of California, Los Angeles, California, USA**
M. Bachtis, R. Cousins, A. Datta, J. Hauser, M. Ignatenko, M.A. Iqbal, T. Lam, E. Manca, W.A. Nash, D. Saltzberg, B. Stone, V. Valuev

**University of California, Riverside, Riverside, California, USA**
R. Clare, M. Gordon, G. Hanson, W. Si, S. Wimpenny[†]

**University of California, San Diego, La Jolla, California, USA**
J.G. Branson, S. Cittolin, S. Cooperstein, D. Diaz, J. Duarte, R. Gerosa, L. Giannini, J. Guiang, R. Kansal, V. Krutelyov, R. Lee, J. Letts, M. Masciovecchio, F. Mokhtar, M. Pieri, M. Quinnan, B.V. Sathia Narayanan, V. Sharma, M. Tadel, E. Vourliotis, F. Würthwein, Y. Xiang, A. Yagil

**University of California, Santa Barbara - Department of Physics, Santa Barbara, California, USA**
L. Brennan, C. Campagnari, G. Collura, A. Dorsett, J. Incandela, M. Kilpatrick,

J. Kim, A.J. Li, P. Masterson, H. Mei, M. Oshiro, J. Richman, U. Sarica, R. Schmitz, F. Setti, J. Sheplock, D. Stuart, S. Wang

**California Institute of Technology, Pasadena, California, USA**
A. Bornheim, O. Cerri, A. Latorre, J.M. Lawhorn, J. Mao, H.B. Newman, T. Q. Nguyen, M. Spiropulu, J.R. Vlimant, C. Wang, S. Xie, R.Y. Zhu

**Carnegie Mellon University, Pittsburgh, Pennsylvania, USA**
J. Alison, S. An, M.B. Andrews, P. Bryant, V. Dutta, T. Ferguson, A. Harilal, C. Liu, T. Mudholkar, S. Murthy, M. Paulini, A. Roberts, A. Sanchez, W. Terrill

**University of Colorado Boulder, Boulder, Colorado, USA**
J.P. Cumalat, W.T. Ford, A. Hassani, G. Karathanasis, E. MacDonald, N. Manganelli, F. Marini, A. Perloff, C. Savard, N. Schonbeck, K. Stenson, K.A. Ulmer, S.R. Wagner, N. Zipper

**Cornell University, Ithaca, New York, USA**
J. Alexander, S. Bright-Thonney, X. Chen, D.J. Cranshaw, J. Fan, X. Fan, D. Gadkari, S. Hogan, J. Monroy, J.R. Patterson, J. Reichert, M. Reid, A. Ryd, J. Thom, P. Wittich, R. Zou

**Fermi National Accelerator Laboratory, Batavia, Illinois, USA**
M. Albrow, M. Alyari, O. Amram, G. Apollinari, A. Apresyan, L.A.T. Bauerdick, D. Berry, J. Berryhill, P.C. Bhat, K. Burkett, J.N. Butler, A. Canepa, G.B. Cerati, H.W.K. Cheung, F. Chlebana, G. Cummings, J. Dickinson, I. Dutta, V.D. Elvira, Y. Feng, J. Freeman, A. Gandrakota, Z. Gecse, L. Gray, D. Green, S. Grünendahl, D. Guerrero, O. Gutsche, R.M. Harris, R. Heller, T.C. Herwig, J. Hirschauer, L. Horyn, B. Jayatilaka, S. Jindariani, M. Johnson, U. Joshi, T. Klijnsma, B. Klima, K.H.M. Kwok, S. Lammel, D. Lincoln, R. Lipton, T. Liu, C. Madrid, K. Maeshima, C. Mantilla, D. Mason, P. McBride, P. Merkel, S. Mrenna, S. Nahn, J. Ngadiuba, D. Noonan, V. Papadimitriou, N. Pastika, K. Pedro, C. Pena[89], F. Ravera, A. Reinsvold Hall[90], L. Ristori, E. Sexton-Kennedy, N. Smith, A. Soha, L. Spiegel, S. Stoynev, J. Strait, L. Taylor, S. Tkaczyk, N.V. Tran, L. Uplegger, E.W. Vaandering, I. Zoi

**University of Florida, Gainesville, Florida, USA**
C. Aruta, P. Avery, D. Bourilkov, L. Cadamuro, P. Chang, V. Cherepanov, R.D. Field, E. Koenig, M. Kolosova, J. Konigsberg, A. Korytov, K.H. Lo, K. Matchev, N. Menendez, G. Mitselmakher, A. Muthirakalayil Madhu, N. Rawal, D. Rosenzweig, S. Rosenzweig, K. Shi, J. Wang

**Florida State University, Tallahassee, Florida, USA**
T. Adams, A. Al Kadhim, A. Askew, N. Bower, R. Habibullah, V. Hagopian, R. Hashmi, R.S. Kim, S. Kim, T. Kolberg, G. Martinez, H. Prosper, P.R. Prova, O. Viazlo, M. Wulansatiti, R. Yohay, J. Zhang

**Florida Institute of Technology, Melbourne, Florida, USA**
B. Alsufyani, M.M. Baarmand, S. Butalla, T. Elkafrawy[54], M. Hohlmann, R. Kumar Verma, M. Rahmani, F. Yumiceva

**University of Illinois Chicago, Chicago, USA, Chicago, USA**
M.R. Adams, C. Bennett, R. Cavanaugh, S. Dittmer, R. Escobar Franco, O. Evdokimov, C.E. Gerber, D.J. Hofman, J.h. Lee, D. S. Lemos, A.H. Merrit, C. Mills, S. Nanda, G. Oh, B. Ozek, D. Pilipovic, T. Roy, S. Rudrabhatla, M.B. Tonjes,

N. Varelas, X. Wang, Z. Ye, J. Yoo

**The University of Iowa, Iowa City, Iowa, USA**
M. Alhusseini, D. Blend, K. Dilsiz[91], L. Emediato, G. Karaman, O.K. Köseyan, J.-P. Merlo, A. Mestvirishvili[92], J. Nachtman, O. Neogi, H. Ogul[93], Y. Onel, A. Penzo, C. Snyder, E. Tiras[94]

**Johns Hopkins University, Baltimore, Maryland, USA**
B. Blumenfeld, L. Corcodilos, J. Davis, A.V. Gritsan, L. Kang, S. Kyriacou, P. Maksimovic, M. Roguljic, J. Roskes, S. Sekhar, M. Swartz, T.Á. Vámi

**The University of Kansas, Lawrence, Kansas, USA**
A. Abreu, L.F. Alcerro Alcerro, J. Anguiano, P. Baringer, A. Bean, Z. Flowers, D. Grove, J. King, G. Krintiras, M. Lazarovits, C. Le Mahieu, C. Lindsey, J. Marquez, N. Minafra, M. Murray, M. Nickel, M. Pitt, S. Popescu[95], C. Rogan, C. Royon, R. Salvatico, S. Sanders, C. Smith, Q. Wang, G. Wilson

**Kansas State University, Manhattan, Kansas, USA**
B. Allmond, A. Ivanov, K. Kaadze, A. Kalogeropoulos, D. Kim, Y. Maravin, K. Nam, J. Natoli, D. Roy, G. Sorrentino

**Lawrence Livermore National Laboratory, Livermore, California, USA**
F. Rebassoo, D. Wright

**University of Maryland, College Park, Maryland, USA**
E. Adams, A. Baden, O. Baron, A. Belloni, A. Bethani, Y.M. Chen, S.C. Eno, N.J. Hadley, S. Jabeen, R.G. Kellogg, T. Koeth, Y. Lai, S. Lascio, A.C. Mignerey, S. Nabili, C. Palmer, C. Papageorgakis, M.M. Paranjpe, L. Wang, K. Wong

**Massachusetts Institute of Technology, Cambridge, Massachusetts, USA**
J. Bendavid, W. Busza, I.A. Cali, Y. Chen, M. D'Alfonso, J. Eysermans, C. Freer, G. Gomez-Ceballos, M. Goncharov, P. Harris, D. Hoang, D. Kovalskyi, J. Krupa, L. Lavezzo, Y.-J. Lee, K. Long, C. Mironov, C. Paus, D. Rankin, C. Roland, G. Roland, S. Rothman, Z. Shi, G.S.F. Stephans, J. Wang, Z. Wang, B. Wyslouch, T. J. Yang

**University of Minnesota, Minneapolis, Minnesota, USA**
B. Crossman, B.M. Joshi, C. Kapsiak, M. Krohn, D. Mahon, J. Mans, B. Marzocchi, S. Pandey, M. Revering, R. Rusack, R. Saradhy, N. Schroeder, N. Strobbe, M.A. Wadud

**University of Mississippi, Oxford, Mississippi, USA**
L.M. Cremaldi

**University of Nebraska-Lincoln, Lincoln, Nebraska, USA**
K. Bloom, M. Bryson, D.R. Claes, C. Fangmeier, F. Golf, J. Hossain, C. Joo, I. Kravchenko, I. Reed, J.E. Siado, G.R. Snow†, W. Tabb, A. Wightman, F. Yan, D. Yu, A.G. Zecchinelli

**State University of New York at Buffalo, Buffalo, New York, USA**
G. Agarwal, H. Bandyopadhyay, L. Hay, I. Iashvili, A. Kharchilava, C. McLean, M. Morris, D. Nguyen, J. Pekkanen, S. Rappoccio, H. Rejeb Sfar, A. Williams

**Northeastern University, Boston, Massachusetts, USA**
G. Alverson, E. Barberis, Y. Haddad, Y. Han, A. Krishna, J. Li, M. Lu,

G. Madigan, D.M. Morse, V. Nguyen, T. Orimoto, A. Parker, L. Skinnari, A. Tishelman-Charny, B. Wang, D. Wood

**Northwestern University, Evanston, Illinois, USA**
S. Bhattacharya, J. Bueghly, Z. Chen, K.A. Hahn, Y. Liu, Y. Miao, D.G. Monk, M.H. Schmitt, A. Taliercio, M. Velasco

**University of Notre Dame, Notre Dame, Indiana, USA**
R. Band, R. Bucci, S. Castells, M. Cremonesi, A. Das, R. Goldouzian, M. Hildreth, K.W. Ho, K. Hurtado Anampa, C. Jessop, K. Lannon, J. Lawrence, N. Loukas, L. Lutton, J. Mariano, N. Marinelli, I. Mcalister, T. McCauley, C. Mcgrady, K. Mohrman, C. Moore, Y. Musienko[13], H. Nelson, M. Osherson, R. Ruchti, A. Townsend, M. Wayne, H. Yockey, M. Zarucki, L. Zygala

**The Ohio State University, Columbus, Ohio, USA**
A. Basnet, B. Bylsma, M. Carrigan, L.S. Durkin, C. Hill, M. Joyce, A. Lesauvage, M. Nunez Ornelas, K. Wei, B.L. Winer, B. R. Yates

**Princeton University, Princeton, New Jersey, USA**
F.M. Addesa, H. Bouchamaoui, P. Das, G. Dezoort, P. Elmer, A. Frankenthal, B. Greenberg, N. Haubrich, S. Higginbotham, G. Kopp, S. Kwan, D. Lange, A. Loeliger, D. Marlow, I. Ojalvo, J. Olsen, D. Stickland, C. Tully

**University of Puerto Rico, Mayaguez, Puerto Rico, USA**
S. Malik

**Purdue University, West Lafayette, Indiana, USA**
A.S. Bakshi, V.E. Barnes, S. Chandra, R. Chawla, S. Das, A. Gu, L. Gutay, M. Jones, A.W. Jung, D. Kondratyev, A.M. Koshy, M. Liu, G. Negro, N. Neumeister, G. Paspalaki, S. Piperov, A. Purohit, J.F. Schulte, M. Stojanovic, J. Thieman, A. K. Virdi, F. Wang, W. Xie

**Purdue University Northwest, Hammond, Indiana, USA**
J. Dolen, N. Parashar, A. Pathak

**Rice University, Houston, Texas, USA**
D. Acosta, A. Baty, T. Carnahan, S. Dildick, K.M. Ecklund, P.J. Fernández Manteca, S. Freed, P. Gardner, F.J.M. Geurts, A. Kumar, W. Li, O. Miguel Colin, B.P. Padley, R. Redjimi, J. Rotter, E. Yigitbasi, Y. Zhang

**University of Rochester, Rochester, New York, USA**
A. Bodek, P. de Barbaro, R. Demina, J.L. Dulemba, C. Fallon, A. Garcia-Bellido, O. Hindrichs, A. Khukhunaishvili, P. Parygin[85], E. Popova[85], R. Taus, G.P. Van Onsem

**The Rockefeller University, New York, New York, USA**
K. Goulianos

**Rutgers, The State University of New Jersey, Piscataway, New Jersey, USA**
B. Chiarito, J.P. Chou, Y. Gershtein, E. Halkiadakis, A. Hart, M. Heindl, D. Jaroslawski, O. Karacheban[28], I. Laflotte, A. Lath, R. Montalvo, K. Nash, H. Routray, S. Salur, S. Schnetzer, S. Somalwar, R. Stone, S.A. Thayil, S. Thomas, J. Vora, H. Wang

**University of Tennessee, Knoxville, Tennessee, USA**

H. Acharya, D. Ally, A.G. Delannoy, S. Fiorendi, T. Holmes, N. Karunarathna, L. Lee, E. Nibigira, S. Spanier

**Texas A&M University, College Station, Texas, USA**
D. Aebi, M. Ahmad, O. Bouhali[96], M. Dalchenko, R. Eusebi, J. Gilmore, T. Huang, T. Kamon[97], H. Kim, S. Luo, S. Malhotra, R. Mueller, D. Overton, D. Rathjens, A. Safonov

**Texas Tech University, Lubbock, Texas, USA**
N. Akchurin, J. Damgov, V. Hegde, A. Hussain, Y. Kazhykarim, K. Lamichhane, S.W. Lee, A. Mankel, T. Mengke, S. Muthumuni, T. Peltola, I. Volobouev, A. Whitbeck

**Vanderbilt University, Nashville, Tennessee, USA**
E. Appelt, S. Greene, A. Gurrola, W. Johns, R. Kunnawalkam Elayavalli, A. Melo, F. Romeo, P. Sheldon, S. Tuo, J. Velkovska, J. Viinikainen

**University of Virginia, Charlottesville, Virginia, USA**
B. Cardwell, B. Cox, J. Hakala, R. Hirosky, A. Ledovskoy, A. Li, C. Neu, C.E. Perez Lara

**Wayne State University, Detroit, Michigan, USA**
P.E. Karchin

**University of Wisconsin - Madison, Madison, Wisconsin, USA**
A. Aravind, S. Banerjee, K. Black, T. Bose, S. Dasu, I. De Bruyn, P. Everaerts, C. Galloni, H. He, M. Herndon, A. Herve, C.K. Koraka, A. Lanaro, R. Loveless, J. Madhusudanan Sreekala, A. Mallampalli, A. Mohammadi, S. Mondal, G. Parida, D. Pinna, A. Savin, V. Shang, V. Sharma, W.H. Smith, D. Teague, H.F. Tsoi, W. Vetens, A. Warden

**Authors affiliated with an institute or an international laboratory covered by a cooperation agreement with CERN**
S. Afanasiev, V. Andreev, Yu. Andreev, T. Aushev, M. Azarkin, A. Babaev, A. Belyaev, V. Blinov[98], E. Boos, V. Borshch, D. Budkouski, V. Bunichev, M. Chadeeva[98], V. Chekhovsky, A. Dermenev, T. Dimova[98], D. Druzhkin[99], M. Dubinin[89], L. Dudko, A. Ershov, G. Gavrilov, V. Gavrilov, S. Gninenko, V. Golovtcov, N. Golubev, I. Golutvin, I. Gorbunov, A. Gribushin, Y. Ivanov, V. Kachanov, L. Kardapoltsev[98], V. Karjavine, A. Karneyeu, V. Kim[98], M. Kirakosyan, D. Kirpichnikov, M. Kirsanov, V. Klyukhin, D. Konstantinov, V. Korenkov, A. Kozyrev[98], N. Krasnikov, A. Lanev, P. Levchenko[100], N. Lychkovskaya, V. Makarenko, A. Malakhov, V. Matveev[98], V. Murzin, A. Nikitenko[101,102], S. Obraztsov, V. Oreshkin, A. Oskin, V. Palichik, V. Perelygin, M. Perfilov, S. Polikarpov[98], V. Popov, O. Radchenko[98], V. Rusinov, M. Savina, V. Savrin, V. Shalaev, S. Shmatov, S. Shulha, Y. Skovpen[98], S. Slabospitskii, V. Smirnov, D. Sosnov, V. Sulimov, E. Tcherniaev, A. Terkulov, O. Teryaev, I. Tlisova, A. Toropin, L. Uvarov, A. Uzunian, P. Volkov, A. Vorobyev†, G. Vorotnikov, N. Voytishin, B.S. Yuldashev[103], A. Zarubin, I. Zhizhin, A. Zhokin

†: Deceased
[1]Also at Yerevan State University, Yerevan, Armenia
[2]Also at TU Wien, Vienna, Austria
[3]Also at Institute of Basic and Applied Sciences, Faculty of Engineering, Arab Academy for

Science, Technology and Maritime Transport, Alexandria, Egypt
[4]Also at Ghent University, Ghent, Belgium
[5]Also at Universidade Estadual de Campinas, Campinas, Brazil
[6]Also at Federal University of Rio Grande do Sul, Porto Alegre, Brazil
[7]Also at UFMS, Nova Andradina, Brazil
[8]Also at Nanjing Normal University, Nanjing, China
[9]Now at The University of Iowa, Iowa City, Iowa, USA
[10]Also at University of Chinese Academy of Sciences, Beijing, China
[11]Also at University of Chinese Academy of Sciences, Beijing, China
[12]Also at Université Libre de Bruxelles, Bruxelles, Belgium
[13]Also at an institute or an international laboratory covered by a cooperation agreement with CERN
[14]Also at Cairo University, Cairo, Egypt
[15]Also at Suez University, Suez, Egypt
[16]Now at British University in Egypt, Cairo, Egypt
[17]Also at Birla Institute of Technology, Mesra, Mesra, India
[18]Also at Purdue University, West Lafayette, Indiana, USA
[19]Also at Université de Haute Alsace, Mulhouse, France
[20]Also at Department of Physics, Tsinghua University, Beijing, China
[21]Also at Tbilisi State University, Tbilisi, Georgia
[22]Also at The University of the State of Amazonas, Manaus, Brazil
[23]Also at Erzincan Binali Yildirim University, Erzincan, Turkey
[24]Also at University of Hamburg, Hamburg, Germany
[25]Also at RWTH Aachen University, III. Physikalisches Institut A, Aachen, Germany
[26]Also at Isfahan University of Technology, Isfahan, Iran
[27]Also at Bergische University Wuppertal (BUW), Wuppertal, Germany
[28]Also at Brandenburg University of Technology, Cottbus, Germany
[29]Also at Forschungszentrum Jülich, Juelich, Germany
[30]Also at CERN, European Organization for Nuclear Research, Geneva, Switzerland
[31]Also at Physics Department, Faculty of Science, Assiut University, Assiut, Egypt
[32]Also at Wigner Research Centre for Physics, Budapest, Hungary
[33]Also at Institute of Physics, University of Debrecen, Debrecen, Hungary
[34]Also at Institute of Nuclear Research ATOMKI, Debrecen, Hungary
[35]Now at Universitatea Babes-Bolyai - Facultatea de Fizica, Cluj-Napoca, Romania
[36]Also at Faculty of Informatics, University of Debrecen, Debrecen, Hungary
[37]Also at Punjab Agricultural University, Ludhiana, India
[38]Also at UPES - University of Petroleum and Energy Studies, Dehradun, India
[39]Also at University of Visva-Bharati, Santiniketan, India
[40]Also at University of Hyderabad, Hyderabad, India
[41]Also at Indian Institute of Science (IISc), Bangalore, India
[42]Also at IIT Bhubaneswar, Bhubaneswar, India
[43]Also at Institute of Physics, Bhubaneswar, India
[44]Also at Deutsches Elektronen-Synchrotron, Hamburg, Germany
[45]Also at Sharif University of Technology, Tehran, Iran
[46]Also at Department of Physics, University of Science and Technology of Mazandaran, Behshahr, Iran
[47]Also at Helwan University, Cairo, Egypt
[48]Also at Italian National Agency for New Technologies, Energy and Sustainable Economic Development, Bologna, Italy

[49]Also at Centro Siciliano di Fisica Nucleare e di Struttura Della Materia, Catania, Italy
[50]Also at Università degli Studi Guglielmo Marconi, Roma, Italy
[51]Also at Scuola Superiore Meridionale, Università di Napoli 'Federico II', Napoli, Italy
[52]Also at Fermi National Accelerator Laboratory, Batavia, Illinois, USA
[53]Also at Università di Napoli 'Federico II', Napoli, Italy
[54]Also at Ain Shams University, Cairo, Egypt
[55]Also at Consiglio Nazionale delle Ricerche - Istituto Officina dei Materiali, Perugia, Italy
[56]Also at Riga Technical University, Riga, Latvia
[57]Also at Department of Applied Physics, Faculty of Science and Technology, Universiti Kebangsaan Malaysia, Bangi, Malaysia
[58]Also at Consejo Nacional de Ciencia y Tecnología, Mexico City, Mexico
[59]Also at Trincomalee Campus, Eastern University, Sri Lanka, Nilaveli, Sri Lanka
[60]Also at Saegis Campus, Nugegoda, Sri Lanka
[61]Also at INFN Sezione di Pavia, Università di Pavia, Pavia, Italy
[62]Also at National and Kapodistrian University of Athens, Athens, Greece
[63]Also at Ecole Polytechnique Fédérale Lausanne, Lausanne, Switzerland
[64]Also at University of Vienna Faculty of Computer Science, Vienna, Austria
[65]Also at Universität Zürich, Zurich, Switzerland
[66]Also at Stefan Meyer Institute for Subatomic Physics, Vienna, Austria
[67]Also at Laboratoire d'Annecy-le-Vieux de Physique des Particules, IN2P3-CNRS, Annecy-le-Vieux, France
[68]Also at Near East University, Research Center of Experimental Health Science, Mersin, Turkey
[69]Also at Konya Technical University, Konya, Turkey
[70]Also at Izmir Bakircay University, Izmir, Turkey
[71]Also at Adiyaman University, Adiyaman, Turkey
[72]Also at Necmettin Erbakan University, Konya, Turkey
[73]Also at Bozok Universitetesi Rektörlügü, Yozgat, Turkey
[74]Also at Marmara University, Istanbul, Turkey
[75]Also at Milli Savunma University, Istanbul, Turkey
[76]Also at Kafkas University, Kars, Turkey
[77]Also at Hacettepe University, Ankara, Turkey
[78]Also at Istanbul University - Cerrahpasa, Faculty of Engineering, Istanbul, Turkey
[79]Also at Yildiz Technical University, Istanbul, Turkey
[80]Also at Vrije Universiteit Brussel, Brussel, Belgium
[81]Also at School of Physics and Astronomy, University of Southampton, Southampton, United Kingdom
[82]Also at University of Bristol, Bristol, United Kingdom
[83]Also at IPPP Durham University, Durham, United Kingdom
[84]Also at Monash University, Faculty of Science, Clayton, Australia
[85]Now at an institute or an international laboratory covered by a cooperation agreement with CERN
[86]Also at Università di Torino, Torino, Italy
[87]Also at Bethel University, St. Paul, Minnesota, USA
[88]Also at Karamanoğlu Mehmetbey University, Karaman, Turkey
[89]Also at California Institute of Technology, Pasadena, California, USA
[90]Also at United States Naval Academy, Annapolis, Maryland, USA
[91]Also at Bingol University, Bingol, Turkey
[92]Also at Georgian Technical University, Tbilisi, Georgia

[93]Also at Sinop University, Sinop, Turkey
[94]Also at Erciyes University, Kayseri, Turkey
[95]Also at Horia Hulubei National Institute of Physics and Nuclear Engineering (IFIN-HH), Bucharest, Romania
[96]Also at Texas A&M University at Qatar, Doha, Qatar
[97]Also at Kyungpook National University, Daegu, Korea
[98]Also at another institute or international laboratory covered by a cooperation agreement with CERN
[99]Also at Universiteit Antwerpen, Antwerpen, Belgium
[100]Also at Northeastern University, Boston, Massachusetts, USA
[101]Also at Imperial College, London, United Kingdom
[102]Now at Yerevan Physics Institute, Yerevan, Armenia
[103]Also at Institute of Nuclear Physics of the Uzbekistan Academy of Sciences, Tashkent, Uzbekistan